[redacted]
THESIS

LIBRARY
Michigan State
University

This is to certify that the

dissertation entitled

TRANSLATION OF TWO CONTACTING SPHERES IN
A VISCOELASTIC FLUID

presented by

Mohammad Amin Jefri

has been accepted towards fulfillment
of the requirements for

Ph.D. degree in Chemical Engineering

K Jayaraman
Major professor

Date June 15, 1983

MSU
LIBRARIES

RETURNING MATERIALS:
Place in book drop to remove this checkout from your record. FINES will be charged if book is returned after the date stamped below.

ROOM USE ONLY

DO NOT CIRCULATE

TRANSLATION OF TWO CONTACTING SPHERES IN A VISCOELASTIC FLUID

By

Mohammad Amin Jefri

A DISSERTATION

Submitted to
Michigan State University
in partial fulfillment of the requirements
for the degree of

DOCTOR OF PHILOSOPHY

Department of Chemical Engineering

1983

TRANSLATION OF TWO CONTACTING SPHERES IN A VISCOELASTIC FLUID

By

Mohammad Amin Jefri

This work was undertaken to study the effect of a viscoelastic fluid on the translation of two contacting spherical particles of unequal size in creeping flow. The elastic effect of the medium was investigated theoretically by employing a second order fluid model and developing a numerical scheme that evaluates the elastic effect on the drag force. The accuracy of the scheme was established by carrying out a detailed error analysis at each step of this scheme. It was revealed by analyzing the numerical results, that the region near the stagnation points at the surface of the larger sphere has the major contribution to the elastic effect on the drag, while the region at the contact point has no contribution. The results obtained for several size ratios of the large to small sphere where the numerical scheme is valid showed an appreciable elastic effect on the drag. This effect increased with increasing size ratio, up to a ratio of 3.

Experiments carried out on the settling of these particles in a solution of 0.2 wt.% Separan in corn syrup at particle Reynolds numbers in the range of 10^{-4} to 10^{-6} yielded the following results. First, it is seen that a stable orientation exists in the direction of the applied force (gravity) along the line of centers with the larger sphere underneath. Secondly, the deviation from Newtonian drag for equal spheres is zero. This agrees with previous theoretical results. In the case of unequal spheres, a 10 percent reduction in the drag coefficient below the Newtonian value is observed, at a Weissenberg number of 0.1. This reduction is seen to increase with increasing Weissenberg number. Good agreement was seen when comparing the experimental and theoretical results.

To my parents--Zain Almasri and Amin Jefri

To my wife, Hend

To my son, Faris

ACKNOWLEDGMENTS

I would like to thank Dr. K. Jayaraman, my major advisor, for his sincere guidance, patience, and deep involvement in this dissertation. My thanks also go to Drs. E. Grulke, P. Wood, and L. Vallejo for their valuable comments.

To my mother, father, wife, and son Faris, thank you for your support and encouragement over the years.

I would also like to thank the Government of Saudi Arabia for financially supporting me during the period of my study.

Finally, thanks to all my friends, especially Dr. Ekong Ekong, for his friendship.

TABLE OF CONTENTS

Chapter Page

LIST OF TABLES

LIST OF FIGURES

Figure		Page

NOMENCLATURE

A	unknown function of s in Equation (3.37)
A_C	plate area of viscometer in cm
$\underline{\underline{A}}_1, \underline{\underline{A}}_2$	dimensionless Rivlin-Ericksen tensors of exterior fluid
a	small sphere radius (cm)
a_1	coefficient of exponential in f_1 in Equation (3.63)
B	unknown function of s in Equation (3.37)
$\underline{\underline{\mathscr{B}}}$	coefficient matrix for solving for A(s)--D(s), see Equation (3.54)
b_1	multiplier of the exponential function f_1
b_2, b_3	function of α in Equation (3.62)
C	unknown function of s in Equation (3.37)
$\underline{c}$	unknown column vector in Equation (3.54)
C_d	drag coefficient
Cd_e	elastic drag coefficient
Cd_s	Newtonian drag coefficient
C_o	characteristic particle dimension
D	unknown function of s in Equation (3.37)
D_c	drop cylinder diameter
$\hat{\underline{\underline{D}}}$	reference field deformation gradient
$\underline{\underline{D}}$	dimensional deformation gradient
$\underline{\underline{D}}_o^*$	dimensionless deformation gradient in Equation (3.29)
d	sphere diameter

d_1	diameter of viscometer plate
$\underline{e}_z$	unit vector along z-direction
$\underline{F}$	drag force vector
F_G	drag force on contacting particles surface
$\underline{F}_o$	drag force vector due to Newtonian contribution
F_N	Newtonian drag force
$\underline{F}_1$	first non-Newtonian contribution to the total drag
$\underline{F}_2$	second non-Newtonian contribution to the total drag of order
F_{1z}	drag force due to elasticity on surface of doublets
F_{oz}	Newtonian drag in the z-direction
$\mathscr{F}$	twice differentiable function. See Equation (3.34)
f	function of x, η, and ξ given in Equation (3.51)
$\underline{\underline{f}}$	deformation gradient in Equation (1.8), (1.10)
f_o	function of x, η, and ξ at small s values in the Hankel transforms in Equation (3.66)
f_1	exponential decaying function in the Hankel transforms 0 to ∞ and 0 to x_u given by Equation (3.63)
f_N	correction factor to the Newtonian fluid for contacting particles
$\|\Delta f\|$	absolute error in evaluating $f(s,\xi)$--See Table 3.4
$\underline{G}$	hydrodynamic couple
g	gravitational acceleartion
g(s)	function of s in Equation (3.78)
g_1	function of ξ and η in Equation (3.50)
H	transfer function of load cell
HT1-HT6	analytical solution of the Hankel transforms 0 to ∞ See Equations (3.73), (3.74)

I_1, I_6	Hankel transforms given by Equation (3.51)
$\underline{\underline{I}}$	unit tensor
i	complex number = $\sqrt{-1}$
i_1--i_6	integrand of the Hankel transforms at small value of x
$\underline{i}$	arbitrary unit vector
J_o	Bessel function of the first kind and order 0
J_1	Bessel function of the first kind and order 1
J_m	Bessel function of the first kind and order m
K	wall correction factor
$\bar{K}$	raw sum norm condition number in Equation (3.59)
$\underline{\underline{K}}$	wall effect tensor for single sphere settling
k	ratio of large sphere to small sphere radius
K_0^{11}, $K_0^{(2)}$	time constants of Equation (1.8)
Le	distance required to attain terminal velocity See Equation (4.5)
ℓ	characteristic container length
M	particle mass
M'	fluid mass displaced by particle
m	order of Bessel function
N_1	first normal stress difference (Newton/meter^2)
n	number of simultaneous equations
$\underline{n}$	outward unit normal
P	pressure
Q	integrand function of ξ and η of a double integral over ξ and η in Equation (3.47)
Re	Reynolds number
r	r-direction of a cylindrical polar coordinates system

$\underline{r}$	position vector
S_∞	fluid surface far from the particle
S_o	fluid surface just about the particle
S_p	particle surface
s	Hankel transform variable. See Equation (3.35)
T	function of α given by Equation (3.68)
T_o	torque on particle surface
T_1 to T_3	function of ψ in Equation (3.48)
$\underline{T}$	torque vector in Equation (1.9)
$\underline{T}_o$	Newtonian torque
$\underline{T}_1$	non-Newtonian torque vector in Equation (1.9)
$\underline{\underline{T}}$	stress tensor of Rivlin-Ericksen type. See Equation (1.3)
$\underline{\underline{T}}_1$	stress tensor for viscoelastic contribution
$\underline{\underline{T}}_o$	stress tensor for reference fluid
t	time (sec)
$\bar{t}$	mantissa of a single precision floating point number
U	uniform translation velocity (cm/sec)
$\hat{U}$	reference uniform translation velocity (cm/sec)
U_∞	bounded uniform translation velocity
$\underline{U}$	uniform translation velocity vector
$\underline{u}^{(1)}$	dimensional velocity vector in Equation (1.3)
$\underline{u}^{(1)+}$	dimensional transpose velocity vector in Equation (1.3)
z	z-direction of a cylindrical polar coordinates system
V_f	fluid volume surrounding doublets
$\underline{v}$	fluid velocity field vector

$\underline{v}_1$ $\underline{v}_2$	non-Newtonian velocity field vector in Equation (3.5)
$\underline{v}_o$	Newtonian fluid velocity vector
$\hat{\underline{v}}_o$	reference fluid velocity field vector
We	modified Weissenberg number $(\nu_1 + 2\nu_1)\frac{U}{a}$
$\bar{W}e$	conventional Weissenberg number, ν_1 U/z,$\frac{N_1}{\tau}$
We*	$\dot{\gamma}_{av}\lambda_o$
x	argument of Bessel function $\equiv s\eta$. See Equation (3.51)
Xe, Xs	correction factor for drag force for contacting and single sphere (elastic effect)
x_ℓ	limit for integrating Hankel transfoms - min [$\cdot 1\eta$, .3] See Euqation (3.66)
x_u	limit for integrating Hankel transform = 10 η. See Equation (3.72)

Greek Letters

α	1/k
α_c	ratio of densities defined by Equation (4.5)
α_o--α_4	material constants of Equation (1.3)
Γ	gamma function
γ	exponent in Equation (3.78) to make g(s) bounded
$\dot{\gamma}$	shear rate
$\dot{\gamma}_{av}$	average surface shear rate
$\underline{\underline{\delta}}$	unit tensor
η	dimensionless tangent sphere coordinate
λ	material constant in Equation (4.4)
λ_o	relaxation time (sec)
μ	fluid viscosity)

μ_o	zero shear viscosity (poise)
μ_s	Stokes' law viscosity
ν_1, ν_2	ratios of normal stress coefficient to viscosity
ξ	dimensionless tangent sphere coordinates
$\underline{\underline{\Pi}}$	stress tensor of Equation (3.9)
$\underline{\underline{\Pi}}_o$, $\hat{\underline{\underline{\Pi}}}_o$	stress tensors of Equation (3.6), (3.11)
π	PI = 3.1415927
ρ	density
ρ_f, ρ_p	fluid and particle density (gm/cm^3)
$\underline{\underline{\sigma}}$	shear tensor in Equations (1.3), (2.1) and (3.1)
τ	shear stress
ϕ	azimuthal angle
ψ	axisymmetrical stream function
ψ_1	first normal stress coefficient ($N_1/\dot{\gamma}^2$)
$\underline{\omega}$	angular velocity vector

<u>Miscellaneous Symbols</u>

D/Dt	material derivative
$\mathcal{D}/\mathcal{D}t$	co-rotational derivative
∇	Nabla operator
∇^2	Laplace operator
$\cdot$	dot product
:	double dot product
*	dimensionless quantities
$\underline{\underline{\Sigma}}_1$	second order tensor defined by Equation (3.15)
Λ^2	operator defined by Equation (3.34)

CHAPTER I

INTRODUCTION

1.1 Introduction

The flow of suspensions in viscoelastic liquids occurs commonly in a variety of industrial processes, ranging from the manufacture of filled polymer composites, paints, and coating to the injection of fracturing and drilling fluids into rock formations. There is a great need to know how the solids in the flow affect the bulk viscoelastic properties and how the solids interact with each other. In general, the rigorous solution of multiparticulate flow is too complex to solve with present techniques. Therefore, we have chosen a simple two contacting spheres problem in a viscoelastic fluid, hoping that the proper analysis of this system would give some insights into multiparticulate problems. The study of such suspensions presents a wide variety of unexplained phenomena dealing with particle motions in sedimentation as well as shear flows and with their bulk properties.

Sigli and Coutanccau (1977) have studied the translation of a solid sphere in a circular cylinder where the ratio of sphere diameter to cylinder diameter is greater than 0.25. They found that the presence of the wall increased the effect of fluid elasticity. Gauthier et al. (1971a,b) and Highgate and Whorlow (1970) observed that in couette flow of viscoelastic fluid, neutrally buoyant rigid spheres migrate toward the cylinder wall while neutrally buoyant Newtonian drops migrate away from the wall to an equilibrium position. Gauthier et al. (1977a,b) also observed that rigid particles migrate to the axis is Poiseuille flow even at Reynolds numbers of 10^{-4} while in Newtonian liquids no cross flow migration is observed at these Reynolds numbers. Furthermore, in liquids which are predominantly shear thinning, migration toward the wall is observed.

Understanding these phenomena must be through studying the particle mechanics and dynamics. In particular, the motion in the unbounded domain is hoped to provide the viscoelastic medium effect relative to the Newtonian medium which has been studied extensively for a variety of particle motions in an unbounded domain. The interest of this research is in the elastic effect on the translational motion of rigid particles and clusters in a quiescent viscoelastic medium. In what follows work on particle motion in viscoelastic and Newtonian liquids are reviewed.

1.2 Particle Motion in Uniform Newtonian Flows

The work on particle motion in Newtonian fluids goes back a long way since Stokes (1819-1903) studied the resistance of a solid body moving relative to a fluid, in which the viscosity was taken into account. Later in 1857 that study was published where Stokes linearized the equations of motion for viscous incompressible fluid. Consequently, the famous Stokes law which described the drag force on falling spherical objects in an unbounded medium was obtained as:

$$\underline{F} = 6\pi\mu\, \underline{U}\, a \tag{1.1}$$

Brenner (1965) has reviewed later work with nonspherical particles and with inertial or wall effects only a brief review is included here.

Stimson and Jeffery (1926) determined the drag force on the surface of two separate equal or unequal spheres along their line of centers. Their solution was for uniform slow viscous flow that is described by the quasistatic creeping equation of motion:

$$\mu\nabla^2\underline{v} = \nabla P$$

$$\nabla \cdot \underline{v} = 0 \tag{1.2}$$

The flow considered is for a body of revolution parallel to its symmetry axis, the exact solution involved using the spherical bipolar coordinates system to find Stokes stream function for the fluid motion. Brenner (1964), in a series of articles, presented solutions for the Stokes resistance to a slightly deformed rigid sphere and for an arbitrary shape particle. The solution was for both uniform flow and shear flow at low Reynolds numbers. In all cases the results were obtained by solving the creeping flow equation for the specific particle and flow condition in question. In the case of non-symmetrical particles, the rotational motion was considered along with translation. An extension to Stimson's solution was carried out by Goldman et al. (1966). The problem they solved is the same two spherical solid particles moving slowly in an unbounded quiescent viscous fluid; with orientation of particle. In their case it was an arbitrary orientation relative to the particle motion direction. The solution is a superposition of the results (of two spheres side by side) for the translation and rotation each considered in the absence of the other. Brenner (1961) presented an exact solution for spherical particles moving toward a plane surface. Two types of walls were considered, a solid wall and a free surface. Correction to Stokes law was given as a function of the ratio of the distance from the wall to the sphere radius. The results obtained were pertinent to end-effects in the falling-ball viscometer. The axisymmetrical stream function obtained by Stimmson and Jeffery in terms of the bipolar coordinates was utilized in the solution. Dean and O'Neill (1963) analyzed the case where the fluid motion is caused by rotation of the sphere along an axis that is parallel to the bounding rigid plane. A successive approximation method was used to solve an infinite set of linear equations which describe the problem. A numerical solution was obtained as a function of the separation distance from the wall. The problem in which the sphere only translates in the same manner as the previous problem was later solved by O'Neill (1964). The solution is for axisymmetric flow around the sphere; where the bipolar stream function of Stimmson was used again.

Their solutions were in the form of infinite series which converged very slowly as the distance between the bounding solid wall and the sphere went to zero; Goldman et al. (1967) proposed an asymptotic approximation obtained by the method of the lubrication theory to overcome this problem. A corresponding solution to that of Brenner (1961) (i.e., sphere translating toward a wall) for small gap width was also carried out by Cox and Brenner (1967). A singular perturbation expansion technique was used for calculating the hydrodynamic force on the sphere surface as the separation distance tends to zero. A general solution for a more general axisymmetric particle was also included. The same solution technique adapted by Cox and Brenner (1967), for the same problem, was also used later by Cooley and O'Neill (1969b). In addition to the plane wall, they also considered a case where a stationary spherical object is approached by the moving sphere. In their work, use was made of a contacting sphere coordinate system to facilitate the solution when contact is achieved between the sphere and the wall or the sphere and the stationary sphere.

So far mostly uniform flows were mentioned. This is, in part, due to the bulk of results available and to the fact that fewer problems have been attempted in shear flow. Lin et al. (1970) extended the problem of arbitrarily oriented two sphere problem in uniform flow in a viscous fluid solved by Godlman et al. (1966) to one in a shear field. The analysis and solution procedure is parallel to that of the uniform flow problem. The problem of a sphere approaching a plane wall was also treated there. In both cases, the hydrodynamic forces and torques experienced by the spheres during the course of their motion were given as a function of the distance separating them.

1.3 Particle Motion in Viscoelastic Fluids

The study of particle motion of a sphere in a viscoelastic fluid was begun by Leslie and Tanner (1961) who carried out a retarded motion expansion, which effectively reduces the constitutive behavior to that of the nth-order fluid which is usually associated with the names Rivlin and Ericksen. This constitutive behavior is given by:

$$p\underline{\underline{I}} + \underline{\underline{T}} = \alpha_o\underline{\underline{A}}_1 + \alpha_1\underline{\underline{A}}_2 + \alpha_2\underline{\underline{A}}_1^2 + \alpha_3\underline{\underline{A}}_3 + \alpha_4(\underline{\underline{A}}_1\underline{\underline{A}}_2 + \underline{\underline{A}}_2\underline{\underline{A}}_1)$$

$$+ \text{ higher terms} \qquad (1.3)$$

where

$$\underline{\underline{A}}_1 = \nabla\underline{u} + \nabla\underline{u}^+$$

$$\underline{\underline{A}}_n = \frac{D\underline{\underline{A}}_{n-1}}{Dt} + \underline{\underline{A}}_{n-1} \cdot \nabla\underline{u} + \nabla\underline{u}^+ \cdot \underline{\underline{A}}_{n-1}$$

and α_o to α_4 are material constants related to the viscosity and normal stress. The first three terms are the terms of what is known as the second order fluid (to be discussed later). Leslie and Tanner (1961) reported the effect of the viscoelastic medium on the drag for uniform creeping flow past a spherical object with the Oldroyd fluid model (1958). They carried out a perturbation expansion up to order two in Weissenberg number.

$$\underline{F} = \underline{F}_o + \bar{W}e\underline{F}_1 + \bar{W}e^2\underline{F}_2 \qquad (1.4)$$

The solution obtained is valid for $Re \ll \bar{W}e \ll 1$. Their results showed a reduction in the drag below that obtained by Stoke's law.

In general, the solution to particle motion in a viscoelastic medium is centered around an expansion of the Weissenberg number which is expressed as:

$$\bar{W}e = \frac{N_1}{\tau} \tag{1.5}$$

N_1 is the first normal stress difference, τ is the shear stress. The expansion is done around Stokes solution. Even though such expansion restricts the viscoelastic effect to a secondary role, nevertheless, for the class of particle motions which involve weak viscoelastic characteristics, the "retarded motion" expansion has been shown to yield qualitatively correct predictions of particle motions, both in uniform streaming flow and in shear flow (Tiefenbruk and Leal, 1979; Chan and Leal, 1979). These authors investigated the cross flow migration of neutrally buoyant drops which are suspended in a non-Newtonian fluid described by the second order fluid. They considered the hydrodynamically induced migration. The predicted results obtained by their theoretical analysis were found to be in good agreement with experimental observations.

Giesekus (1962) obtained the correction to Stoke's drag for both translation and rotation of a rigid sphere at the same flow conditions as those of Leslie and Tanner. The medium is described by a third order fluid model. This is represented by the first four terms in Equation (1.3). The results obtained were consistent with Leslie's. Other workers also used the third order fluid like

Caswell and Schwarz (1962) to find that drag reduction is observed at order $\mathcal{W}e^2$.

It is worth while to present a word about the second order fluid model which had been used by a number of workers. If the fluid relaxation time is small (but finite) compared to the time scale motion U/a, the fluid motion will be "rheologically slow" so that the second order model may be used. As mentioned earlier, this model is part of the general Rivlin Eriksen retarded expansion which indicates that the flow is both slow and slowly varying with time. It is useful in predicting elastic effects with a non-shear dependent viscosity. Due to the non-linearities of both the governing equation of motion for particle motion in viscoelastic fluids and the constitutive equations, most of the solutions have been limited to creeping flow, with the equation of motion

$$\nabla \cdot \underline{\sigma} = 0 \tag{1.6}$$

The hydrodynamic force, F_{hyd}, and torque, T_{hyd}, on the particle surface are given by:

$$F_{hyd} = \int_{S_p} \underline{\underline{\sigma}} \cdot \underline{n} \, dS$$

$$T_{hyd} = \int_{S_p} (\underset{\sim}{n} \cdot \underline{\underline{\sigma}}) \times \underline{r} \, ds \tag{1.7}$$

where S_p indicates the integration over the particle surface and $\underline{n}$ is an outward unit normal in the direction of the force.

Brunn (1977a) has considered the general problem of a transversely isotropic particle moving in a second order fluid. Such a particle has three planes of symmetry, two of which are identical. Examples are bodies of revolution with fore-aft symmetry. The analysis included both uniform and simple shear flow. The solution was carried out in the framework of a complete asyptotic solution, but without carrying out the details necessary for numerical evaluation of the coefficients which characterize the particle's motion. The interest was about particle preferred orientation. For the flow condition considered there, the second order fluid model was given as:

$$\underline{\underline{\sigma}}^{(1)} = 2\mu[K_0^{(11)}\underline{f}^{(1)} \cdot \underline{f}^{(1)} + K_0^{(2)}\ \underline{f}^{(2)}] \tag{1.8}$$

and

$$\underline{f}^{(1)} = \frac{1}{2}\left[\frac{\partial \underline{u}^{(1)}}{\partial \underline{r}} + \left(\frac{\partial \underline{u}^{(1)}}{\partial \underline{r}}\right)^{\dagger}\right]$$

$$\underline{f}^{(2)} = \frac{\partial \underline{f}^{(1)}}{\partial t} + \underline{u}^{(1)} \cdot \frac{\partial}{\partial \underline{r}}\,\underline{f}^{(1)} + \underline{\omega}^{(1)}\quad \underline{f}^{(1)} - \underline{f}^{(1)} \cdot \underline{\omega}^{(1)},$$

where

$\underline{\omega}^{(1)}$ is the angular velocity vector

$\underline{u}^{(1)}$, $\underline{u}^{(1)\dagger}$ is the velocity vector and its transpose

$K_0^{(11)}$ and $K_0^{(2)}$ are two time constants related to the viscosity and normal stress of the fluid.

It is by the contribution of these constants to the total hydrodynamic force $\underline{F}$ and couple $\underline{G}$, information was obtained on those preferred orientation. It was shown that a transversely isotropic particle in a quiescent field will have a terminal orientation in the direction of the external force. In this case, the particle would not rotate once it reaches the terminal state. A particle with its symmetry axis in the plane of the shear will not leave that plane while a particle with its axis parallel to the vorticity axis will always maintain that orientation. For long transversely isotropic particle, Leal (1975) used the slender-body approximation to calculate the hydrodynamic force and torque for simple translation. It was shown that the particle will acquire a terminal orientation that is parallel to the axis of symmetry in the direction of the external force. This was also seen to be the case experimentally. In simple shear flow the results were identical to those of Brunn (1977a). Brunn (1979) investigated the effect of particle shape on the orientation. He considered a near sphere particle and included the particle shape in the analysis. The medium was taken to be represented by the second order fluid. The result of particle sedimentation gave the same conclusion as that of a perfect sphere. This is a terminal orientation in the direction of minimum resistance. The results showed no such agreement for shear flow. In this case, it is shown that the particle migrates in the direction of its axis provided that this is the vorticity axis. In elongational flow, the behavior is qualitatively the same as in a Newtonian fluid. In a review by Brunn

(1980) the motion of rigid particles in viscoelastic fluid was surveyed. The second order fluid model was used to describe the medium. A general formulation for arbitrary rigid particle in a steady motion of negligible inertial effect was considered. A regular perturbation expansion around the Newtonian solution in power of small Weissenberg number was assumed to obtain an expression for the drag force and torque on the particle surface.

$$\underline{F} = \underline{F}_0 + \bar{W}e\, \underline{F}_1 + \ldots$$
$$\underline{T} = \underline{T}_0 + \bar{W}e\, \underline{T}_1 + \ldots \qquad (1.9)$$

where the subscript 0 is for Newtonian contribution and the subscript 1 is for the non-Newtonian (normal stress) contribution. In pure translation the contribution from $\underline{F}_1$ was obtained via application of the reciprocal theorem which is given as a volume integral around the total fluid volume surrounding the particle.

$$\underline{i} \cdot \underline{F}_1 = 2\mu \int_{V_f} d\underline{V}[\underline{\underline{f}}_0 \cdot \underline{\underline{f}}_0] : \hat{\underline{\underline{f}}}_0 \qquad (1.10)$$

where

$\underline{i}$ is an arbitrary vector,

μ is the viscosity

$\underline{\underline{f}}_0$, $\hat{\underline{\underline{f}}}_0$ are the Newtonian and reference field deformation gradient

Brunn (1976) had stressed the difficulty of evaluating the integral of Equation (1.10). He clarified that the difficulty is not due to the volume integral itself, but to the tedious repeated tensorial product $\underline{f}_0 \cdot \underline{\underline{f}}_0 : \hat{\underline{\underline{f}}}$. The same method of analysis was also outlined by Leal (1975). The merit in using the reciprocal theorem is in that there is no need for obtaining the velocity field in order to obtain the force and torque on the particle surface. Leal also found that a slender or symmetric rod-like particle in a simple shear flow has a correction in the drag force at order one rather than at order two in Weissenberg number as for a sphere.

In the next chapter particle interaction is going to be discussed and the problem statement is to be presented. Chapter III and IV are devoted to the theoretical and experimental analysis. Finally, Chapter V would present the conclusion and recommendation.

CHAPTER II

MOTION OF AGGREGATES

2.1 Particle Interaction

2.1.1 Effect of Particle Size

Increasing the concentration of particles and shear rate in suspensions leads to the formation of particle doublets due to the hydrodynamic interaction. In general, suspensions of single particles will behave differently from suspension of agglomerates. This is caused by the difference in shape between agglomerates and single particles and by the fluid entrapped in the interstices between the particles. When the particle size is of 1μm or less, other factors which are known as colloidal forces effect the interaction and stability of doublets in addition to the hydrodynamic force. The first of the colloidal forces is the Brownian. These have been reviewed by Russell (1980). This force is due to random collision between particles due to fluctuation in thermal conditions. The dominance of this force over the electrostatic force is for particle sizes of nanometers. Electrostatic effect is dominant for particle sizes in the range of .1 to 10μm in diameter. This has been treated by Overbeek (1948). At this size, two electrostatic effects are encountered between the particles; an attractive field as a result of the Van der Waals forces and a repulsive field due to particle surface charge. The repulsion effect acts as an opposing force against the attraction. Thus, the superiority of either the attraction or repulsion effect is the limiting factor for forming an aggregated or a floctuated system. The stability of the doublets formed was investigated by several workers. Papenhyijzen (1972) investigated the effect of high and low deformation on aggregated suspension. A network model describing the particle arrangement as a random chain formation was developed. The relative order of magnitude of the effects of hydrodynamic and non-hydrodynamic forces on breaking these chains was calculated for two different suspensions. It was found that the hydrodynamic force is of the same order of magnitude as the non-hydrodynamic. Hoffman (1974) performed a theoretical and experimental study of the role of interactive forces on the dilatant viscosity behavior in concentrated suspensions of polymer resins in shear flow. The phenomona was explained by the effect of the shear rate on the layer of ordered chains of particles which pass one over another in the direction of flow. It is the disorder of such an arrangement, caused by shear rate increase, that results in dilatancy. A mathematical model was postulated to describe this behavior. Experimental results gave strong evidence to the importance of the repulsive force and shear stress effect. The mathematical model has not been conclusive yet. Zeichner and Schowalter (1977) carried out a similar study of the interparticles forces in a shear flow on the stability of colloidal systems.

2.2 Hydrodynamic Effect

When the particle size is above those of colloidal size only hydrodynamic force effects exist. Michele et al. (1977) observed that rigid spheres, as well as air bubbles of 60 to 70 μm diameter suspended in visoelastic polymer solutions subjected to laminar shear flow, aligned themselves to form finite chains. They reported also that when two spheres come into contact in such shear flows, no rotation was observed. Riddle et al. (1977) observed pairs of identical rigid spheres (of diameter 0.3 to 0.6 cm) falling along their line of centers in viscoelastic fluids and found that for initial sparations less than a critical value, the spheres come in contact. All observations indicate the formation of chains of particles in suspensions of both Newtonian and viscoelastic fluids. The study of hydrodynamic effects on these systems started investigating the effect of the interaction between two particles.

A theoretical analysis of O'Neill (1969b) studied the slow viscous flow caused by the motion of two equal spheres almost in contact. The spheres were perpendicular to their line of centers. Two cases were considered: one of a translation with uniform equal velocities and the other is of rotation with equal and opposite angular velocities. The drag force for each sphere was obtained for the first problem and the value of each was less than that of a single sphere in the same fluid. The method of solution involved the use of the contacting spheres coordinates. The solution of the creeping flow equation was obtained in terms of several Hankel transforms expressed in terms of these coordinates. In the second problem a singular purturbation expansion around the limit of zero separation between the spheres was carried out. In the same year Cooley and O'Neill (1969a) were able to solve the problem of two arbitrary contacting spheres translating slowly in a viscous incompressible fluid. This problem is the same problem we are going to solve in a viscoelastic fluid. These workers expressed the axisymmetric stream function in the same coordinates of O'Neill, mentioned earlier, as a Hankel transform too. The drag force exerted by the Newtonian fluid on either sphere is less than the drag on a single sphere, over a range of ratios of sphere diameter. The same problem was solved later for simple shear flow by Simon and Goren (1971) and Nir and Acrivos (1972).

In a viscoelastic medium, which is the main concern of this work, the study of the hydrodynamic effect on interacting particles has just started. Brunn (1977b) found that equal spherical particles in contact in a second order fluid would yield no correction to Stokes' drag if the solution was considered at order We. For the case where the particles are separated from each other in such a way that the distance between the spheres divided by the spheres radius is much greater than one, the spheres seem to converge and they orient themselves along their center line. No data exist on the effect of changing size ratio for contacting particles in these fluid. The experimental work that was carried by Riddle et al. (1977) had been for fluids which possess considered shear thinning behavior and so they could not be compared to theories which assume constant shear viscosity as the second order fluid model does.

2.3 Bulk Stress

The previous factors which influence particle interaction have been studied by a number of investigators in an attempt to determine an effective viscosity for concentrated suspensions of Newtonian medium. Adler (1978) used the cell model to get a concentration dependent effective viscosity. The defect of the model is its dependence on the shape of the cell. Frankel and Acrivos (1967) used the classical hydrodynamic lubrication theory to study the same systems by calculating dissipated energy in the gap between the spherical particles. Both the cell model and the lubrication method suffers from neglecting particle interaction in the analysis.

Polymeric suspensions have been investigated experimentally by Highgate and Whorlew (1970). Three different viscoelastic systems of various types of rigid spherical particles have been studied. The size of the particle is 100 μm in diameter and at concentration of 10% by volume or less. The relative viscosity, defined by ratio of viscosity of suspension to viscosity of suspending fluid, was measured along with the first normal stress difference. This had been done for several solid concentrations within the above range. The results showed that comparing suspension properties to the suspending medium at the same shear stress was a function of concentration only; whereas if the comparison is made at the same shear rate both concentration and shear rate dependence was noticed. The same observations were reported by Kataoka et al. (1978). Until recently, no theoretical explanation was available.

Sun and Jayaraman (1982) have derived the bulk stress for suspensions of neutrally buoyant spherical particles in a second order fluid medium. They showed that the bulk viscosity of the suspension has a shear thinning factor which is directly related to the elasticity of the medium. Their expressions are borne out by the data of Highgate and Whorlow for systems of concentration up to 7%. These results suggest that if an understanding of systems of higher concentrations (moderate) is to be achieved, a basic understanding of the role of elasticity in the motion of doublets must be pursued. Thus we exclude colloidal systems and dispersion forces from any future consideration within the scope of this work.

2.4 Objective of Present Research

Understanding the behavior of aggregates in flowing polymer liquids is still in a very early stage. This in part is due to the fact that most theoretical analysis has been centered around single particle; while most practical systems are composed of doublets and chains. It is hoped that studying the effect of medium elasticity on the drag experienced by two rigid, contacting spheres in uniform translation would add some light to the subject of filled polymer systems.

2.5 Statement of the Problem

Two rigid spheres in contact, one of radius a and another of radius ka with their line of centers along the z-axis in a cylindrical polar coordinates as shown in Figure 2.1 were considered. The pair translates along the z-axis with a constant velocity U in an incompressible viscoelastic fluid at negligible particle Reynolds numer, Re $\sim$ a $U\rho_f/\mu_o$ where ρ_f = fluid density and μ_0 = zero shear rate viscosity of the fluid. If the fluid relaxation time is small (but finite) compared to the time scale of motion $\frac{U}{a}$, the fluid motion will be "rheologically slow" so that the second order stress constitutive equation may be used:

$$\underline{\underline{\sigma}} = -P\underline{\underline{\delta}} + 2\mu\,[\underline{\underline{D}} - \frac{\nu_1 \mathscr{D}\underline{\underline{D}}}{2\,\mathscr{D}t} + (\nu_1 + 2\nu_2)(\underline{\underline{D}} \cdot \underline{\underline{D}})] \tag{2.1}$$

where

$\underline{\underline{\delta}}$ = is a unit tensor

$\underline{\underline{D}}$ = rate of deformation gradient tensor given by

$$\underline{\underline{D}} = \frac{1}{2}\,(\nabla\underline{v} + \nabla\underline{v}^{\dagger}) \tag{2.2}$$

$\mu\,\nu_1$ and $\mu\nu_2$ $\equiv$ are the primary and secondary normal stress coefficient. $\mathscr{D}\,/\,\mathscr{D}t$ $\equiv$ denotes the corotational derivative given by

$$\frac{\mathscr{D}\underline{\underline{D}}}{\mathscr{D}t} = \frac{\partial\underline{\underline{D}}}{\partial t} + \{\underline{\underline{D}} \cdot \nabla\underline{\underline{D}}\} + \frac{1}{2}\,(\underline{\underline{\omega}} \cdot \underline{\underline{D}}\} - \{\underline{\underline{D}} \cdot \underline{\underline{\omega}}\}) \tag{2.3}$$

This model will allow us to isolate the elastic effect on the translation of these contacting spheres, since it has a non-shear dependent

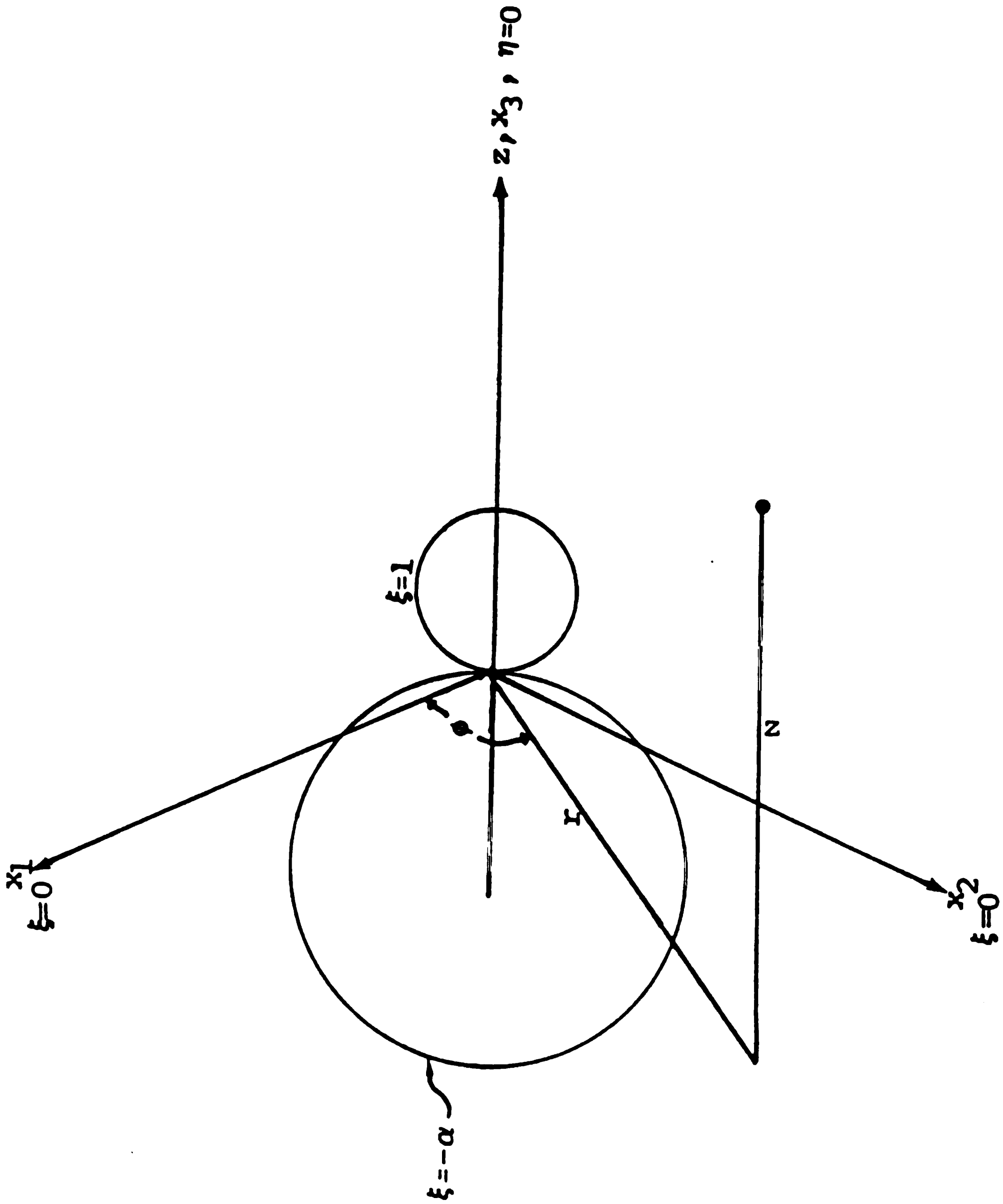

Figure 2.1.--Schematic diagram of spheres and coordinates.

viscosity μ. Thus in the next chapter we will derive an expression for the drag force on the surface of the spheres due to the elasticity of the medium.

CHAPTER III

DRAG CALCULATION FOR TWO TOUCHING SPHERES

The drag on two touching spheres of arbitrary sizes translating in a second order fluid is evaluated in this chapter. First, the governing equation of motion and the solution procedure are laid down. Next, a volume integral is developed for the elastic effect with the integrand in the most useful form. This volume integral is then evaluated by a sequence of numerical steps. The errors occurring in each numerical step are discussed.

3.1 Equation of Motion

The axisymmetrical fluid motion described by the problem statement of Section 2.3 may be represented by the equations:

$$\nabla \cdot \underline{\underline{\sigma}} = 0, \ \nabla \cdot \underline{v} = 0 \tag{3.1}$$

where $\underline{\underline{\sigma}}$ is the second order stress constitutive equation given earlier by equation (2.1) as:

$$\underline{\underline{\sigma}} = -p\underline{\underline{\delta}} + 2\mu[\underline{\underline{D}} - \frac{\nu_1 \mathscr{D}\underline{\underline{D}}}{2\,\mathscr{D}t} + (\nu_1 + 2\nu_2)(\underline{\underline{D}} \cdot \underline{\underline{D}})] \tag{3.2}$$

The boundary conditions require that

$$\begin{aligned} \underline{v} &= U\underline{e}_z \quad \text{on either sphere} \\ \underline{v} &= \underline{0} \quad \text{far from the spheres} \end{aligned} \tag{3.3}$$

Since only uniform translation is considered, in Equation (3.2) the term containing $\frac{\mathscr{D}\underline{\underline{D}}}{\mathscr{D}t}$ given by equation (2.3) and the term containing $\underline{\underline{D}} \cdot \underline{\underline{D}}$ are significant for this analysis. Thus a modified Weissenberg number, We is defined as:

$$We = (\nu_1 + 2\nu_2) \frac{U}{a} \tag{3.4}$$

while the conventional Weissenberg number is, $\bar{We} = \nu_1 U/a$. For small values of We (Re << We << 1), which is the case in the problem considered here, the velocity field $\underline{v}$ and the hydrodynamic force on the two spheres $\underline{F}$ may be expressed as a regular perturbation expansion in powers of We.

$$\underline{v} = \underline{v}_0 + We\,\underline{v}_1 + We^2\,\underline{v}_2 + \ldots$$

$$\underline{F} = \underline{F}_0 + We\,\underline{F}_1 + We^2\,\underline{F}_2 + \ldots \tag{3.5}$$

where $\underline{v}_0$, $\underline{F}_0$ denote solutions for a Newtonian fluid, with the same boundary conditions,using only the first two terms of Equation (3.2) and $\underline{v}_1$, $\underline{F}_1$ the correction obtained with the other two terms of Equation (3.2). No attempt is going to be made to evaluate $\underline{v}_1$, since it is possible to solve for $\underline{F}_1$ without it as shown by Brunn (1980). This is done by applying the reciprocal theorem which was also used by Leal (1975). The background of this theorm, as well as its application to determine the elastic contribution $\underline{F}_1$ are presented below.

3.1.1 Reciprocal Theorem (Background)

The reciprocal theorem is a useful device with regard to problems involving the resistance of particles and pressure drops due to fluid moving with respect to particles in creeping flow. Many of the developments and uses of this theorem stem from the work of Lorentz (1906). The theorem can be stated as follows. Let there be a closed surface which is bounding a volume of fluid where we know the velocity and stress fields for a certain steady, incompressible creeping flow in a certain geometry; the theorem says that the force and torque on any surface witin that volume for a different fluid and a different creeping flow but the same geometry may be obtained without solving for the velocity and stress fields in the latter situation. The details of this statement can be best explained by showing its use for a specific case as presented below.

We assume that we know the solution to an incompressible Newtonian fluid in creeping flow for a certain geometry with the equation of motion and continuity.

$$\nabla \cdot \hat{\underline{\underline{\Pi}}}_0 = 0 \quad \text{and} \quad \underline{\nabla} \cdot \hat{\underline{v}}_0 = 0 \tag{3.6}$$

where

$$\hat{\underline{\underline{\Pi}}}_0 = - \hat{P}_0 \underline{\underline{\delta}} + 2\mu(\nabla \hat{\underline{v}}_0 + \nabla \hat{\underline{v}}_0^{+}) \tag{3.7}$$

Next we consider an incompressible viscoelastic fluid within the same geometry as the first fluid and also in creeping flow situation, the relevant equations are

$$\nabla \cdot \underline{\underline{\Pi}} = 0 \quad \text{and} \quad \nabla \cdot \underline{v} = 0 \tag{3.8}$$

where

$$\underline{\underline{\Pi}} = - p_o \underline{\underline{\delta}} + 2\mu(\nabla \underline{v}_o + \nabla \underline{v}_o^+) - \bar{P}_1 \underline{\underline{\delta}}$$

$$+ 2\mu \left[\underline{\underline{D}} - \frac{\nu_1}{2} \frac{\mathscr{D}\underline{\underline{D}}}{\mathscr{D}t} + (\nu_1 + 2\nu_2)\, \underline{\underline{D}} \cdot \underline{\underline{D}} \right] \tag{3.9}$$

is the stress tensor of the second order fluid model. Furthermore, let us say that we are interested in getting the contribution at the first perturbation in We for the second fluid such as the force on any surface within the total volume that is enclosing the fluid. Equation (3.8) may be rewritten with O(We) terms as

$$\nabla \cdot (\underline{\underline{\Pi}}_0 + We\bar{\underline{\underline{\Pi}}}_1 + We\bar{\underline{\underline{\Sigma}}}_1) = 0$$

$$\nabla \cdot (\underline{v}_0 + We\underline{v}_1) = 0 \tag{3.10}$$

where

$$\bar{\underline{\underline{\Pi}}}_1 = - \bar{p}_1 \underline{\underline{\delta}} + 2\mu(\nabla \underline{v}_1 + \nabla \underline{v}_1^+)$$

$$\underline{\underline{\Pi}}_0 = - p_o \underline{\underline{\delta}} + 2\mu(\nabla \underline{v}_o + \nabla \underline{v}_o^+)$$

$$\bar{\underline{\underline{\Sigma}}}_1 = 2\mu \left[- \frac{\nu_1}{2} \frac{\mathscr{D}\underline{\underline{D}}_o}{\mathscr{D}t} + (\nu_1 + 2\nu_2)\, \underline{\underline{D}}_o \cdot \underline{\underline{D}}_o \right]$$

$$\underline{\underline{D}}_o = \frac{1}{2}(\nabla \underline{v}_o + \nabla \underline{v}_o^+) \tag{3.11}$$

Giesekus (1963) has shown that the divergence of the term

$$- \frac{\nu_1}{2} \frac{\mathscr{D}\underline{\underline{D}}_o}{\mathscr{D}t}$$

may be rewritten as the gradient of a scalar function

$$- \mu\nu_1\nabla \cdot \frac{\mathscr{D}\underline{\underline{D}}_o}{\mathscr{D}t} \equiv \frac{-\mu\nu_1}{2} \nabla P_1^1 \tag{3.12}$$

where

$$P_1^1 = \underline{v}_o \cdot \nabla P_o + \mu (\underline{\underline{D}}_o : \underline{\underline{D}}_o).$$

Now we define

$$P_1 = \bar{P}_1 + \frac{\mu\nu_1}{2} P_1^1 \tag{3.13}$$

Notice that P_1 is isotropic. Thus, according to Equation (3.10), we may write

$$\nabla \cdot \underline{v}_1 = 0$$

$$\nabla \cdot \underline{\underline{\Pi}}_1 = - \nabla \cdot \underline{\underline{\Sigma}}_1 \tag{3.14}$$

where

$$\underline{\underline{\Pi}}_1 = - P_1 \underline{\underline{\delta}} + 2\mu (\nabla\underline{v}_1 + \nabla\underline{v}_1^+)$$

$$\underline{\underline{\Sigma}}_1 = 2\mu(\nu_1 + 2\nu_2) \underline{\underline{D}}_o \cdot \underline{\underline{D}}_o \tag{3.15}$$

The nonhomogeneous term in the stress equation now involve only the quadratic combination $\underline{\underline{D}}_0 \cdot \underline{\underline{D}}_0$. The reciprocal theorem may be written for the fields $(\hat{v}_0, \hat{\underline{\underline{\Pi}}}_0)$ and $(\underline{v}_1, \underline{\underline{\Pi}}_1)$ from the given equations of motion as

$$\int_{V_f} \left[\left[\nabla \cdot (\underline{\underline{\Pi}}_1 + \underline{\underline{\Sigma}}_1) \right] \cdot \hat{\underline{v}}_0 - \left[\nabla \cdot \hat{\underline{\underline{\Pi}}}_0 \right] \cdot \underline{v}_1 \right] dV = 0 \tag{3.16}$$

where V_f is the volume of fluid considered. Substituting the tensor identities

$$[\nabla \cdot (\underline{\underline{\Pi}}_1 + \underline{\underline{\Sigma}}_1)] \cdot \hat{\underline{v}}_0 = \nabla \cdot [(\underline{\underline{\Pi}}_1 + \underline{\underline{\Sigma}}_1) \cdot \hat{\underline{v}}_0] - (\underline{\underline{\Pi}}_1 + \underline{\underline{\Sigma}}_1) : \nabla \hat{\underline{v}}_0$$

$$[\nabla \cdot \hat{\underline{\underline{\Pi}}}_0] \cdot \underline{v}_1 = \nabla \cdot [\hat{\underline{\underline{\Pi}}}_0 \cdot \underline{v}_1] - \hat{\underline{\underline{\Pi}}}_0 : \nabla \underline{v}_1 \tag{3.17}$$

$$\int_{V_f} \nabla \cdot [(\underline{\underline{\Pi}}_1 + \underline{\underline{\Sigma}}_1) \cdot \hat{\underline{v}}_0 - \hat{\underline{\underline{\Pi}}}_0 \cdot \underline{v}_1] \, dV$$

$$= \int_{V_f} \left[(\underline{\underline{\Pi}}_1 + \underline{\underline{\Sigma}}_1) : \nabla \hat{\underline{v}}_0 - \hat{\underline{\underline{\Pi}}}_0 : \nabla \underline{v}_1 \right] dV \tag{3.18}$$

Applying Gauss' divergence theorem to the left hand side, we obtain

$$\int_{S_o + S_\infty} \left[\underline{n} \cdot (\underline{\underline{\Pi}}_1 + \underline{\underline{\Sigma}}_1) \cdot \hat{\underline{v}}_o - \underline{n} \cdot \underline{\underline{\Pi}}_0 \cdot \underline{v}_1 \right] dS$$

$$= \int_{V_f} \left[\underline{\underline{\Pi}}_1 : \nabla\hat{\underline{v}}_0 - \hat{\underline{\underline{\Pi}}}_0 : \nabla\underline{v}_1 \right] dV + \int \underline{\underline{\Sigma}}_1 : \nabla\hat{\underline{v}}_o \, dV \tag{3.19}$$

Note here that the area integral is evaluated over the entire surface bounding the fluid. This comprises a fluid surface just about the particle, S_o, as well as a fluid surface S_∞ far from the particle. Also, the normal $\underline{n}$ is directed away from the fluid at the fluid-particle boundary. Furthermore, as shown in Appendix A

$$\int_{V_f} [\underline{\underline{\Pi}}_1 : \nabla\hat{\underline{v}}_o - \hat{\underline{\underline{\Pi}}}_0 : \nabla\underline{v}_1] \, dV = 0 \tag{3.20}$$

so that we may write

$$\int_{S_o + S_\infty} \left[\underline{n} \cdot (\underline{\underline{\Pi}}_1 + \underline{\underline{\Sigma}}_1) \cdot \hat{\underline{v}}_o - \underline{n} \cdot \hat{\underline{\underline{\Pi}}}_0 \cdot \underline{v}_1 \right] dS$$

$$= \int_{V_f} \underline{\underline{\Sigma}}_1 : \nabla \hat{\underline{v}}_o \, dV \tag{3.21}$$

Note here that the volume integral on the right hand side involves only velocity fields in a Newtonian fluid, $\underline{v}_o$ and $\hat{\underline{v}}_o$. In order to apply the reciprocal theorem in this form successfully, the complementary or known fields $(\hat{\underline{v}}_o, \hat{\underline{\underline{\Pi}}}_0)$ must be chosen to leave only one unknown on the left hand side, such as the o(We) contribution to force on the particle in the other problem.

3.1.2 Application of the Reciprocal Theorem

Pursuing the objective outlined in the last section, of leaving only one unknown on the left hand side of Equation (3.21), let us choose the complementary problem such that $\hat{\underline{v}}_o = 0$ far from the particle on S_∞ ; that is the fluid is quiescent far from the particle. Further, to obtain the z - component of the force contribution at o(We) on the particle, let us choose a uniform translation of the particle along the z - direction for the complementary problem, i.e.,

$$\hat{\underline{v}}_o = \hat{U}\underline{e}_z \quad \text{on} \quad S_p \text{ the particle surface} \tag{3.22}$$

The other problem of interest with unknown velocity and stress fields in a second order fluid is also one of a uniformly translating particle in a quiescent fluid since the velocity is specified on the particle surface

$$\underline{v} = U\underline{e}_z \quad \text{on } S_p \tag{3.23}$$

This is met by the zeroth order term $\underline{v}_o$ and

$$\underline{v}_1 = 0 \quad \text{on } S_p \tag{3.24}$$

Finally, the fluid here too is quiescent far from the particle

$$\underline{v}_1 = 0 \quad \text{on } S_\infty \tag{3.25}$$

and we obtain from Equation (3.21)

$$- \hat{U}\, F_{1z} = \int_{V_f} \underline{\underline{\Sigma}}_1 : \nabla \underline{\hat{v}}_o \, dV \tag{3.26}$$

where F_{1z} is the z- component of the O(We) contribution to force on the particle surface. If we choose, $\hat{U} = U$, we obtain

$$F_{1z} = - \frac{2\mu}{U} (\nu_1 + 2\nu_2) \int_{V_f} (\underline{\underline{D}}_o \cdot \underline{\underline{D}}_o) : \nabla \underline{v}_o \, dV \tag{3.27}$$

or

$$F_{1z} = \frac{-2\mu}{U} (\nu_1 + 2\nu_2) \int_{V_f} (\underline{\underline{D}}_o \cdot \underline{\underline{D}}_o) : \underline{\underline{D}}_o \, dV \tag{3.28}$$

Working with nondimensional quantities on the right hand side (length scale a, velocity scale U) $\underline{\hat{v}}_o$ the same as $\underline{v}_o$ here,

$$F_{1z} = -2\mu(\nu_1 + 2\nu_2)\, U^2 \int_{V_f^*} (\underline{\underline{D}}_o^* \cdot \underline{\underline{D}}_o^*) : \underline{\underline{D}}_o^* \, dV^* \tag{3.29}$$

or

$$F_{1z} = -2(\mu Ua)We \int_{V_f^*} (\underline{\underline{D}}_o^* \cdot \underline{\underline{D}}_o^*) : \underline{\underline{D}}_o^* \, dV^* \tag{3.30}$$

with nondimensional quantities denoted by an asterisk.

This relation given by equation (3.30) is a direct consequence of the result of the reciprocal theorem as given by equation (3.21). It is seen that we could avoid evaluating $\underline{v}_1$ since $\underline{F}_1$ at order one in Weissenberg number is associated with terms involving $\underline{v}_o$. At this point we would like to stress that all the work in the remaining part of this chapter is centered around evaluating this volume integral as given by equation (3.30).

3.2. Use of the Newtonian Solution

The dimensionless, axisymmetric velocity field, $\underline{v}_o^*$ needed for determining the volume integral of Equation (3.30) may be obtained from a stream function ψ in cylindrical coordinates as

$$\underline{v}_o^* = (v_r^*, o, v_z^*); \; v_r^* = \frac{1}{r^*}\frac{d\psi}{dz^*} \; ; \; v_z^* = \frac{-1}{r^*}\frac{d\psi}{dr^*} \tag{3.31}$$

Several investigators have solved for this stream function in various coordinates. Cooley and O'Neill (1969a) approached this problem using tangent sphere coordinates (mentioned briefly in Chapter I) which are related to cylindrical coordinate by the relations

$$Z^* = \frac{2\,\xi}{\xi^2 + \eta^2}\;;\; r^* = \frac{2\eta}{\xi^2 + \eta^2},\; \phi = \phi$$

or

$$\eta + i\xi = \frac{2i}{(z^* + ir^*)} \qquad i = \sqrt{-1} \tag{3.32}$$

Figure 3.1 is a schematic diagram of the spheres and the coordinates. In terms of these coordinates, the surfaces of the two spheres are given by $\xi = 1$ and $\xi = -\alpha \equiv -1/k$. The region occupied by the fluid is given by $-\alpha < \xi < 1$ and $0 < \eta < \infty$. The point of contact of the two spheres is given by $\eta = \infty$; and the region far away from the spheres by $\xi = \eta = 0$.

Cooley and O'Neill showed that the equation of motion for creeping flow of an incompressible Newtonian fluid about the pairs of spheres may be written in terms of the axisymmetric stream function as

$$\Lambda^4 \psi = 0 \tag{3.33}$$

where the operator Λ^4 is defined in tangent sphere coordinates by

$$\Lambda^2 \left[(\xi^2 + \eta^2)^{-\frac{1}{2}}\, \mathscr{F}(\xi, \eta)\right]$$

$$= \frac{1}{4}\,(\xi^2 + \eta^2)^{3/2} \left[\frac{\partial^2 \mathscr{F}}{\partial \xi^2} - \frac{2}{\eta}\frac{\partial \mathscr{F}}{\partial \eta} + \frac{\partial^2 \mathscr{F}}{\partial \eta^2}\right] \tag{3.34}$$

where $\mathscr{F}(\xi,\eta)$ is any twice differentiable function. The solution to Equation (3.33) was then obtained by them as Hankel transform involving

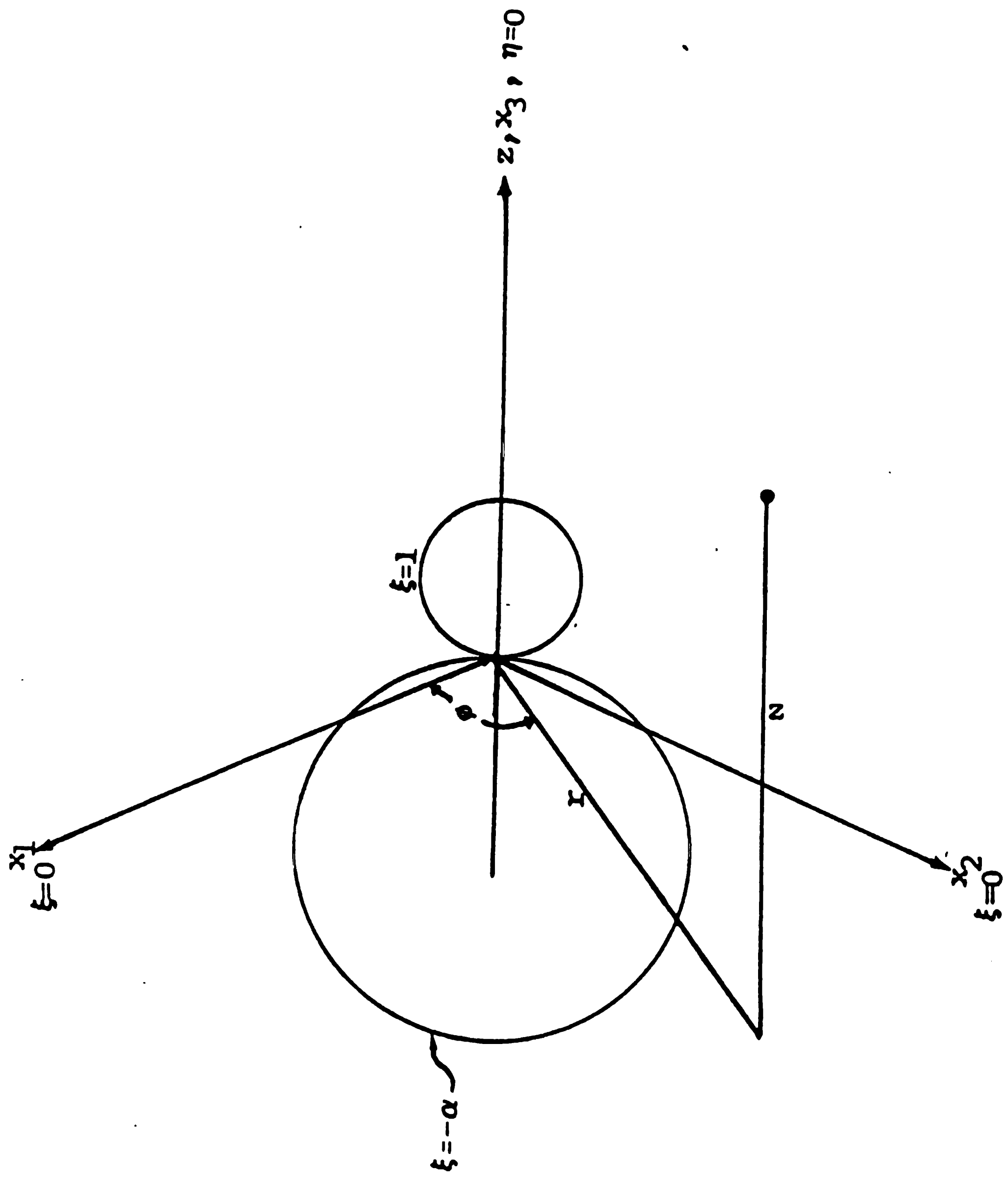

Figure 3.1. Schematic diagram of the spheres and coordinates.

J_1, a Bessel function of first kind and order 1.

$$\psi = \frac{\eta}{(\xi^2 + \eta^2)^{3/2}} \int_0^\infty \{(A + \xi C) \sinh s\xi + (B + \xi D) \cosh s\xi\} J_1(s\eta)\, ds \qquad (3.35)$$

where A, B, C, D are functions of s found from the no-slip boundary conditions on the moving sphere surfaces, $\xi = (\xi_1 = 1,\ \xi_2 = -\alpha)$ which can be written as

$$\psi - -2\eta^2(\xi^2 + \eta^2)^{-2}$$

$$\text{at } (\xi = \xi_1,\ \xi_2)$$

$$\frac{\partial\psi}{\partial\xi} = 8\xi\eta^2(\xi^2 + \eta^2)^{-3} \qquad (3.36)$$

These equations, along with Equation (3.35) yield (as shown in detail by Cooley and O'Neill (1969a) a set of four linear equations in the unknowns A, B, C, and D for arbitrary size spheres.

$$A \sinh s\xi_1 + B \cosh s\xi_1 + \xi_1 C \sinh s\xi_1 + \xi_1 D \cosh s\xi_1 =$$

$$-2e^{-s|\xi_1|}(|\xi_1| + s^{-1})$$

$$A \sinh s\xi_2 + B \cosh s\xi_2 + C\xi_2 \sinh s\xi_2 + \xi_2 D \cosh s\xi_2 =$$

$$-2e^{-S|\xi_2|}(|\xi_2| + s^{-1})$$

$$A \cosh s\xi_1 + B \sinh s\xi_1 + C(s^{-1} \sinh s\xi_1 + \xi_1 \cosh s\xi_1) +$$

$$D(s^{-1} \cosh s\xi_1 + \xi_1 \sinh s\xi_1) = 2\xi_1 e^{-s|\xi_1|}$$

$$A \cosh s\xi_2 + B \sinh s\xi_2 + C(s^{-1} \sinh s\xi_2 + \xi_2 \cosh s\xi_2)$$

$$D(s^{-1} \cosh s\xi_2 + \xi_2 \sinh s\xi_2) = 2\xi_2\, e^{-s|\xi_2|} \tag{3.37}$$

Solution of these equations for the unknowns A, B, C and D furnishes the solution to the stream function ψ. The force $\underline{F}_0$ on the pair of spheres has been shown by Cooley and O'Neill (1969a) to be given by

$$\underline{F}_0 = 2\pi\mu a \underline{e}_z \int_0^\infty sBds \tag{3.38}$$

It is to be noted that this is obtained by adding the forces on the individual spheres given in Equation (4.3) of their paper.

In order to evaluate the elastic contribution to drag, the integrand of Equation (3.30), must be expressed in terms of the contacting sphere coordinates. This is because the Newtonian solution of which use is going to be made of here, is given in these coordinates, and the volume of fluid around the spheres is most easily expressed in these coordinates. The procedure involved performing the tensorial operation $\underline{\underline{D}}_0^* \cdot \underline{\underline{D}}_0^* : \underline{\underline{D}}_0^*$ in terms of cylindrical coordinates, followed by coordinates transformation with the aid of Equation (3.32)

$$\underline{\underline{D}}_o^* = \begin{bmatrix} \dfrac{\partial v_r^*}{\partial r^*} & 0 & \dfrac{1}{2}\left(\dfrac{\partial v_r^*}{\partial z^*} + \dfrac{\partial v_z^*}{\partial r^*}\right) \\ 0 & v_r^*/r^* & 0 \\ \dfrac{1}{2}\left(\dfrac{\partial v_r^*}{\partial z^*} + \dfrac{\partial v_z^*}{\partial r^*}\right) & 0 & \dfrac{\partial v_z^*}{\partial z^*} \end{bmatrix}$$

and the dot product $\underline{\underline{D}}_o^* \cdot \underline{\underline{D}}_o^*$ yield

$$\underline{\underline{D}}_o^* \cdot \underline{\underline{D}}_o^* = \begin{bmatrix} \left(\dfrac{\partial v_r^*}{\partial r^*}\right)^2 + 1/4\left(\dfrac{\partial v_r^*}{\partial z^*} + \dfrac{\partial v_z^*}{\partial r^*}\right)^2 & 0 & -\dfrac{v_r^*}{2r^*}\left(\dfrac{\partial v_r^*}{\partial z^*} + \dfrac{\partial v_z^*}{\partial r^*}\right) \\ 0 & \dfrac{v_r^*}{r^{*2}} & 0 \\ \dfrac{-v_r^*}{2r^*}\left(\dfrac{\partial v_r^*}{\partial z^*} + \dfrac{\partial v_z^*}{\partial r^*}\right) & 0 & \left(\dfrac{\partial v_z^*}{\partial z^*}\right)^2 + \dfrac{1}{4}\left(\dfrac{\partial v_r^*}{\partial z^*} + \dfrac{\partial v_z^*}{\partial r^*}\right)^2 \end{bmatrix} \quad . \qquad (3.39)$$

The above quantities yield for

$$\underline{\underline{D}}_o^* \cdot \underline{\underline{D}}_o^* : \underline{\underline{D}}_o^* = - 3[\frac{v_r^{*2}}{r^{*3}} \frac{\partial v_z^*}{\partial z^*} + \frac{v_r^*}{r^*} (\frac{\partial v_z^*}{\partial z^*})^2 + \frac{v_r^*}{4r^*}$$

$$(\frac{\partial v_r^*}{\partial z^*} + \frac{\partial v_z^*}{\partial r^*})^2] \tag{3.40}$$

The velocity components in Equation (3.40) can be expressed in terms of the stream function using Equations (3.31) and some rearrangement to give.

$$\underline{\underline{D}}_o^* \cdot \underline{\underline{D}}_o^* : \underline{\underline{D}}_o^* = \frac{3}{r^{*4}}[- \frac{\partial\psi}{\partial z^*} (\frac{\partial^2\psi}{\partial z^* \partial r^*})^2 + \frac{1}{r^{*2}} (\frac{\partial\psi}{\partial z^*})^2 \frac{\partial^2\psi}{\partial z^* \partial r^*}$$

$$+ r^* \frac{\partial\psi}{\partial z^*} \frac{\partial^2\psi}{\partial z^{*2}} \frac{\partial}{\partial r^*} (- 1/r^* \frac{\partial\psi}{\partial r^*})] \tag{3.41}$$

At this point coordinate transformation is to be performed. To start with, the volume element of Equation (3.30) in tangent sphere coordinates can be written as:

$$dV^* = \frac{d\xi d\eta d\phi}{h_\xi h_\eta h_\phi} = \frac{8 d\xi d\eta d\phi}{(\eta^2 + \xi^2)^{5/2}} \tag{3.42}$$

where h_ξ, h_η, h_ϕ are scale factors which may be obtained with the procedure discussed by Happel and Brenner (1965). The transformation of Equation (3.41) into the contacting spheres coordinate system is a rather lengthy but straight forward process. It involves handling a large number of terms which resulted from repeated use of the chain rule as required for each expression in the above equation. To clarify the previous statement further, $\frac{\partial\psi}{\partial z^*}$ is going to be transformed below. With $\psi = \psi(\eta, \xi)$ given

$$\frac{\partial\psi}{\partial z^*} = \frac{\partial\psi}{\partial\xi}\ \frac{\partial\xi}{\partial z^*} + \frac{\partial\psi}{\partial\eta}\ \frac{\partial\eta}{\partial z^*} \tag{3.43}$$

The partial derivatives $\frac{\partial\xi}{\partial z^*}$, $\frac{\partial\eta}{\partial z^*}$ and others like $\frac{\partial\eta}{\partial r^*}$ and $\frac{\partial\xi}{\partial r^*}$ can be obtained from Equations (3.32) which yield,

$$\frac{\partial\eta}{\partial z^*} = -\ \xi\eta,\ \frac{\partial\xi}{\partial z^*} = \frac{\eta^2-\xi^2}{2}$$

$$\frac{\partial\eta}{\partial r^*} = -\ (\frac{\eta^2-\xi^2}{2}),\ \frac{\partial\xi}{\partial r^*} = -\ \xi\eta \tag{3.44}$$

With the aid of Equation (3.44) the individual terms in Equations (3.41) can be written in terms of the contacting coordinates as:

$$\partial_1\psi \equiv \frac{\partial\psi}{\partial z^*} = \frac{(\eta^2-\xi^2)}{2}\quad \frac{\partial\psi}{\partial\xi} - \eta\xi\ \frac{\partial\psi}{\partial\eta}$$

$$\partial_{11}\psi \equiv \frac{\partial^2\psi}{\partial z^{*2}} = \frac{(\eta^2-\xi^2)}{2}\quad \frac{\partial}{\partial\xi}\ (\partial_1\psi)\ -\ \eta\xi\ \frac{\partial}{\partial\eta}\ (\partial_1\psi)$$

$$\partial_{12}\psi \equiv \frac{\partial^2\psi}{\partial r^*\ \partial\ z^*} = -\xi\eta\ \ \frac{\partial}{\partial\xi}\ (\partial_1\psi) + \frac{\xi^2-\eta^2}{2}\ \frac{\partial}{\partial\eta}\ (\partial_1\psi)$$

$$\partial_2\psi \equiv \frac{1}{r^*}\ \ \frac{\partial\psi}{\partial r^*} = \frac{\eta^2+\xi^2}{2\eta}\ [-\xi\eta\ \ \frac{\partial\psi}{\partial\xi} + \frac{(\xi^2-\eta^2)}{2}\ \frac{\partial\psi}{\partial\eta}\ ]$$

$$\partial_{22}\psi \equiv r^* \frac{\partial}{\partial r^*} (\partial_2\psi) = \frac{2\eta}{\eta^2 + \xi^2} \left[-\xi\eta \frac{\partial}{\partial \xi} (\partial_2\psi) \right.$$

$$\left. + \frac{\xi^2 \eta^2}{2} \frac{\partial}{\partial \eta} (\partial_2\psi) \right] \tag{3.45}$$

Now we can express Equation (3.30) in terms of contacting spheres by utilizing the results of Equation (3.42) and (3.45) which yield

$$\frac{F_{1z}}{\mu a U} = -32\pi \int_{-\alpha}^{1} d\xi \int_{0}^{\infty} d\eta \quad Q(\xi,\eta) \tag{3.46}$$

where

$$Q(\xi,\eta) = \frac{(\eta^2 + \xi^2)^{3/2}}{\eta^4} [T_1(\psi) + T_2(\psi) + T_3(\psi)] \tag{3.47}$$

$$T_1(\psi) = \frac{-3}{16} (\partial_1\psi)(\partial_{12}\psi)^2$$

$$T_2(\psi) = \frac{0.75}{16} \frac{\eta^2 + \xi^2}{\eta^2} (\partial_1\psi)^2 (\partial_{12}\psi)$$

$$T_3(\psi) = \frac{3}{16} (\partial_1\psi)(\partial_{11}\psi)(\partial_{22}\psi) \tag{3.48}$$

The partial derivaties $\frac{\partial\psi}{\partial\xi}$, $\frac{\partial\psi}{\partial\eta}$ and higher order derivatives as needed in the individual terms of Equation (3.45) is obtained as follows from Equation (3.35).

Let us write $\psi = g_1 I_1$

where

$$g_1 = \eta/(\xi^2+\eta^2)^{3/2}$$

$$I_1 = \int_0^\infty f(s,\xi)\, J_1(s\eta)ds \tag{3.49}$$

Hence

$$\frac{\partial\psi}{\partial\eta} = \frac{\partial g_1}{\partial\eta} I_1 + g_1 \frac{\partial I_1}{\partial\eta}$$

$$\frac{\partial\psi}{\partial\xi} = \frac{\partial g_1}{\partial\xi}\ \frac{\partial I_1}{\partial\eta} + g_1 \frac{\partial I_1}{\partial\xi} \tag{3.50}$$

This procedure when followed for the rest of the partial derivatives, with respect to η and ξ, involved in Equation (3.48) yielded other Hankel transforms in addition to the ones in Equation (3.50). At this point it is convenient to define the variable $x = s\eta$ for the argument of the Bessel functions J_1 and J_o arising in these transformations. Later we will see that the quadrature is done over x in order to keep track of the oscillatory integrand. Here we list all the transforms which resulted from the above operations in terms of the variable x.

$$I_1 = \int_0^\infty f(x/\eta,\xi) J_1(x) \frac{dx}{\eta}$$

$$I_2 = \frac{\partial I_1}{\partial \eta} = \int_0^\infty f(x/\eta,\xi)(x \frac{dJ_1}{dx}) \frac{dx}{\eta^2}$$

$$I_3 = \frac{\partial^2 I_1}{\partial \eta^2} = \int_0^\infty f(x/\eta,\xi)(x^2 \frac{d^2 J_1}{dx^2}) \frac{dx}{\eta^3}$$

$$I_4 = \frac{\partial I_1}{\partial \xi} = \int_0^\infty \frac{\partial f}{\partial \xi} J_1(x) \frac{dx}{\eta}$$

$$I_5 = \frac{\partial I_2}{\partial \xi} = \int_0^\infty \frac{\partial f}{\partial \xi} (x \frac{dJ_1}{dx}) \frac{dx}{\eta^2}$$

$$I_6 = \frac{\partial^2 I_1}{\partial \xi^2} = \int_0^\infty \frac{\partial^2 f}{\partial \xi^2} J_1(x) \frac{dx}{\eta}$$

where $f = (A + \xi C) \sinh \frac{x\xi}{\eta} + (B + \xi D) \cosh \frac{x\xi}{\eta}$

$$x \frac{dJ_1}{dx} = x J_0 - J_1$$

and

$$x^2 \frac{d^2 J_1}{dx^2} = (2 - x^2) J_1 - x J_0 \qquad (3.51)$$

It is to be emphasized that I_1 through I_6 have to be obtained before any other numerical calculation can be carried out.

3.3 Results for Equal Spheres

For equal spheres, $\alpha = 1$ and the boundary conditions given by Equation (3.36) lead to nonzero values only for B and C in Equations (3.37) so the stream function ψ is an even function of ξ

$$\psi = \frac{\eta}{(\xi^2 + \eta^2)^{3/2}} \int_0^\infty \{\xi C \sinh s\xi + B \cosh s\xi\} J_1 (s\eta) ds$$

Furthermore, Cooley and O'Neill have noted the explicit expressions

$$B = -[2 + 2s + s^{-1}(1-e^{-2s})]/[s + \sinh s \cosh s]$$

$$C = [1 + 2s-e^{-2s}]/[s + \sinh s \cosh s] \qquad (3.52)$$

This feature is useful here in obtaining an analytical answer for the integral in Equation (3.46). A quick look at the individual terms of Equations (3.45) in terms of the even stream function would show that

$$\begin{aligned}
\partial_1\psi &= \text{even}\\
\partial_{11}\psi &= \text{odd}\\
\partial_{12}\psi &= \text{even}\\
\partial_{22}\psi &= \text{odd}
\end{aligned} \qquad (3.53)$$

and so it is readily seen from Equation (3.48) that for this case, $T_1(\psi)$, $T_2(\psi)$, $T_3(\psi)$--all turn out to be odd functions of ξ. Integration over ξ from -1 to +1 should yield zero. Hence, the drag exerted by a second order fluid on a pair of identical, touching spheres is the same up to O(We) as the drag exerted by a Newtonian fluid with the same viscosity. This result will be used later in the case of arbitrary spheres to check the numerical procedures developed to evaluate the integral in Equation (3.46). It is worth noting here that a pair of identical, touching spheres is a body of revolution with fore-after symmetry and thus belongs to the class of transveresly isotropic particles. For such particles Brunn (1977a) has shown that the O(We) contribution to the drag is zero.

3.4 Numerical Procedure for Evaluating the Drag on Unequal Spheres

In this section we are going to have three subsections. Section 3.4.1 is devoted to evaluating the function $f(s,\xi)$ for unequal spheres; Section 3.4.2 is the detailed evaluation of the Hankel transforms; and Section 3.4.3 to discussing the quadrature scheme over η and ξ. The importance of the first two subsections is because for uneuqal spheres ($\alpha \neq 1$), the functions A, B, C, and D of s (see Equation (3.37)) must be evaluated numerically; so the integral of Equation (3.46) has to be evaluated numerically; managing such an expression is no trivial matter. This is not because of the triple integration that had to be carried out, but rather because of the great need of very accurate numerical evaluations of the function $f(s,\xi)$ and subsequently the Hankel transforms.

3.4.1 Evaluation of $f(s,\xi)$ for Unequal Spheres

The function $f(s,\xi)$ is evaluated thousands of times in the product quadrature scheme used for the multiple integration of Equation (3.46). Hence, the accurate evaluation of A(s), B(s), C(s), and D(s) is at the heart of the lengthy sequence of the numerical steps in this work. These functions of s are obtained as the solution to the four linear equations (3.37). Detailed error estimates for different valuse of s and α may be obtained by writing (3.37) as

$$\underline{\underline{\mathscr{B}}}\,\underline{c} = \underline{d} \tag{3.54}$$

where

$$\underline{c}^T = [A(s), B(s), C(s), D(s)] \tag{3.55}$$

Defining the vector norm of $\underline{c}$ by

$$||\underline{c}||_\infty = \max_i |c_i| \tag{3.56}$$

and the matrix (row sum) norm of $\underline{\underline{\mathscr{B}}}$ by

$$||\underline{\underline{\mathscr{B}}}||_\infty = \max_j \left(\sum_i |\mathscr{B}_{ij}|\right) \tag{3.57}$$

we obtain an upper bound on the relative error $||\delta\underline{c}||/||\underline{c}||$ according to Goult et al. (1974),

$$||\delta \underline{c}||/||c|| \leq \bar{K}(7)(2^{n-1})2^{-\bar{t}} \tag{3.58}$$

where $\bar{K}$ is a condition number defined by

$$\bar{K} \equiv |\mathcal{B}|_{\infty} \; ||\mathcal{B}^{-1}||_{\infty} \tag{3.59}$$

n is the number of Equations (4) and t, the number of bits in the mantissa of a single precision floating point number is 48 on the cyber 750 at Michigan State University. So for a relative error of 10^{-5} say, $\bar{K}$ may be as large as 5×10^{7}. Table 3.1 shows the condition numbers of the matrix $\underline{\underline{\mathcal{B}}}$ for different values of s at several values of α between .05 and 5. It is to be noticed that the values of $\bar{K}$ show a marked increase at both very low and large values of s. Furthermore,

TABLE 3.1.--Condition numbers $\bar{K}$ of $\underline{\underline{\mathcal{B}}}$ at different values of α and s.

	s				
α	0.1	1.0	6.0	10.0	20.0
0.05	$0.1217\text{x}10^{6}$	$0.9038\text{x}10^{2}$	$0.4732\text{x}10^{4}$	$0.3226\text{x}10^{6}$	$0.805\ \text{x}10^{10}$
0.1	$0.1062\text{x}10^{6}$	$0.8075\text{x}10^{2}$	$0.3650\text{x}10^{4}$	$0.2042\text{x}10^{6}$	$0.3096\text{x}10^{10}$
0.2	$0.8221\text{x}10^{5}$	$0.6596\text{x}10^{2}$	$0.2164\text{x}10^{4}$	$0.8139\text{x}10^{5}$	$0.4554\text{x}10^{9}$
0.5	$0.4281\text{x}10^{5}$	$0.4184\text{x}10^{2}$	$0.4469\text{x}10^{3}$	$0.5004\text{x}10^{4}$	$0.1400\text{x}10^{7}$
1	$0.1864\text{x}10^{4}$	$0.2822\text{x}10^{2}$	$0.5633\text{x}10^{2}$	$0.882\ \text{x}10^{2}$	$0.1681\text{x}10^{3}$
5	$0.1073\text{x}10^{4}$	$0.1813\text{x}10^{4}$	$0.3501\text{x}10^{13}$	$0.4992\text{x}10^{20}$	$9.2283\text{x}10^{38}$

the actual magnitude of A, B, C, and D are also larger with decreasing α at large values of s as can be seen in Table 3.2. For

TABLE 3.2.--Change in A, B, C, and D with decreasing α

	s=10 α=.5	s=10 α=.2
A	5.538×10^{-4}	4.762×10^{-2}
B	-5.540×10^{-4}	-4.762×10^{-2}
C	9.989×10^{-4}	0.1832
D	-9.987×10^{-4}	-0.1832

both the small values and large values of s, Cooley and O'Neill (1969a) have asymptotic estimates for A, B, C, and D.

$$A = \frac{-2(\alpha-1)(\alpha^2 + 4\alpha + 1)}{(\alpha + 1)^3 s} \qquad \text{for } s \leq 0.1 \qquad (3.60)$$

$$B = -\frac{2}{s}$$

and for large s.

$$A,\ B,\ C, \text{ and } D \text{ all are } O(se^{-2\beta s}) \qquad (3.61)$$

where $\beta = \min\{1, \alpha\}$

Thus in our evaluation of the function $f(s,\xi)$ to overcome the error in evaluating A, B, C, and D at both small $s \leq .1$ and large $s \geq 10$ we do the following. First at small s the expressions of Equations

(3.60) are used and the function $f(s,\xi)$ at this range of $s \leq .1$ will be referred to as f_0 from now on. On the other hand for large s we obtain with Equation (3.61) for A, B, C, D, the following asymptotic expression for $f(s,\xi)$

$$f \sim se^{-s(\alpha - \xi)} (b_2 + b_3\xi) \tag{3.62}$$

where b_2 and b_3 are functions of α. A plot of $f(s,\xi)$ versus s shows a monotonic decay for the function above s = 7.5 as seen in Figure 3.2. It was seen possible to fit $f(s,\xi)$ with a single exponential function

$$f_1 = b_1 e^{-a_1 s} \tag{3.63}$$

where b_1, a_1 are obtained from fitting $f(s,\xi)$ keeping α,ξ fixed. More will be said about the fitting procedure in the next section. For convenience, the form of Equation (3.63) is used for values of $s \geq 10$. Thus for $s \geq 10$ the function $f(s,\xi)$ is referred to as f_1.

Another look at Table 3.1 would show that the relative error in most cases is less than 10^{-7}; but for $\alpha = 5$ the error at larger values of s becomes enormous. This large error is typical for α greater than 1. However, of all possible values for α, it is enough to consider the range of $0 < \alpha < 1$, because the results for the remaining values may be found by reversing the sign of the right-hand side of Equation (3.37).

The last point that we would like to stress is the magnitude of error in calculating $f(s,\xi)$ as α is decreased. In Table 3.2 we

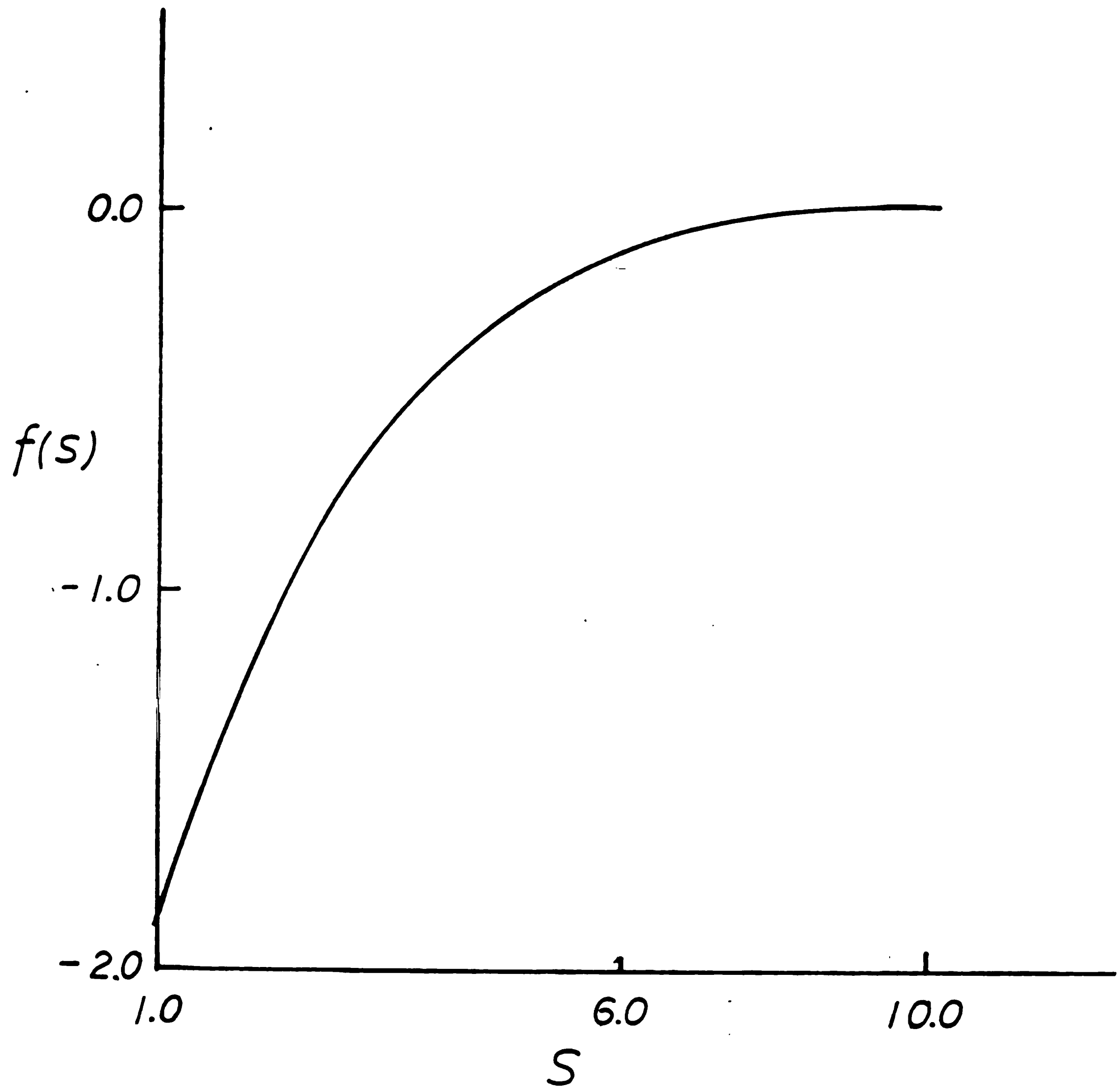

Figure 3.2. Monotonic decay of $f(s,\xi)$ vs s at α = .5, ξ = 0.25

have shown that the values of A, B, C, and D increase in magnitude as α is lowered from .5 to .2 at S = 10. This increase in magnitude has also caused the value of $f(s,\xi)$ to increase markedly for this change in α at s = 10. Thus, the accuracy of evaluating $f(s,\xi)$ is decreased for values of α less than 0.5. The behavior of $f(s,\xi)$ as α is decreased is given in Table 3.3. It is to be noticed that the values of $f(s,\xi)$ increase by one order of magnitude as α is decreased from .5 to .2 at large values of s above s = 1. Finally in Table 3.4 we present the absolute error $|\Delta f|$ in calculating $f(s,\xi)$. $|\Delta f|$ is obtained by finding the error in A, B, C, and D, and multiplying by $f(s,\xi)$. The table shows us the change in the magnitude of the absolute error as α is decreased. It is seen that as α is decreased, the absolute error is higher in two particular situations. The first is that for all values of ξ as α is decreased, the error is largest at s = 10. The second situation is seen to be associated with two distinct regions on the surface of the contacting spheres. These are at the stagnation point on the larger sphere at $\xi = -\alpha$ and in the region far away from the spheres at $\xi = 0$.

These absolute errors would accumulate each time the function $f(s, \xi)$ is evaluated with the numerical scheme. In that scheme the function $f(s,\xi)$ is evaluated 27,000 times on the average. Multiplying this number by Δf would give an upper bound on the total error involved in evaluating $f(s, \xi)$. Using the maximum value of $|\Delta f|$ over s and ξ, we obtain an upper bound of 10^{-4} on total error due to function evaluation at $\alpha = 0.2$.

TABLE 3.3.--Behavior of $f(s,\xi)$ with decreasing α

S	α=.5 ξ=-.5	α = .5 ξ=0.0	α=.5 ξ=1.0
	$f(s,\xi)$	$f(s,\xi)$	$f(s,\xi)$
1	-1.8196	-1.9108	-1.471
6	-0.066383	-0.020822	- .00578
10	-0.008086	-0.000554	- .00009988
	α=.2 ξ=-.2	α=.2 ξ=0.0	α=.2 ξ=1.0
1	-1.965	-1.9881	-1.462
6	- .22088	- .18998	- .00578
10	- .0812	- .047621	- .00009988

TABLE 3.4.--Absolute error in $f(s,\xi)$ as α is decreased

S	α=.5 ξ=-.5	α=.5 ξ=0.0	α=.5 ξ=1.0
	$\|\Delta f\|$	$\|\Delta f\|$	$\|\Delta f\|$
1	1.5×10^{-11}	1.6×10^{-11}	1.21×10^{-11}
6	5.9×10^{-12}	1.85×10^{-12}	5.13×10^{-13}
10	8.1×10^{-12}	5.55×10^{-13}	1.0×10^{-13}
	α =.2 ξ=-.2	α=.2 ξ=0.0	α=.2 ξ=1.0
1	2.5×10^{-11}	2.63×10^{-11}	1.95×10^{-11}
6	9.5×10^{-11}	8.17×10^{-11}	2.5×10^{-12}
10	1.3×10^{-9}	7.62×10^{-10}	1.59×10^{-12}

3.4.2 Evaluation of Hankel Transforms

There are several problems to be addressed as we proceed in describing the procedure of evaluating the Hankel transforms $I_1 \ldots I_6$ given in Equation (3.51). For convenience, only one Hankel transform is going to be used to describe the method of solution. The others are evaluated in a similar fashion. Also, we will use the variable $x = s\eta$ which is the argument of the Bessel function. In particular, we choose the transform

$$I_1 = \frac{1}{\eta}\int_0^{\infty} f(x/\eta,\xi)J_1(x)dx \tag{3.64}$$

As we discussed in Section 3.4.1 that asymptotic expressions f_o and f_1 will be used over a range of small s and a range of large s values repsectively.

Hence

$$\int_0^{\infty} f(x/\eta,\xi)J_1(x)dx = \int_0^{x_\ell} f_o J_1(x)dx + \int_{x_\ell}^{x_u} fJ_1(x)dx + \int_{x_u}^{\infty} f_1 J_1(x)dx \tag{3.65}$$

We note that in Equation (3.65) $x = s\eta$ and as we mentioned earlier it is more convenient for the behavior of the Bessel functions to use x rather than $s\eta$. This is primarily to keep track of the number of cycles over the limits of integration and to provide enough quadrature points in each cycle. The quadrature points which we are referring to here are those of a Gauss Chebyshev quadrature scheme which is used for the numerical integration as will be discussed shortly. In Equation (3.65) $x_\ell = .1\eta$; however, x_ℓ should be less than or equal to 0.3 so that the power series representation of the Bessel function (to be discussed below) is valid. Thus, $x_\ell = \min\,[.1\eta, .3]$; and $X_u = 10\eta$ as established earlier in Section 3.4.1. In the subsequent paragraphs each of those integrals on the right hand side of Equation (3.65) is going to be discussed separately.

In the first integral on the right hand side of Equation (3.65)

$$\int_0^{x_\ell} f_o\, J_1(x)dx \tag{3.66}$$

f_o has been defined in Section 3.4.1 and because of the unbounded functions A(s), B(s) as $s \to 0$ (see Equation (3.60)), for $J_1(x)$, we considered the first few terms of a power series representation of the Bessel function

$$J_1(x) \simeq \frac{x}{2} - \frac{x^3}{16} \qquad x \leq 0.3$$

When this is done, the integrand of Equation (3.66) is no more unbounded and can be written as:

$$i_1 = f_o J_1(x) = (T\eta/2)\sinh(\frac{x\xi}{\eta}) - (\frac{Tx^2\eta}{16})\sinh(\frac{x\xi}{\eta})$$
$$- \eta\cosh(\frac{x\xi}{\eta}) + (\frac{x^2\eta}{8})\cosh(\frac{x\xi}{\eta}) \tag{3.67}$$

where $\quad T = \dfrac{-2\ (\alpha-1)(\alpha^2 + 4\alpha + 1)}{(\alpha + 1)^3}$ (3.68)

The integration of Equation (3.66) was carried out numerically using Gauss-Chebyshev quadrature scheme. The integrands for the rest of the Hankel transforms $I_2 \ldots I_6$ for this limit $0 \rightarrow x_\ell$ were obtained by a similar procedure and are listed below.

$$i2 = (1 - \frac{3x^2}{\eta^2})((T/2)\sinh(\frac{x\xi}{\eta}) - \cosh(\frac{x\xi}{\eta}))$$

$$i3 = \frac{1}{\eta}(\frac{-3x^2}{4\ \eta^2})((T/2)\sinh(x\xi/\eta) - \cosh(\frac{x\xi}{\eta}))$$

$$i4 = (T\cosh(x\xi/\eta) + 2\sinh(\frac{x\xi}{\eta}))\ J_1(x)$$

$$i5 = \frac{1}{\eta}(T\ \cosh(\frac{x\xi}{\eta}) - 2\ \sinh(\frac{x\xi}{\eta}))(\frac{x}{\eta}\ J_0(x) - J_1(x))$$

$$i6 = (\frac{Tx}{\eta}\ \sinh(\frac{x\xi}{\eta})\ - 2\frac{x}{\eta}\ \cosh(\frac{x\xi}{\eta}))J_1(x) \tag{3.69}$$

The second integral on the right hand side of Equation (3.65) over the range x_ℓ to x_u was obtained with the Gauss Chebyshev quadrature scheme. Here the function f is the actual function as given with the original Hankel transform in Equation (3.51). A(s), B(s), C(s), and D(s) are evaluated by the Gauss-elimination routine from Equation (3.37), and no truncation is used for the Bessel function. The number of quadrature points supplied was based on determining the number of cycles for that range of integration, and at least three points per cycle were supplied.

Finally the third integral on the right hand side of Equation (3.65) is to be discussed. In Section 3.4.1 we mentioned that the errors in evaluating A(s) -- D(s) is also large at large s. We also mentioned that

$$f_1 = b_1 e^{-a_1 s} \tag{3.70}$$

This form has been obtained by observing the behavior of $f(s,\xi)$ at large values of s. Figure 3.3 shows this behavior where a monotonic decay is observed after about $s = \frac{x}{\eta} = 7.5$. It should be mentioned that for the other Hankel transforms $I_2 \ . \ . \ . \ I_6$, their function of s are born by derivatives of $f(s,\xi)$ with respect to ξ as can be seen in Equation (3.51). The behavior of these functions at large s is shown in Figures 3.4 and 3.5 where a similar monotonic decay is observed at about the same value of $s = \frac{x}{\eta} = 7.5$. Thus, fitting each of $f(s,\xi)$, $\frac{\partial f(s,\xi)}{\partial \xi}$ and $\frac{\partial^2(s,\xi)}{\partial \xi}$ by an exponential near s = 10 would prevent the error in evaluating A(s)--B(s) at larger value of s. In f_1, b_1 and a_1 are determined by the fitting procedure of $f, \frac{\partial f}{\partial \xi}, \frac{\partial^2 f}{\partial \xi^2}$ for each set of α and ξ separately. For each α, several values of ξ between $-\alpha$ and 1 were picked and a range of s values (between 7 and 12), that was seen to yield a uniform decay, was chosen.

Even though we have been able to overcome the problem of evaluating those functions of s at large s by the exponential fit, we have noticed that for α less than 0.33 there was a considerable difference between the values of the functions $f(s,\xi)$, $\frac{\partial f(s,\xi)}{\partial \xi}$, $\frac{d^2 f(s,\xi)}{\partial \xi^2}$ and their exponential fit f_1, f_1', f_1''. The difference is larger and more significant between $\frac{\partial f(s,\xi)}{\partial \xi}$, $\frac{\partial^2 f(s,\xi)}{\partial \xi^2}$ and f_1', f_1''. For example, when $\alpha = 0.2$, the fitting error associated with $\frac{\partial f}{\partial \xi}$ is of order 10^{-4} and the error associated with $\frac{\partial^2 f}{\partial \xi^2}$ is of order 10^{-2}, while the error with f is of order 10^{-6}. However, in the case of $\alpha = 0.5$, the fitting errors are much smaller. Thus, once more we see that this range of α values would have one additional error to that discussed in Section 3.4.1 in evaluating the function because of the fitting procedure. It should be stressed that this error especially in fitting $\frac{\partial f(s,\xi)}{\partial \xi}$ and $\frac{\partial^2 f(s,\xi)}{d\partial^2 \xi}$ is going to be large as we repeat their evaluation in the numerical scheme for these α values less than 0.33.

The Hankel transforms of a decaying exponential is available as

$$\int_0^\infty e^{-a_1 s} J_1(s\eta)ds = \frac{\sqrt{a_1^2 + \eta^2} - a_1}{\eta\sqrt{a_1^2 + \eta^2}} \tag{3.71}$$

Hence, we may write the last integral of Equation (3.65) as

$$\int_{x_u}^\infty f_1 J_1 (x)dx = HT_1 - \int_0^{x_u=10\eta} f_1 J_1(x)dx$$

$$= b_1 \frac{\sqrt{a_1^2 + \eta^2} - a_1}{\eta\sqrt{a_1^2 + \eta^2}} - \int_0^{x_u=10\eta} b_1 \frac{e^{-a_1 x}}{\eta} J_1(x)dx \tag{3.72}$$

And the expressions for the remaining Hankel transforms in the limit $0 \to \infty$ are

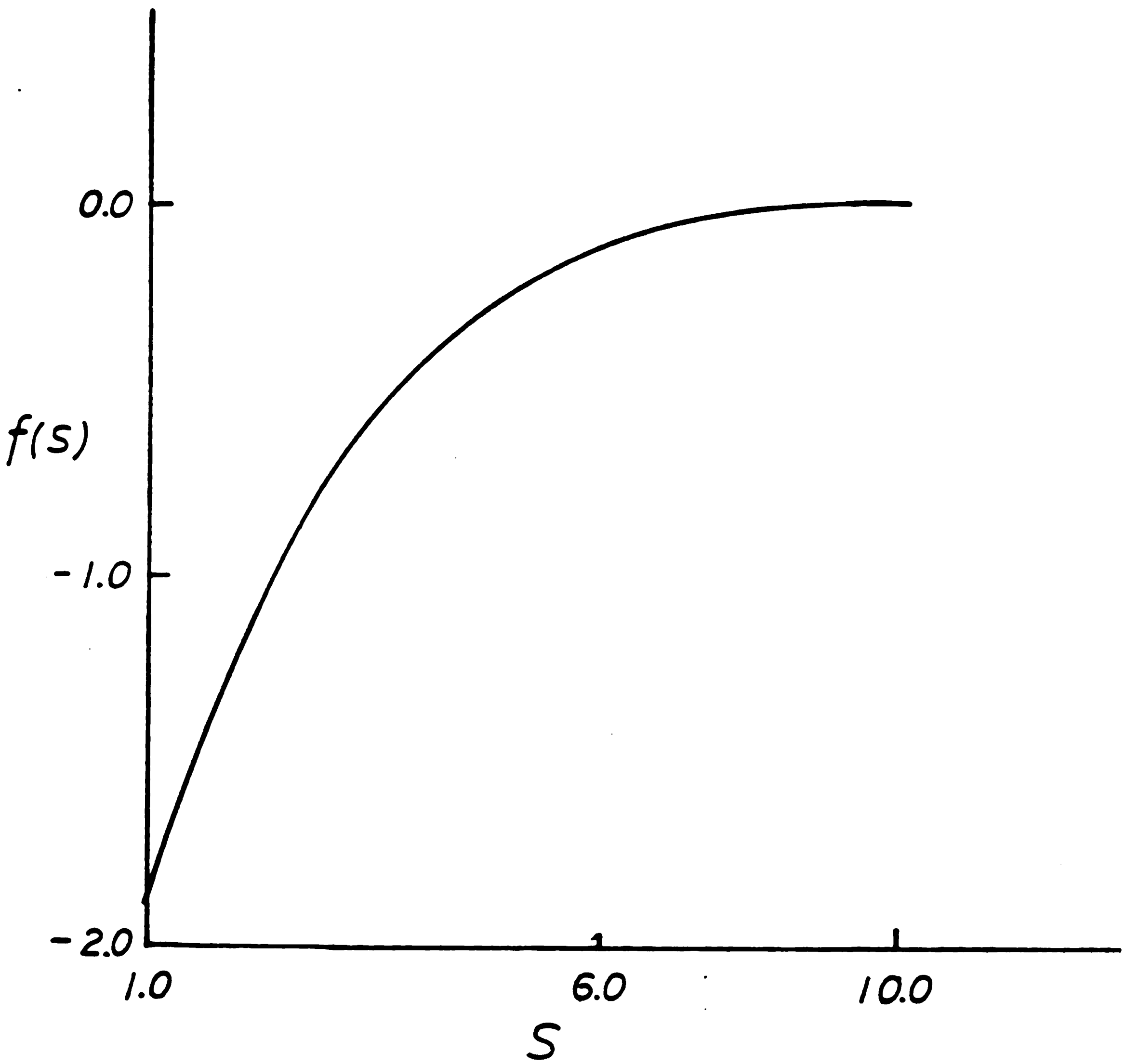

Figure 3.3. Monotonic decay of $f(s,\xi)$ vs. s for $\alpha = 0.5$, $\xi = 0.25$.

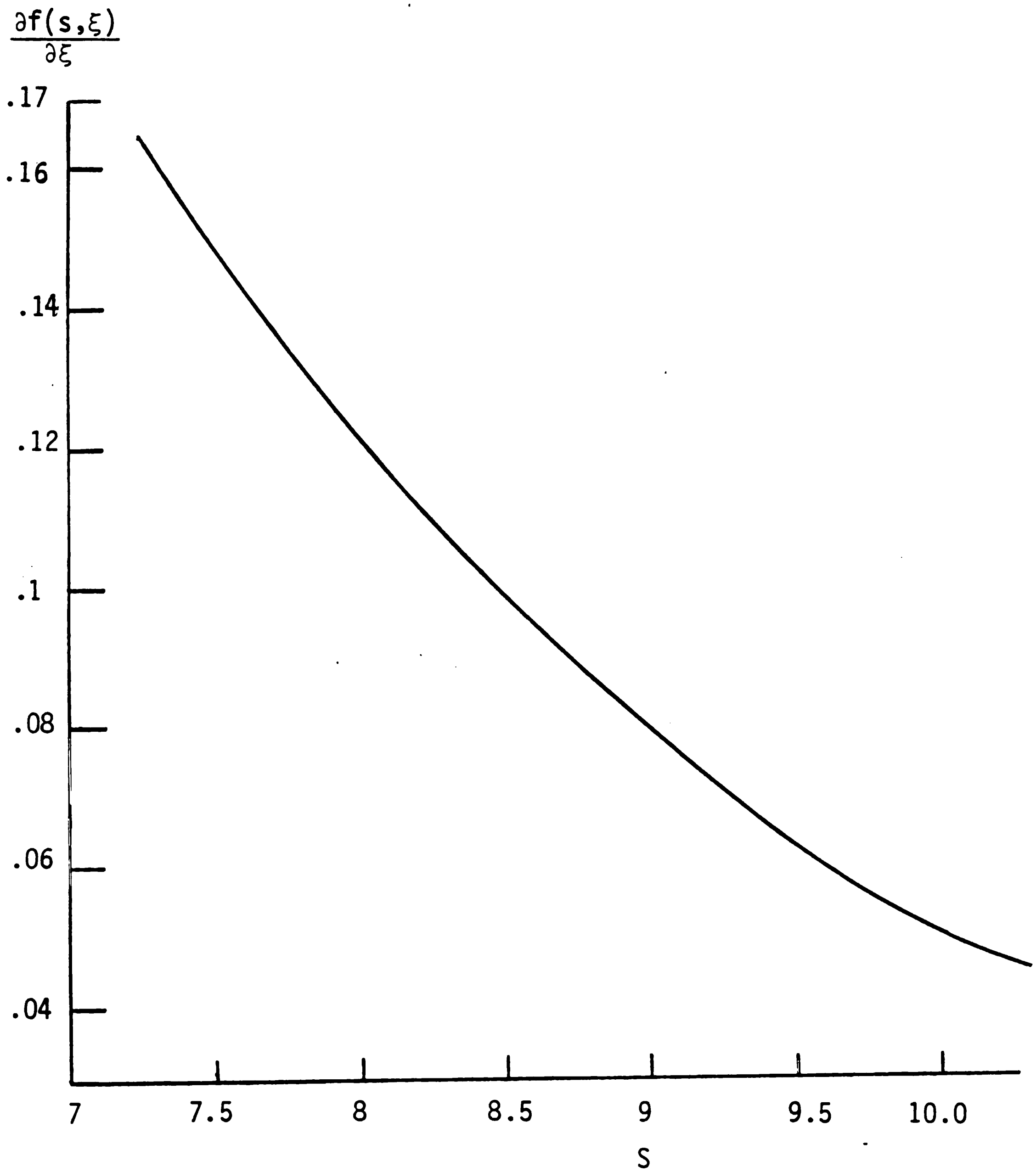

Figure 3.4. Monotonic decay of $\frac{\partial f(s,\xi)}{\partial \xi}$ vs. s for $\alpha = 0.5$, $\xi = 0.25$.

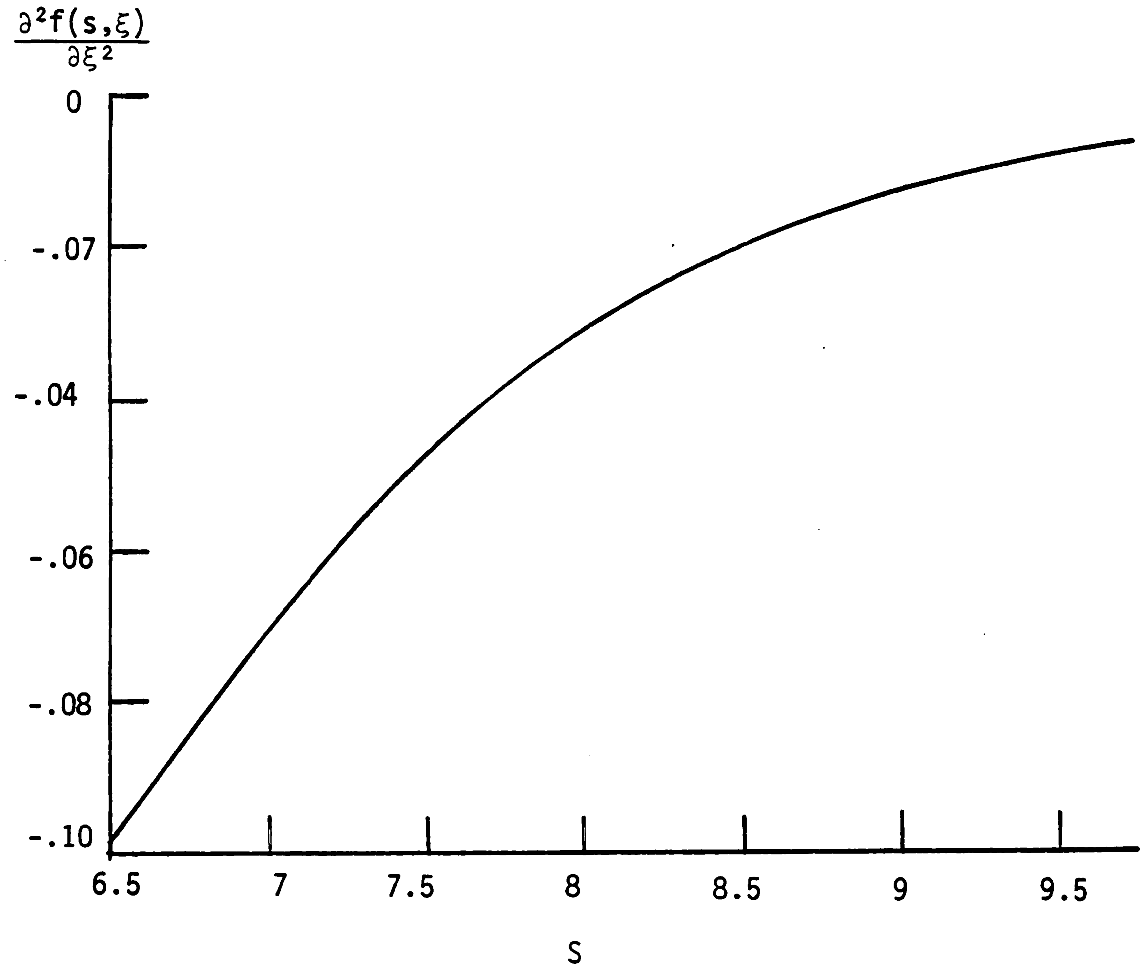

Figure 3.5.--Monotonic decay of $\frac{\partial^2 f}{\partial \xi^2}$ vs s for α = .5, ξ= 0.25.

$$HT2 = \frac{\partial HT1}{\partial \eta} = b_1 \left(\frac{a_1^3 + 2a_1\eta^2 - (a_1^2 + \eta^2)^{3/2}}{\eta^2(a_1^2 + \eta^3)^{3/2}} \right) \tag{3.73}$$

$$HT3 = \frac{\partial^2 HT1}{\partial \eta^2} = b_1 \left(\frac{2}{\eta^3} \left(1 - \frac{a_1}{\sqrt{\eta^2 + a_1^2}}\right) - \frac{a_1}{\eta(\eta^2 + a_1^2)^{3/2}} \right.$$

$$\left. - \frac{3a_1\eta}{(\eta^2 + a_1^2)^{5/2}} \right) \tag{3.74}$$

It is to be noticed that HT4 and HT6 are given by expression similar to that for HT1 in Equation (3.72), but with different coefficients. Their coefficients are a_4, b_4, and a_6, b_6 respectively and obtained from fitting $\frac{\partial f}{\partial \xi}$ and $\frac{\partial^2 f}{\partial \xi^2}$. HT5 is similar to HT2 with a_5 and b_5 obtained from fitting $\frac{\partial f}{\partial \xi}$. The indices associated with HT's are for the purpose of identifying the specific Hankel transform $I_1 \ldots I_6$ in Equation (3.51). The other integral on the right hand side of Equation (3.72) is

$$\int_0^{x_u = 10\eta} b_1 \, e^{-a_1 x/\eta} \, J_1(x)dx \tag{3.75}$$

This integral was obtained numerically using the same quadrature scheme.

Now that we have discussed the individual integrals and explained the motivation behind that procedure, we rewrite Equation (3.65)

$$I_1 = \int_0^\infty f(x/\eta,\xi(J_1(x)dx$$

$$= \int_0^{x_\ell = .1\eta \text{ or } .3} [T\eta(\frac{1}{2} - \frac{x^2}{16})\sinh(\frac{x\xi}{\eta}) + \eta(\frac{x^2}{8} - 1)\cosh(\frac{x\xi}{\eta})]dx$$

$$+ \int_{x_\ell = .1\eta \text{ or } .3}^{x_u = 10\eta} f(x/\eta,\xi)J_1(x)dx$$

$$+ b\,(\frac{\sqrt{a_1^2 + \eta^2} - a_1}{\eta\sqrt{a_1^2 + \eta^2}}) - \int_0^{x_u = 10\eta} b_1 e^{-a_1\frac{x}{\eta}} J_1(x)dx \qquad (3.76)$$

This form is the one that was used in the numerical evaluation. An additional check on the numerical values of these Hankel transforms is available from the work of Soni and Soni (1973) on asymptotic estimates at large η. These estimates are discussed in the next section.

3.4.3 Quadrature Scheme over η and ξ

It was mentioned earlier that in terms of the contacting spheres coordinates employed here, the region at which $\eta = \infty$ is the point of contact of the spheres and the region of $\eta = \xi = 0$ is the region far from the spheres. The contribution to the elastic effect at the contact point was investigated through the use of asymptotic estimates of the six Hankel transforms given in Equation (3.51) as $\eta \to \infty$ and by writing the integral over η as follows.

$$\int_0^\infty Q(\eta,\xi,I_1\ .\ .\ .I_6)d\eta = \int_0^{10} Q(\eta,\xi,\ I_1\ .\ .\ .I_6)\ d\eta$$

$$+ \int_{10}^\infty Q(\eta,\xi,\text{ asymptotic estimates of I's})\ d\eta \qquad (3.77)$$

where the asymptotic estimates of the Hankel transforms were obtained by a theorem of Soni and Soni (1973). Soni and Soni have related the behavior of a function of s that is unbounded at $s \to 0$ of the form $s^{-\gamma}g(s)$ where $\gamma > 0$ and $0 < \gamma < m + 3/2$ with the limit of its Hankel transform at $\eta \to \infty$.

$$\lim_{\eta\to\infty} \int_0^\infty \sqrt{s\eta}\ J_m(s\eta)\ s^{-\gamma}g(s)ds$$

$$= -2^{-\gamma+\frac{1}{2}} \frac{\Gamma\ (m/2 - \gamma/4 + 3/4)}{\Gamma\ (m/2 - \gamma/4 + 1/4)}\ \eta^{\gamma}\ \ g(0^+) \qquad (3.78)$$

where the function g(s) is bounded over the entire range of s. It is to be noticed that in Equation (3.78) $s^{\frac{1}{2}-\gamma}\ g(s)$ is equal to the specific function of s in the various Hankel transforms. Further the form of equation (3.67) has $\eta^{\frac{1}{2}}$ which is not present in our definition of the Hankel transforms, so we have to multiply the results of Equation (3.73) by $\eta^{-\frac{1}{2}}$. The coefficient γ is chosen in such a way as to make $f(s,\xi)$ bounded at $s = 0$, m is the order of Bessel function. Application of Equation (3.78) to the six Hankel transforms showed that as $\eta \to \infty$ the following estimates are obtained:

$$I_1 = -2$$
$$I_2 = 0$$
$$I_3 = 0$$
$$I_4 = 0$$
$$I_5 = 0$$
$$I_6 = 0 \qquad (3.79)$$

In the last integral of Equation (3.77) when infinity was replaced by 15 or 20 and using the results of Equation (3.79) along with other functions of ξ and η yielded values of the order of 10^{-5} which were practically zero. This result had established two things. First, the point of contact of the spheres yield no contribution to whatever result we get for the elastic effect on the drag. Second the value of $\eta = 10$ is a reasonable upper limt for η.

On the other hand, at low η the value of the integrand is large, particularly at $\xi \leq 0$. It is useful to note here that the range of low η with ξ near 0 describes the region far away from the spheres while the range of low η with ξ near $-\alpha$ describes the stagnation points region about the larger sphere. More will be said in Section 3.6 about the contributions from different regions to the elastic effect on the drag.

3.5 Contribution from Different Regions

We proceed to look at the integrand $Q(\xi,\eta)$ of the double integral over η and ξ in Equation (3.46). This integrand involves large sequence of algebric expressions. It is useful to look at the behavior of $Q(\xi,\eta)$ in different regions of fluid around the spheres. In Section 3.4.3 we have already shown that the region near the equatorial section of the spheres and in particular the point of contact has no contribution to the drag. This region is that of $\eta \to$ infinity. On the other hand, in the regions of low values of η and nonzero values of ξ we observed a different behavior. The numerical values of the integrand $Q(\xi,\eta)$ for $\alpha = .2$ are listed in Table 3.5. The values of η and ξ are those at which the integrand started to have an appreciable magnitude. Let us first look at low values of η, with ξ approaching zero, which represent the region far away from spheres as can be seen from

$$z^* = \frac{2\xi}{\eta^2 + \xi^2} , \quad r^* = \frac{2\eta}{\xi^2 + \eta^2}$$

The values of $Q(\xi,\eta)$ are significant in this region as shown in Table 3.5 Next we looked at the region near $\xi \simeq -\alpha$ and at low η which describe the stagnation points on the surface of the rear sphere. It was seen that this region contribute the most to the elastic effect on the drag. The range of low η values over which the integrand $Q(\xi,\eta)$ takes on appreciable magnitude is larger around the larger sphere ($\xi < 0$) than around the small sphere ($\xi > 0$).

The large contribution from the stagnation point region is understandable in the light of previous work. Of particular importance to us is the work of Leal (1975) where he treated the

Table 3.5.--Integrand after integrating over x (α=.2, k=5)

ξ	η	$Q(\xi,\eta)$
0.79	0.007	0.29
0.713	0.007	0.29
0.63	0.007	0.26
0.54	0.007	0.23
0.447	0.007	-0.21
0.087	0.007	0.42
0.01	0.062	-0.60
0.01	0.007	-950.7
-0.056	0.062	253.8
-0.056	0.007	-2.08
-0.112	0.332	-1.01
-0.112	0.17	5.74
-0.112	0.062	165.8
-0.112	0.007	2.71
-0.154	0.17	18.38
-0.154	0.062	93.83
-0.154	0.007	-641.3
-0.183	0.062	64.74
-0.183	0.007	-1.31
-0.198	0.062	1.56
-0.198	0.007	0.21

case of a long, slender rod-like cone without fore-aft symmetry. In that work, the drag force due to the elasticity of the medium was represented by two integrals. The first is a surface integral which is evaluated at the surface of the particle using asymptotic expression for the integrand. These expressions are not valid for the region close to the ends of the particle. Further in the volume integral it was seen that the region of fluid close to the particle is dominant; and because of the slender body approximation the stagnation points at both ends of the particles where omitted. However, the fact that we have an appreciable contribution even near $\xi = 0$ (i.e., far from the spheres) is at variance with the result of Leal. It is to be mentioned that the shape of our particles is different from Leal's and this may explain this variance in the results for this region.

We would like to conclude this section by presenting an estimate of the error associated with the integration over ξ and η. It was just seen that the region of small η and $\xi < 0$ has the largest contribution to the drag on the spheres surfaces. Thus, when we evaluated the numerical value of the integral of Equation (3.46) for equal spheres ($\alpha = 1$) where a high degree of accuracy was available in the Hankel transforms evaluation, we obtained a final answer of 0.12. This value was obtained by integrating over ξ from -1 to 0 and over η from 0 to 1 which are the regions of major contribution to the drag. The integration from $-\alpha$ to 0 over ξ and 1 to 10 over η has a value of 10^{-4} which is practically zero. Before we can say anything about the value 0.12 for the integral of equal spheres, we further investigated the effect of changing the number of quadrature points over the range $-\alpha$ to 0 over ξ and 0 to 1 over η for several α values. As can be seen in Table 3.6 that the effect of increasing

TABLE 3.6.--Effect of increasing number of quadrature points on integral shown

α	30 points each $\int_{-\alpha}^{0} d\xi \int_{0}^{1} d\eta$	50 Points each $\int_{-\alpha}^{0} d\xi \int_{0}^{1} d\eta$
0.33	0.98	0.95
0.50	0.48	0.46
0.67	0.28	0.27

the number from 30 to 50 has an effect on the second decimal point of the integral value. The other integral $-\alpha$ to 0 over ξ and 1 to 10 over η is also very small 0 (10^{-4}). Thus, we conclude that even with this increase in the number of quadrature points, the first decimal point is unchanged. We also know that in the integration over ξ and η the integrand does not involve α. Thus, we say that since for equal spheres the result of Equation (3.46) should be zero, therefore, the value of 0.12 is error due to the quadrature over ξ and η. This magnitude is also associated with other values of α's $\neq 1$ which we will present their final results in the next section.

3.6 Results for Unequal Spheres

Before we present the results of the drag correction factor $F_{1z}/6\pi\mu Ua$ due to the elastic medium for unequal spheres ($\alpha \neq 1$), we would like to recall attention to Sections 3.4.1 and 3.4.2. In Section 3.4.1 we aimed at establishing confidence in the numerical evaluation of the function $f(s,\xi)$ of the Hankel transform. We have seen that as α is decreased from 0.5 to 0.2 the absolute error $|\Delta f|$ increased by an order of magnitude. Furthermore, we showed that as we repeat the evaluation of $f(s,\xi)$ the error adds up to reach an upper bound of 10^{-4} for $\alpha = .2$. In Section 3.5.2 we discussed the error involved in fitting $\frac{\partial f(s,\xi)}{\partial \xi}$ and $\frac{\partial^2 f(s,\xi)}{\partial \xi^2}$ at α less than 0.33 and said that the order of magnitude of the difference between these functions and the fitting function f_1 is large. We also mentioned that the difference will add up as we repeat evaluating these functions. Thus, in light of these points, it was decided that values of $\alpha \geq .33$ where the upper bound of the total error in evaluating all the functions of s and also the difference between the functions and their fitting values is of order 10^{-8} to 10^{-4}, is an acceptable degree of accuracy. In Table 3.7 we present the result for unequal spheres for $k = \frac{1}{\alpha}$ between 1.5 and 3 or α between .33 and .67. The table includes both $\frac{F_{1z}}{6\pi\mu Ua}$ and $\frac{F_{oz}}{6\pi\mu Ua}$ the corresponding Newtonian drag correction factor for those particle size ratios. These results show that there is an appreciable elastic effect on the drag at order one in Weissenberg number. Also, it is seen that this effect increases as k is increased.

TABLE 3.7.--Drag on pair of contacting spheres--elastic contributions

K	$-F_{oz}/6\pi\mu Ua$	$-F_{1z}/6\pi\mu Ua$
1	1.29	.64
1.5	1.66	1.23
2	2.09	1.89
3	3.04	3.42

Note: $F_z = F_{oz} + \text{We } F_{1z}$

Before we conclude this chapter we would like to recall that the problem treated here is that of two contacting spherical particles translating along their center line in the positive z-direction with the small sphere leading. We mentioned earlier in Section 3.5.1 that the case where the spheres translates in the negative z- direction with the larger sphere leading can be considered by changing the signs of the right hand sides of Equation (3.37). The sign of the quantity F_{1z} is not going to be affected by this sign change of Equation (3.37) since it is associated with the quadratic quantity $\underline{\underline{D}}_0 \cdot \underline{\underline{D}}_0$. For the case of spheres translating in the positive z direction F_{0z} acts in the negative z-direction; the net drag

$$F = F_{oz} + \text{We}F_{1z}$$

If we consider We = .1 and for $\alpha = 1.5$

$$F = -6\pi\mu Ua(1.66) - .6\pi\mu Ua(1.233)$$

which is greater than the Newtonian value. On the other hand, the case where the large sphere is leading in the negative z-direction, F_{oz} acts up in the positive z-direction. Thus

$$F = 6\pi\mu Ua(1.66) - .6\pi\mu Ua(1.233)$$

which is less than the Newtonian value. In Chapter IV we shall discuss the results of Table 3.7 in light of the experimental results.

CHAPTER IV

EXPERIMENTAL PROCEDURE AND RESULTS

4.1 Single Sphere Experiments

Sedimentation is a common method for measuring the drag coefficient of particles translating in a fluid. It is very accurate when care is exercised in both the design and procedure. Several investigators--Sutterby (1973), Sakai et al. (1977/78), Sigli and Coutanceau (1977), Chhabra et al. (1980), Broad and Mena (1974), and Acharya et al. (1976)--have performed such experiments using single-rigid spheres with both Newtonian and viscoelastic fluids. The only measurements needed are settling velocity, particle size, and density and the fluid density. In terms of isolating the effect of fluid elasticity on drag, Boger and coworkers (1980) have obtained the most accurate results using so-called Boger fluids. Most of these experiments were done at very low particle Reynolds numbers. The work of Sigli and Coutanceau (1977) has addressed inertial effects. It was concluded that inertial effects generally opposed the elastic effect. This means that as the Reynolds number is increased, the elastic effect is decreased. Creeping flow conditions are commonly observed since most of the theoretical work applies only to such flow conditions.

The purpose of the present work is to investigate the effect of elasticity on the drag experienced by rigid contacting spheres translating in a non-shear thinning fluid along their line of centers. This is to be performed over a range of Weissenberg number and at low Reynolds number. The remainder of this chapter will include apparatus design, material properties and preparation, experimental procedure, and finally, results.

4.2 Apparatus

4.2.1 Wall Effect Correction for Newtonian Fluids

A drop cylinder made of Plexiglass was designed for the experiment. In this design, the following factors have been taken into consideration, which are very critical from the standpoint of the degree of accuracy. In selecting the cylinder diameter, the wall effect is the major concern. For a single sphere in a Newtonian fluid, Faxen (1932) has made a theoretical analysis of the correction to Stokes law due to the presence of a boundary. The resulting expression for drag is

$$F = 6\pi\mu U a K \tag{4.1}$$

where

$$K = \frac{1}{1-2.104(d/D) + 2.09(d/D)^3 - .95(d/D)^5}$$

d/D is the ratio of sphere to tube diameters

The above expression was verified experimentally by Bacon (1936) for d/D up to 0.32. The linearity of the constitutive relation of Newtonian fluids enabled Brenner (1964) to derive expressions for the first order effect of wall proximity as a correction formula for the terminal velocity given as

$$\underset{=}{U} = \underset{=}{U}_{\infty} + \frac{\underset{=}{K} \cdot \underset{=}{F}}{6\pi\mu\ell} + O(C_0/\ell) \tag{4.2}$$

and a correction force formula obtained by a simple inversion of the above expression. In Equation (4.2), $\underset{=}{U}$ is the velocity of the particle when settling in an infinite medium, $\underset{=}{U}_{\infty}$ is the velocity when the particle is settling under the influence of an outside force $\underset{=}{F}$ at a distance from a boundary whose wall effect tensor is $\underset{=}{K}$ and C_0 is a characteristic particle dimension, usually the radius. The second order tensor $\underset{=}{K}$ was obtained by the method of reflection. Sutterby (1973) studied the wall and inertial effect experimentally over a range of d/D between 0.0025 to 0.125 for a range of Reynolds number between 0.00001 to 3.78. The falling sphere data were correlated as a relationship between $\mu_S/\mu \equiv K$, d/D and Re = $\rho Ud/\mu$. Here μ_s is the fluid viscosity obtained from Stokes law and μ is corrected fluid viscosity. The value of K for several values Re was given in a graphical form and reproduced here as Figure 4.1. Agreement with Faxen results is up to Re = 0.2; where beyond this value inertial effect is appreciable.

4.2.2 Wall Effect Correction for Viscoelastic Fluids

In the case of a viscoelastic material, the wall effect is not fully determined. Unlike the case of viscous flow, the nonlinearities of the fluid's constitutive relations for a viscoelastic

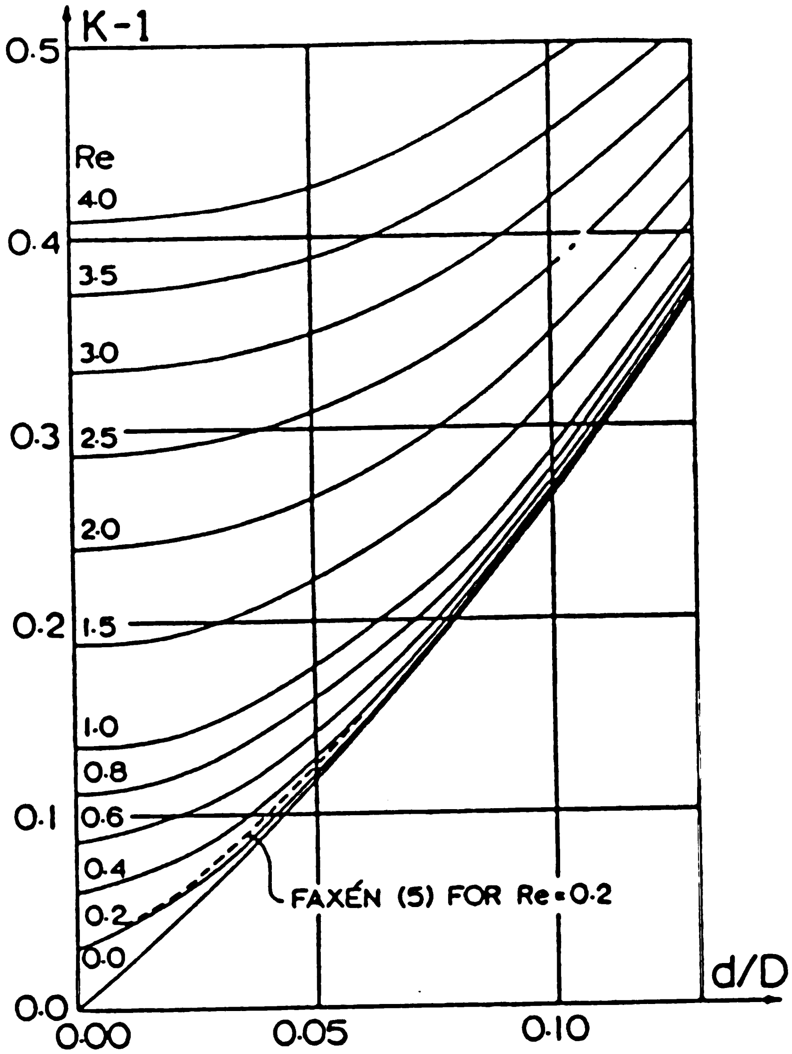

Figure 4.1. Wall correction factor vs. d/D of Sutterby (1973).

medium doesn't in general allow the wall effect to be expressed as a force correction formula. Only a velocity correction factor is possible. Caswell (1970) presented the expression for the first order effect of the wall proximity on particle settling as:

$$\underline{U} = \underline{U}_{\infty} + \underline{\underline{K}} \cdot \underline{F}/6\pi\mu_0 \ell + O(\ell^{-2}) \tag{4.3}$$

The only restriction on the constitutive equation for the validity of the above relation is that it must describe an isotropic fluid which has a lower Newtonian regime with zero shear viscosity. This general relation was examined for the case where the stress expression for the medium is represented by the third order fluid model. Translation induced by a force alone and rotation induced by torque alone was considered. The solution involved velocity perturbation expansions and Green's function method was utilized for obtaining the wall effect tensor $\underline{\underline{K}}$. The final expression for the unbounded velocity was expressed in terms of the zero shear viscosity for a sphere settling in a viscoelastic medium as:

$$\frac{6\pi a U_{\infty}}{-\underline{F}} = \frac{1}{\mu_0} - \frac{\lambda}{\mu_0^{\,3}} \left(\frac{\underline{F}}{6\pi a^2}\right)^2 + O\left(\frac{\underline{F}}{6\pi a^2}\right)^4 \tag{4.4}$$

where

λ is a combination of material constants given in Caswell (1970)

Various experiments were carried out to estimate the critical ratio of particle to tube diameter above which wall effect is significant. Sigli (1977) observed that for a ratio greater than 0.25 the wall proximity increased the effect of fluid elasticity. This effect is seen by a decrease in the particle velocity. Boger and coworkers (1980) had established experimental conditions for negligible wall effects. They investigated situations for d/D between 0.04 and 0.2. It was found that the terminal velocity decreased as the sphere to tube diameter ratio increased, but this reduction in the terminal velocity as a result of the proximity of the tube wall to the falling sphere was less than 2% of the unbounded terminal velocity for the case of d/D = 0.2.

In the present work the diameter of the tube is 200mm. The maximum particle diameter is less than 25.4 mm; so the maximum particle to tube diameter ratio is about 0.125. This selection will provide negligible wall effect. The method of Thomas and Walter (1965) was used to estimate the distance (L_e) required for the sphere to attain their terminal velocity using the following equation:

$$L_e = \frac{170\rho_p^2\alpha_c^4 F}{M\ \mu_0^2} \tag{4.5}$$

where

ρ_p is the particle density

$$\alpha_c = \frac{2\rho_p + \rho_F}{9\rho_f F}$$

$$M' = 4/3\ \pi\rho_f\ a'$$

ρ_f = fluid density

a' = doublet radious = $a^3(1 + k^3)$

k = ratio of large to small sphere diameter

a = small particle radius

F = (M-M')g = net gravational force

M = 4/3 π a' ρ_p and g = gravitational acceleration

The maximum entrance length needed was thus estimated to be less than 200 mm. The designed tube height is 1200 mm, allowing for at least 800 mm of test section. Two sections of 300 mm each were marked along the tube length to improve precision. First, a section of 50 mm from the top was left empty to be able to draw a vacuum on the solution without drawing it out. This section is then followed by a 200 mm liquid filled section for attaining terminal velocity. Following this there are the two sections of 300 mm which are separated by 150 mm. A schematic diagram of the details of the drop cylinder is shown in Figure 4.2. Only measurement considered are those reproduced in the two equal sections. Finally, a section of 200 mm is allowed for the bottom edge effect. The accuracy of this arrangement is seen in the results presented for a Newtonian fluid.

The spheres are supposed to be free from any attachment and fall under gravity along their line of centers. Extreme care is required to have the spheres dropped axially in the fall tube at the start of each experiment. A special centering device, shown in Figure 4.3, was designed for each pair. This device, a Plexiglass funnel positioned in the center of the tube cover. The lower end

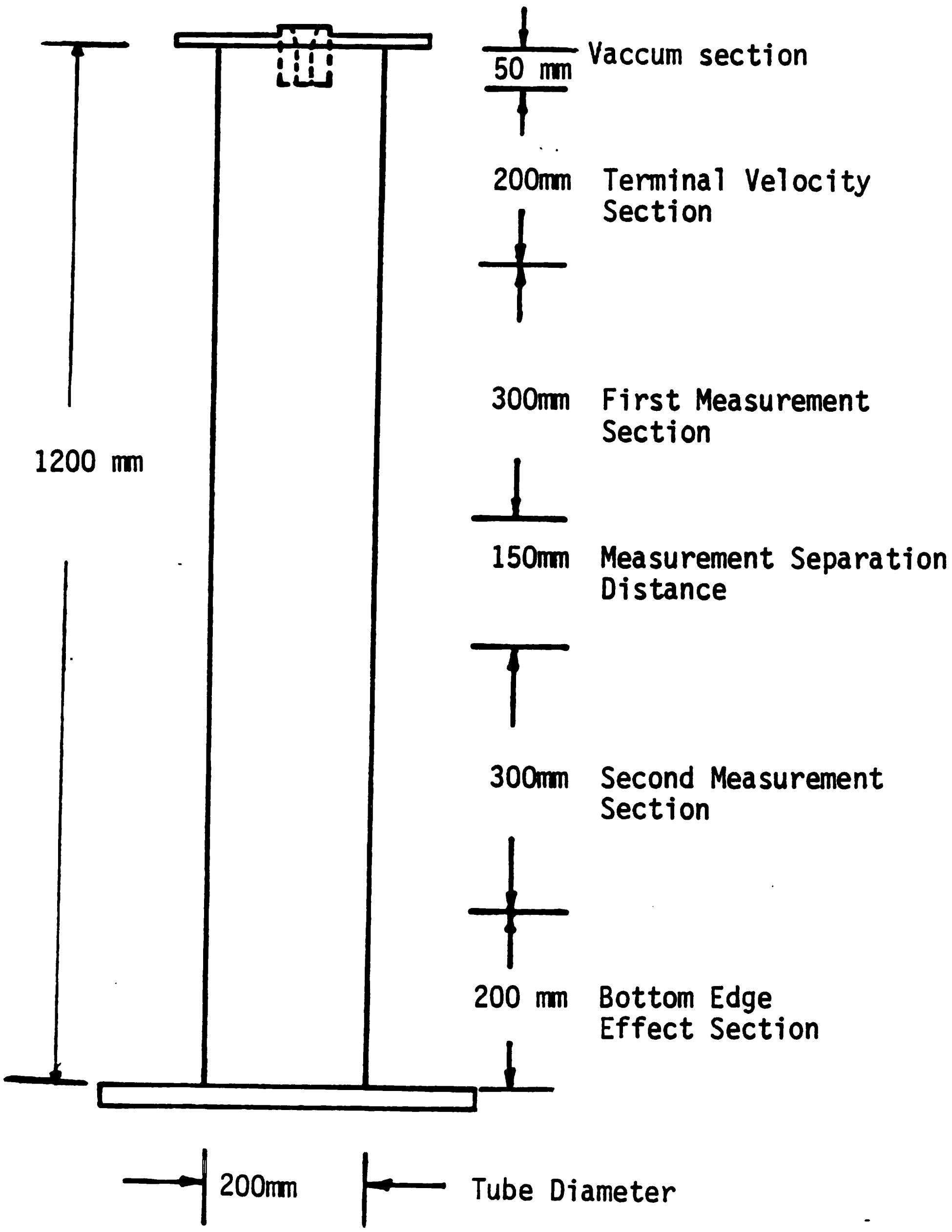

Figure 4.2. Schematic diagram of drop cylinder.

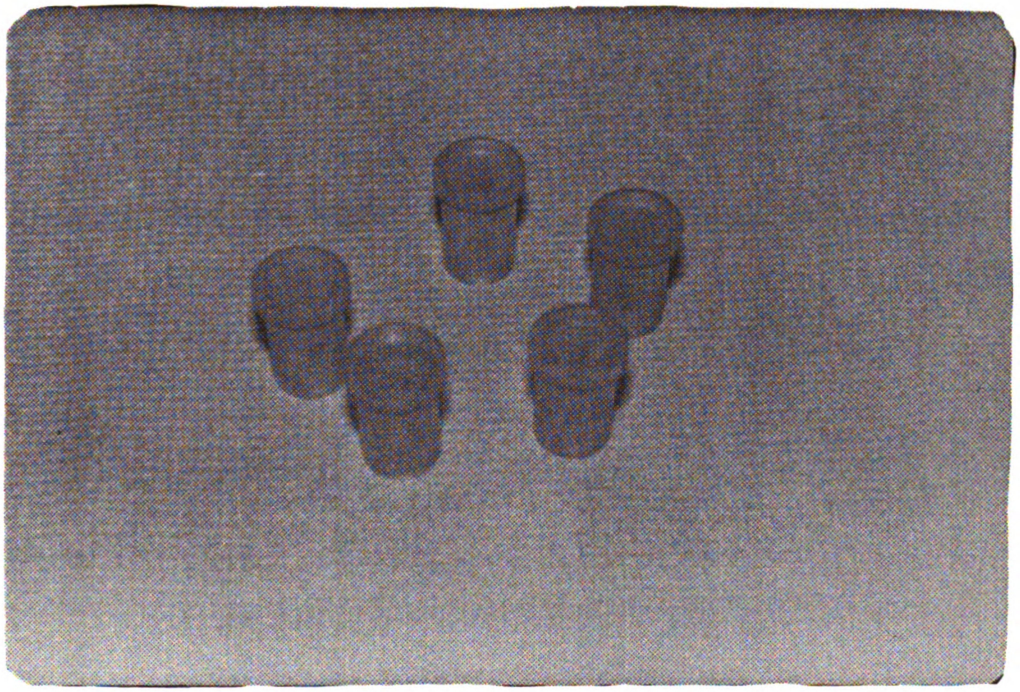

Figure 4.3. Photograph of centering device.

of the funnel is immersed in the fluid and is only 0.001 inch larger than the large sphere. This design yielded good degree of alignment of the pairs along the axis before they enter the fluid. Friction in the funnel was eliminated by making the passage very smooth. The tube wall thickness was 1/4" so as to withstand the pressure of the highly viscous fluid.

4.3 Materials

4.3.1 Test Fluids

For the purpose of isolating the elastic effect on the translation of the doublets, a viscoelastic fluid that has a constant shear viscosity is needed. This fluid has the characteristics of what is referred to as a second order fluid with constant shear viscosity and constant normal stress coefficients.

$$\lim_{\dot{\gamma} \to 0} (\mu(\dot{\gamma})) = \mu_0 \text{ and } \psi_1 = \frac{N_1}{\dot{\gamma}^2} = 2\mu_0\lambda_0 \tag{4.6}$$

where

ψ_1 is the first normal stress coefficient

N_1 is the first normal stress difference,

$\dot{\gamma}$ is the shear rate

λ_0 is a time constant

In the present work two media are used, a Newtonian corn syrup made by A. E. Staley and a viscoelastic solution of Separan® in this corn syrup. The syrup was chosen due to its clarity and high viscosity at the experiment conditions which was 1580 poise at 25°C.

Terminal velocity was obtained over a short distance down the tube and low Reynolds number flow around the spheres was obtained because of such fluid viscosity. The range of Re is between (10^{-4} to 10^{-6}). The Newtonian medium was used for the purpose of confirming the accuracy of the drag measurements. The viscoelastic medium was prepared by dissolving small quantities (0.2 wt.%) of Separan AP30 synthetic polyacrylamide, manufactured by Dow Chemical, in the corn syrup. The polymer was sprinkled in the syrup at different depth in the preparation tank and left for two days to swell. Then a slight rotation of the solution to achieve uniformity of the polymer concentration. The solution obtained was fairly clear and homogeneous. Separan AP-30 has good thermal stability below 210°C, and good resistance to shear degradation.

4.3.2 Preparation of Doublets

Spheres choosen for the experiment were steel ball bearings having extremely small tolerance on diameter and sphericity. The sphere diameter was measured carefully at several points. The density was obtained from the measurements of weight and volume of sphere. Doublets were formed by joining two spheres together over a size ratio of 1 to 7. The joining process was performed very carefully. A commercially available adhesive (Super glue) was used, a small drop was enough to bond the spheres together at a minimum contact point. The surfaces of the spheres were wiped clean and no foreign material such as glue was on them as they were dropped in the cylinder. Figure 4.4 is a photograph of several size doublets.

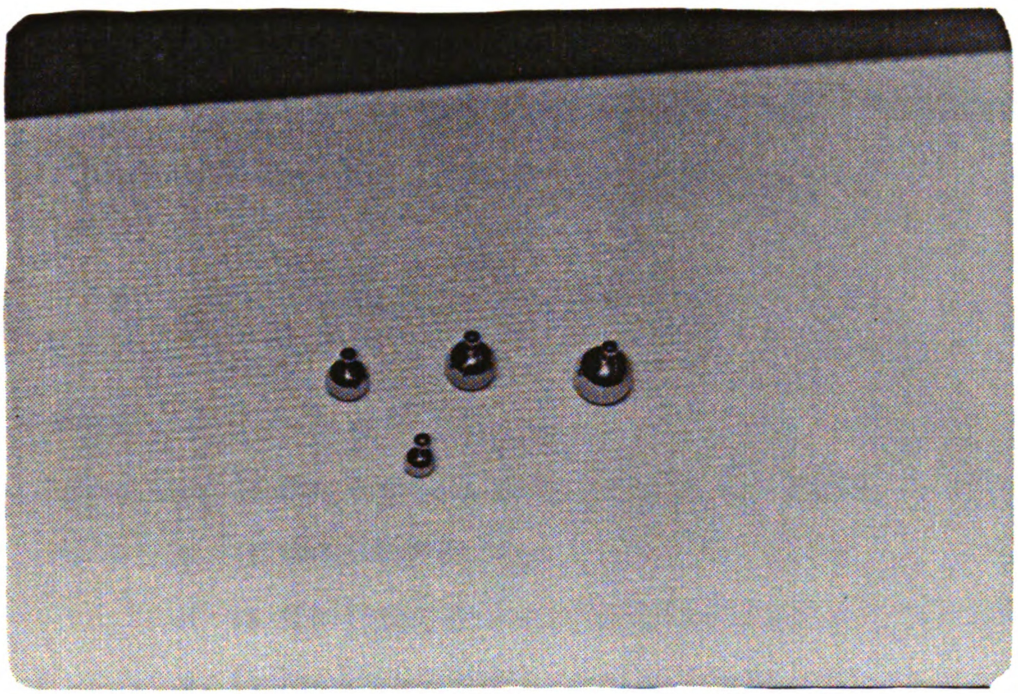

Figure 4.4. Photograph of several size doublets.

4.4 Rheological Properties of Test Fluids

An R-16 Weissenberg Rheogoniometer was used to measure the flow properties of all test fluids. Steady shear measurements were carried out to obtain the torques and forces on the cone and plate and angular velocity of the rotating plate. A cone angle of 0.5522° and a plate diameter of 7.5 cm were used in the measurements. To measure normal stress difference, piezoelectric load cell (922F) connected through an amplifier to a storage oscilloscope were used here. The cell was calibrated before the measurements by placing a certain weight and recording the voltage output. The first normal stress difference is then calculated by:

$$N_1 = \frac{F}{A_c} = \frac{2H\Delta n_1 g}{(\pi/4)d_1^2} \qquad (4.7)$$

where

Δn_1 is the oscilloscope steady-state reading in volts

g is the gravity force

H is the transfer function of the cell in mass/volt

d_1 is the plate diameter and the factor (2) is for the force on the lower and upper platens.

The first normal stress coefficient is then obtained by Equation (4.6).

A standard oil supplied by ASTM was used for viscosity calibration. Temperature control was also used to obtain viscosity-temperature data for comparison with the manufacturer's data. This comparison is shown in Figure 4.5 to be excellent. The Newtonian corn syrup was also characterized at various temperatures. The viscoelastic Separan solution in corn syrup was tested at the experiment condition. The effect of inertia on normal stress measurements was studied very carefully. No normal force was observed with the pure corn syrup. Since the Separan solution has the same density almost as the corn syrup, inertial effects are absents in these measurements. Corn syrup viscosity vs. shear rate is shown in Figure 4.6 and 4.7. The temperature dependence of the viscosity is given in Figure 4.8. Figure 4.9 shows the viscosity vs. shear rate of the elastic fluid. Constant viscosity is observed up to a shear rate of 5 sec^{-1}. For the first normal stress coefficient Figure 4.10 show that ψ_1 is constant again up to $\dot{\gamma} \approx 2$ sec^{-1}. In any case our settling experiments involve shear rates less than or equal to 1 sec^{-1} as will be seen in Table 4.3. The first normal stress difference is shown in Figure 4.11. The flow properties of all test fluids are summarized in Table 4.1. A new sample was used

TABLE 4.1.--Viscosity, relaxation time, and density of test fluids

Test Fluid	Temp C°	μ_0(Poise)	λ_0(sec)	ρ_f(gm/cm^3)
Standard oil	25	740	--	
Corn syrup 200	25	1580	--	1.4288
.2% Separan	25	1760.57	0.26	1.3501

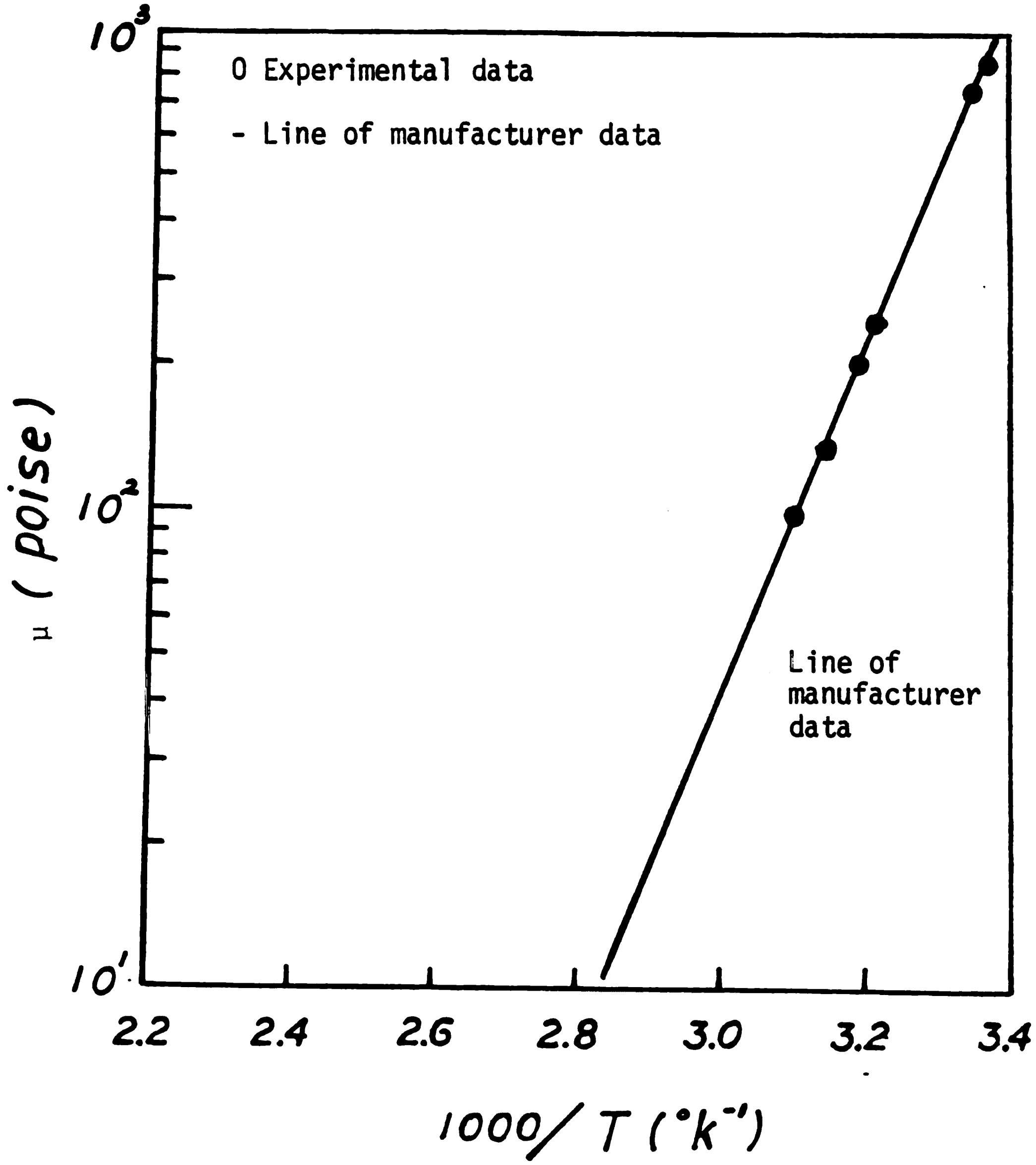

Figure 4.5 Calibration of Weissenberg Rheogoniometer by ASTM Fluid.

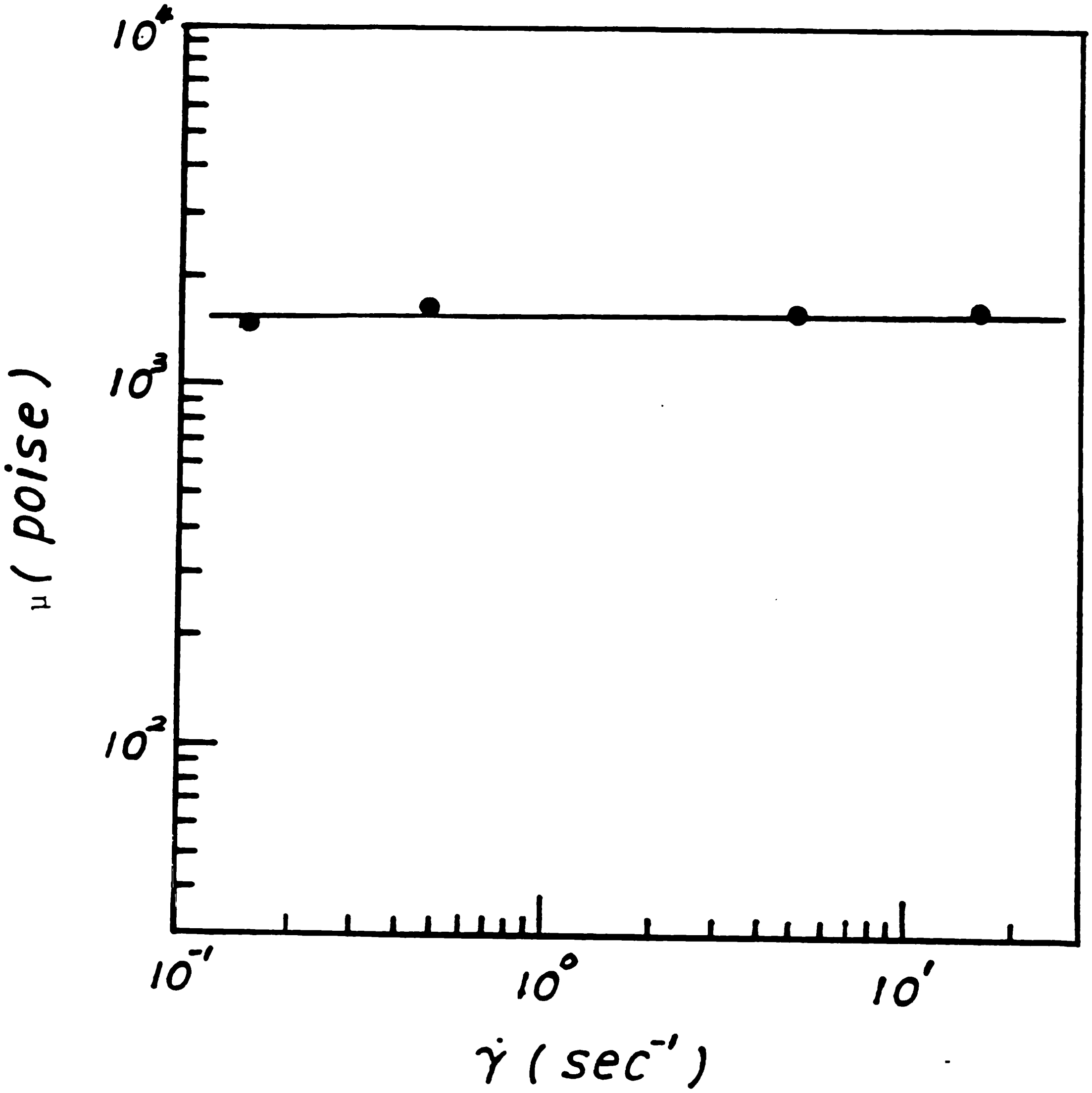

Figure 4.6. Corn syrup viscosity vs. shear rate at 25°C.

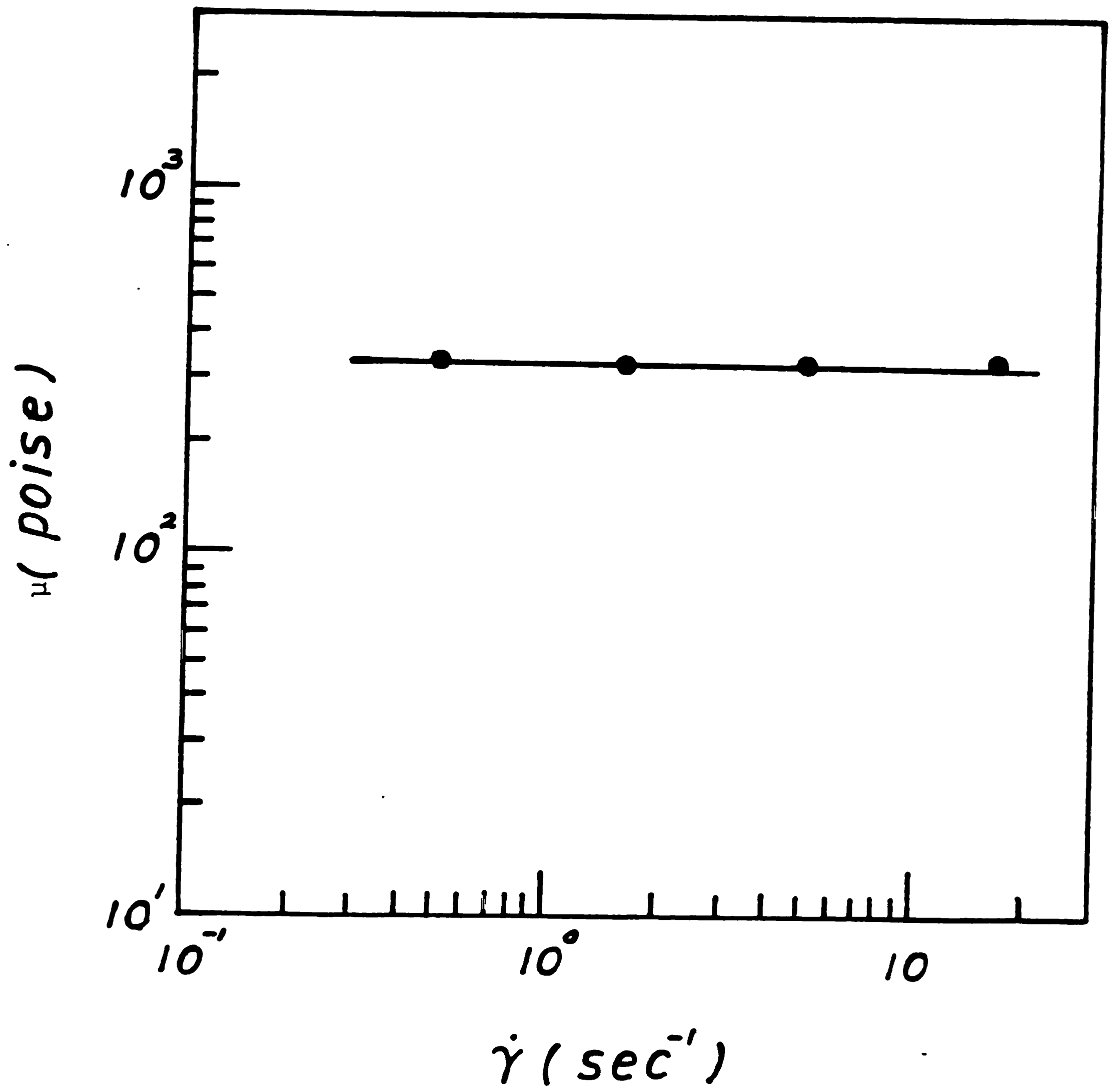

Figure 4.7. Viscosity vs. shear rate for corn syrup at 36°C.

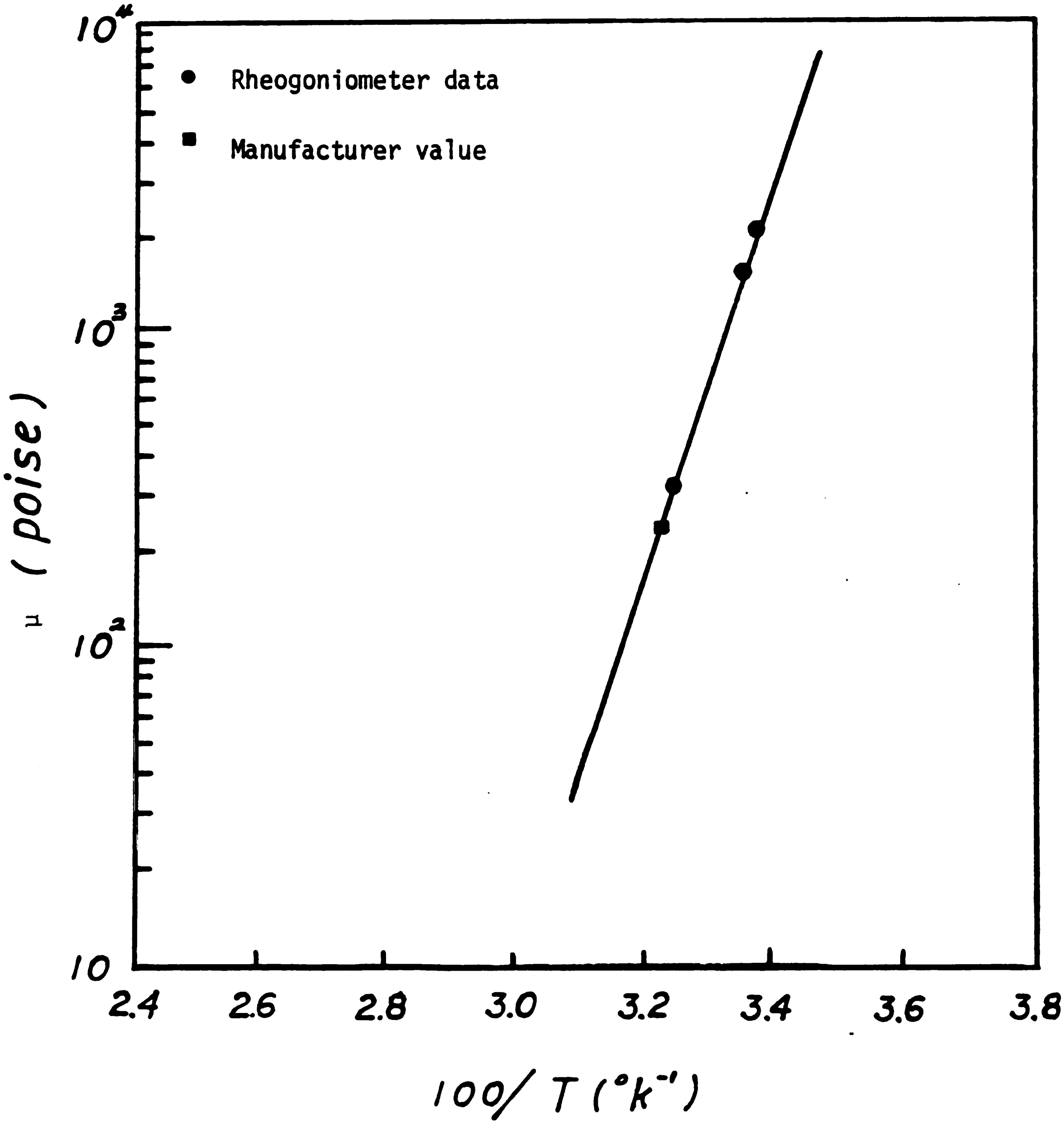

Figure 4.8. Viscosity vs. temperature for corn syrup.

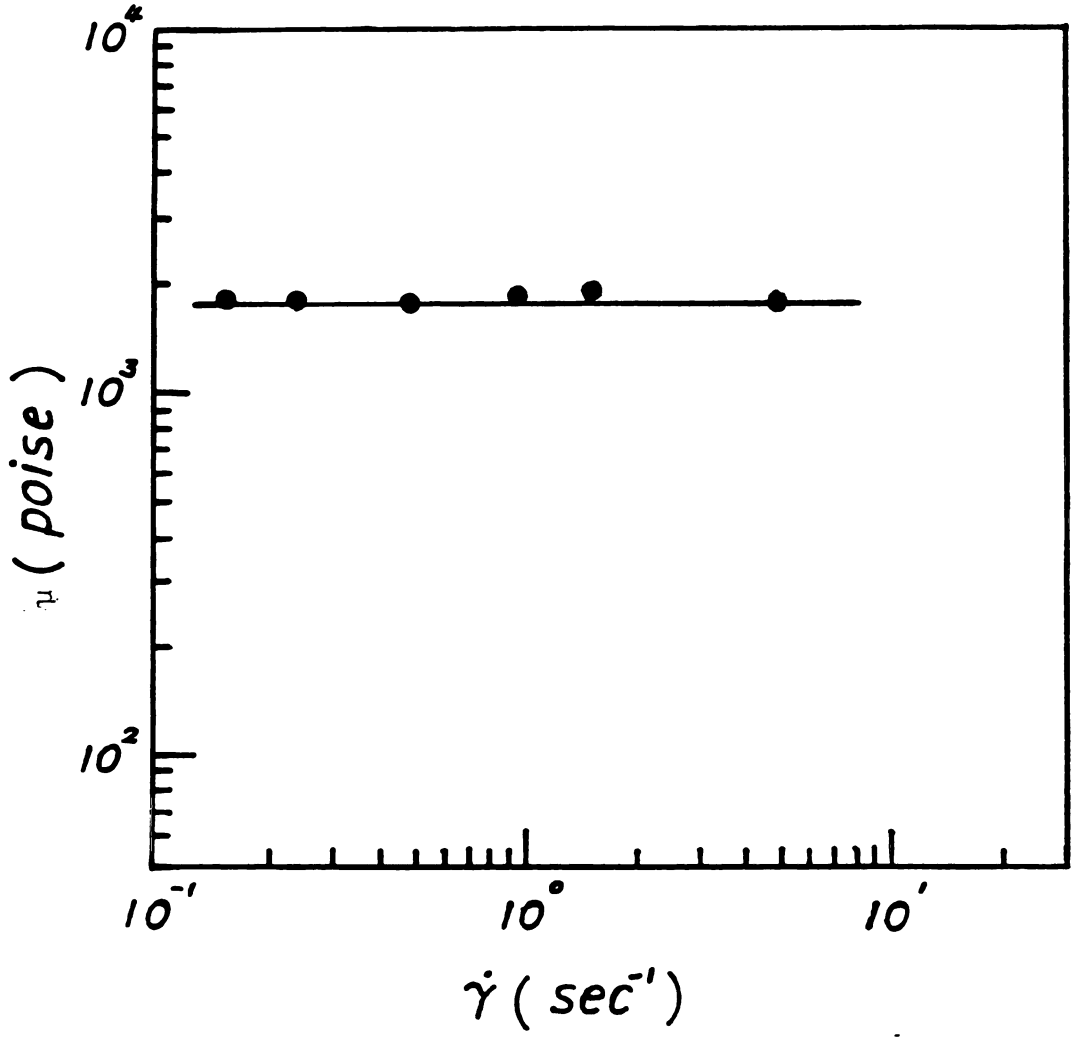

Figure 4.9.--Viscosity vs. shear rate of 0.2% separan in corn syrup at 25°C.

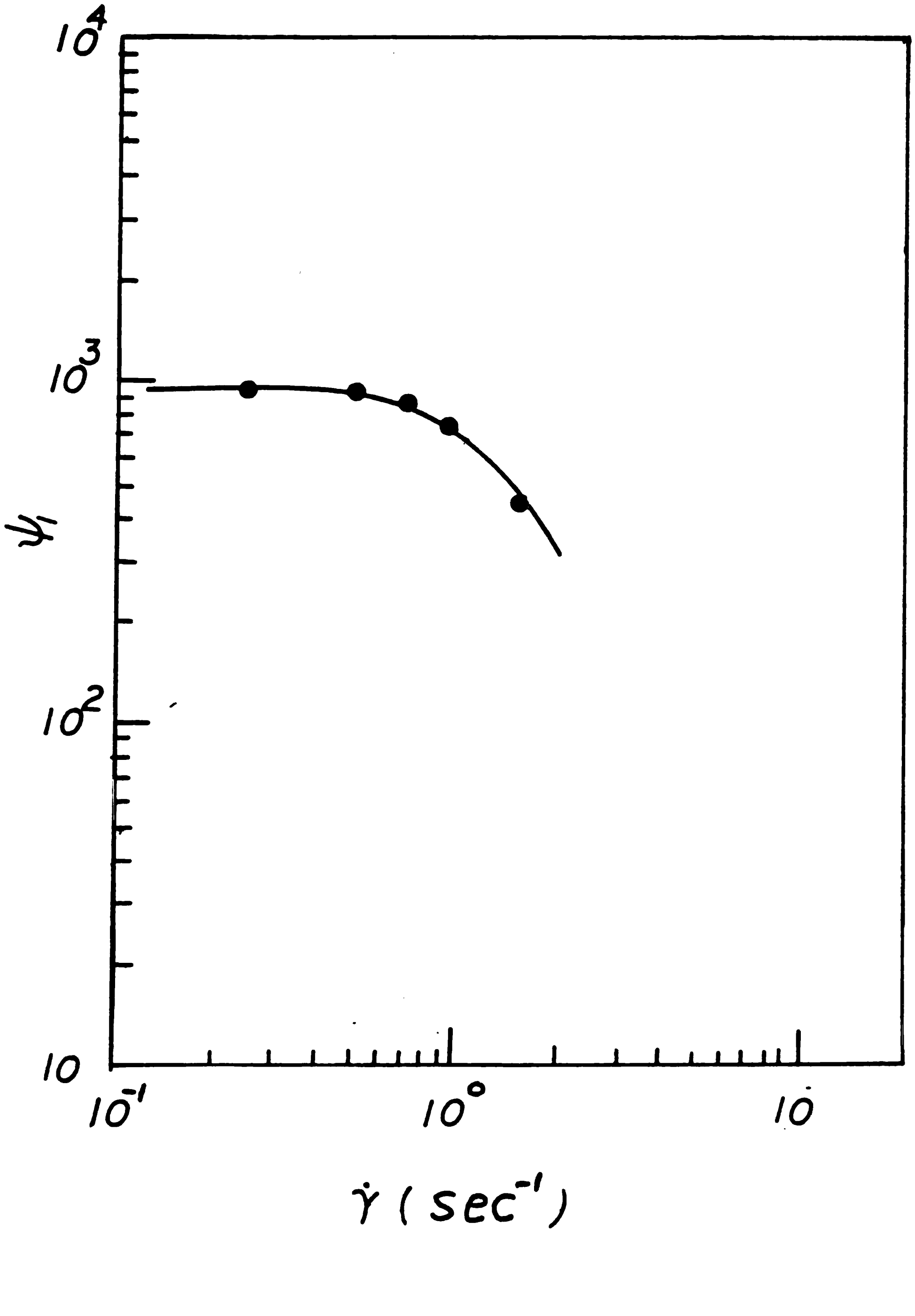

Figure 4.10. Normal stress coefficient vs. shear rate of 0.2% separan in corn syrup.

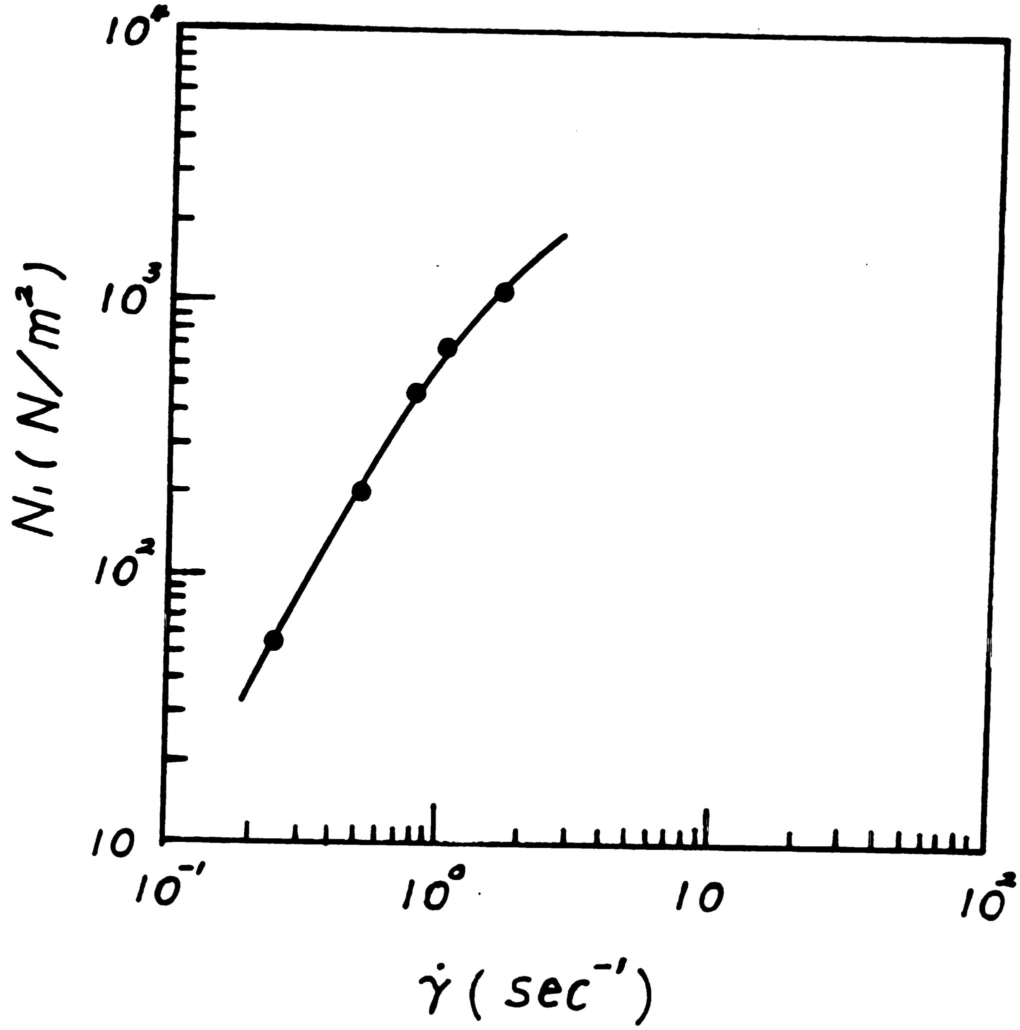

Figure 4.11. First normal stress difference vs. shear rate for 0.2% separan in corn syrup.

at each shear rate. This was necessary to avoid any error due to material degradation or insufficient relaxation time after shearing the sample. Each time a sample is loaded twenty minutes were allowed for the material to relax before a measurement is taken. Evaporation of the sample was cut to a minimum by applying a thin film of silicon oil of comparable viscosity to the exposed sample in the gap between the cone and platen.

4.5 Experimental Procedure

The Newtonian fluid was used first for reproducing available theoretical results and confirming the suitability of the experimental arrangement. Pure corn syrup filled the drop cylinder up to a level that is enough to have the centering device immersed. The cylinder was left in a constant temperature room for few days to allow the entrapped air to escape and thermal equilibrium to be reached. Application of a vaccum on the cylinder helped further speed up the process of getting rid of the air bubbles.

Each pair of spheres was released carefully in the centering device to avoid any eccentricity. The terminal velocity was recorded with two electronic timers, were each section is timed by a separate timer. A period of at least twenty minutes was allowed after each test to avoid any error due to disturbances. This was necessary due to the highly viscous fluids used. This time was also higher for larger doublets. The same procedure was followed for the visco-elastic medium. It is worth noting that it took a longer time to clear the solution from air bubbles.

The orientation of non-spherical particles is an important question to be addressed in sedimentation experiments. Photographs in Figures 4.12, 4.13 show that for both Newtonian and viscoelastic medium the orientation in which the line of centers coincides with the axis of the cylinder and the larger sphere is underneath, is stable and maintained throughout the fall. The same behavior was predicted by Brunn (1977a) for transversely isotropic particle in a quiescent field, as discussed earlier in Chapter I.

4.6 Results

4.6.1 Previous Observations
Non-Contacting Particles

For the purpose of completeness non-contacting spheres were also dropped with two different initial separation distances. This was done in both the Newtonian syrup and the elastic liquid. As expected, in the Newtonian syrup the initial separation has no effect on the spheres as they settle in the tube. On the other hand, in the elastic liquid we observed convergence of the spheres for small initial separation distance and divergence for large separation distance as they settle in the tube as can be seen in Figures 4.14 to 4.20. These phenomena were also reported by Riddle et al. (1977). The fluids used by Riddle were of considerable shear thinning. In our case the elastic fluid is non-shear thinning and thus we attribute these observations to the elasticity of the medium.

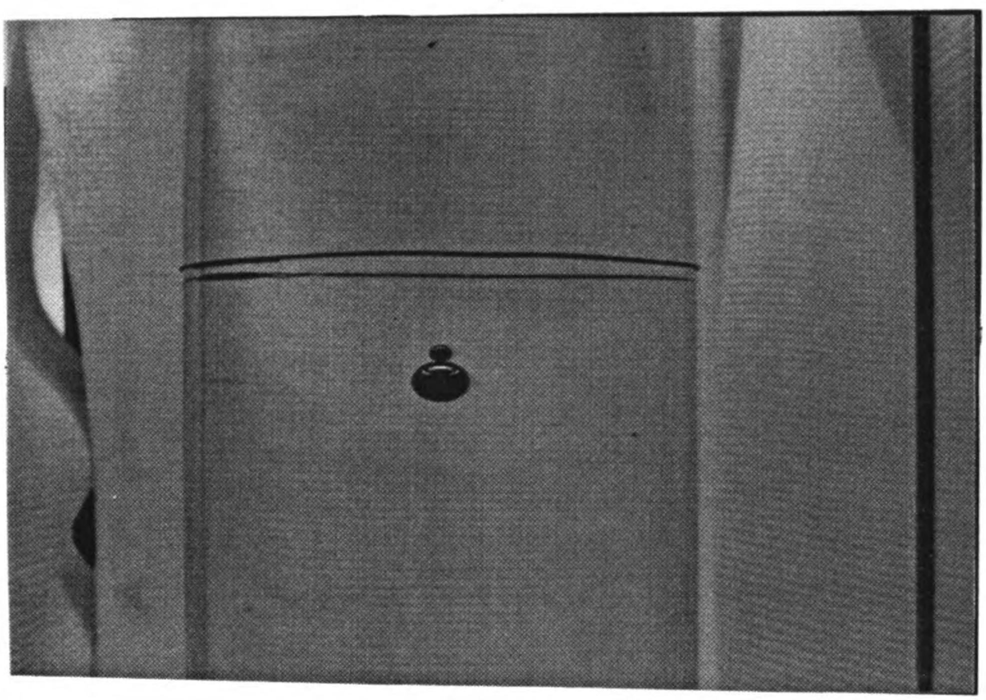

Figure 4.12. Photograph of a doublet in a Newtonian fluid.

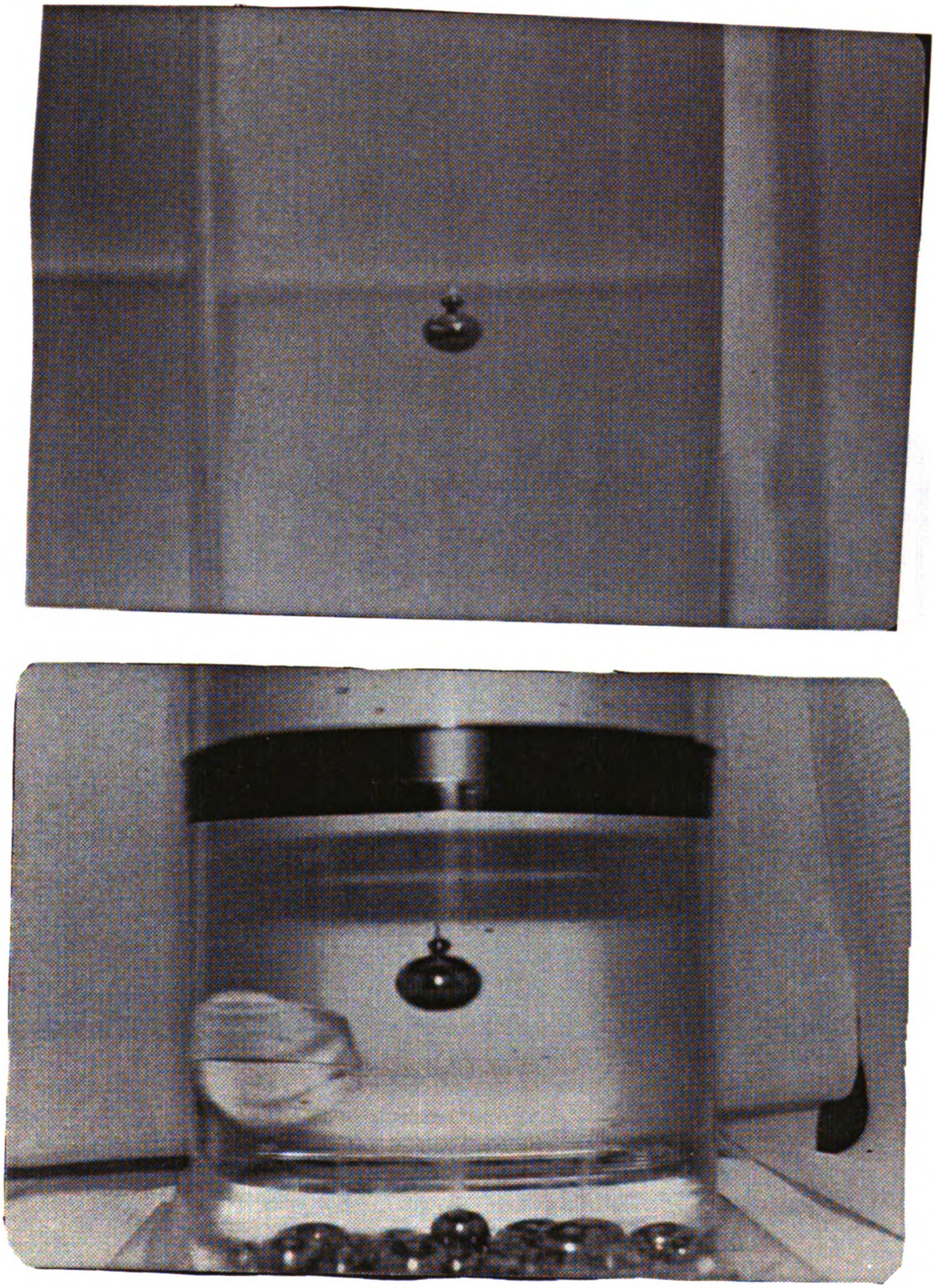

Figure 4.13. Photograph of a doublets in a viscoelastic fluid.

Figure 4.14. Photograph of particles separated by a distance in Newtonian fluid. Top section of the test column.

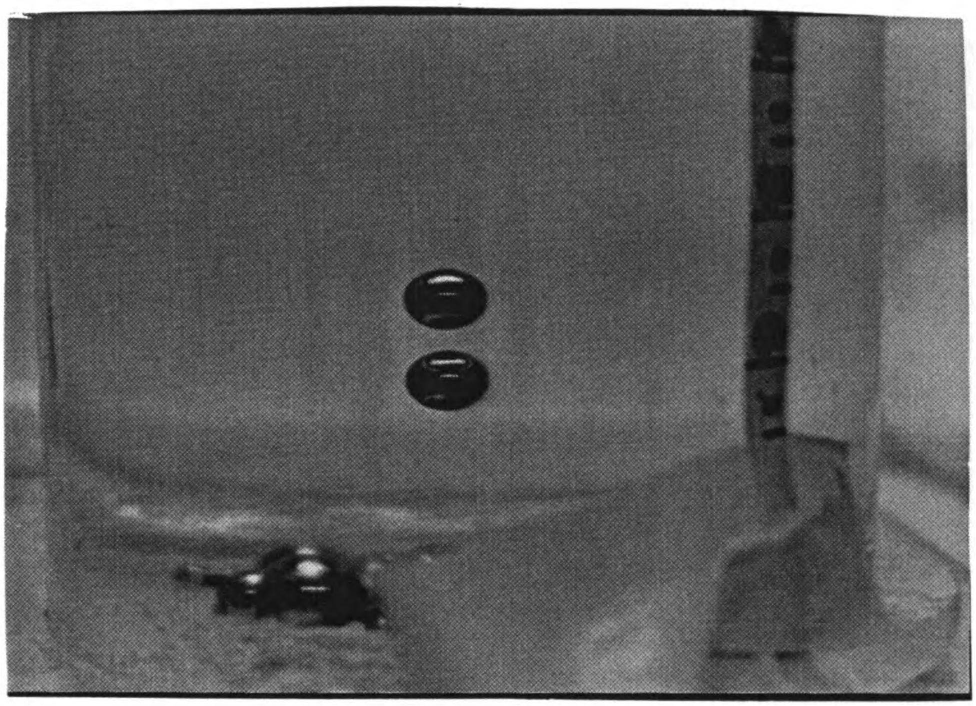

Figure 4.15. Photograph of same particles at the bottom of the test cylinder.

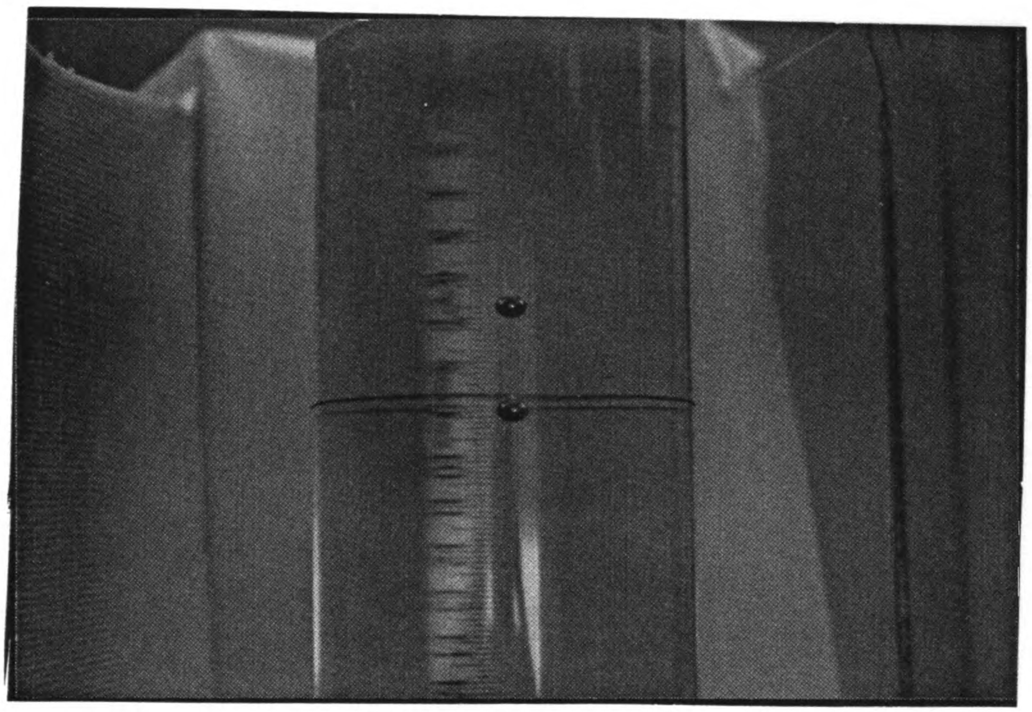

Figure 4.16. Photograph of two particles in viscoelastic fluid at the top of the test cylinder.

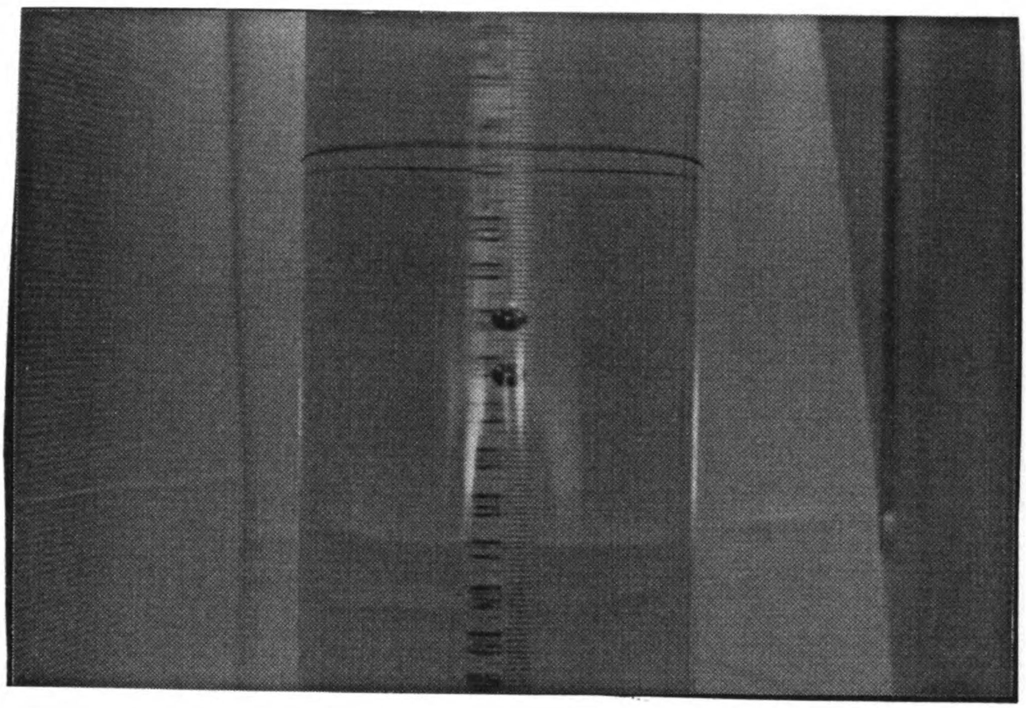

Figure 4.17. Photograph of same two particles after some distance down the tube.

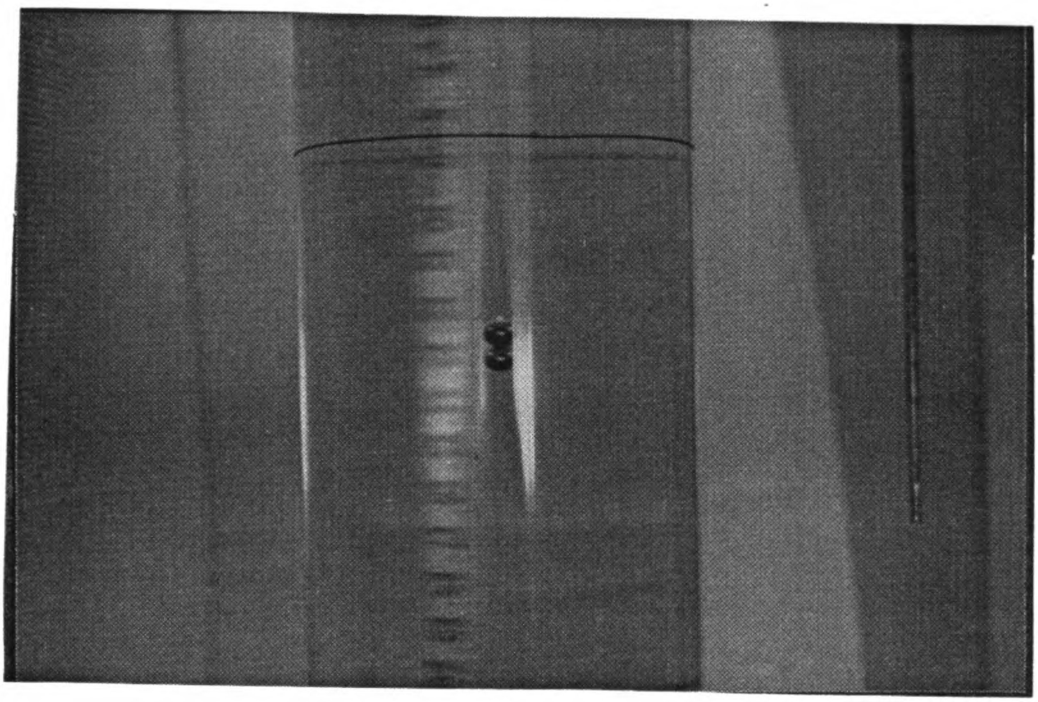

Figure 4.18. Photograph of same particles as they converge.

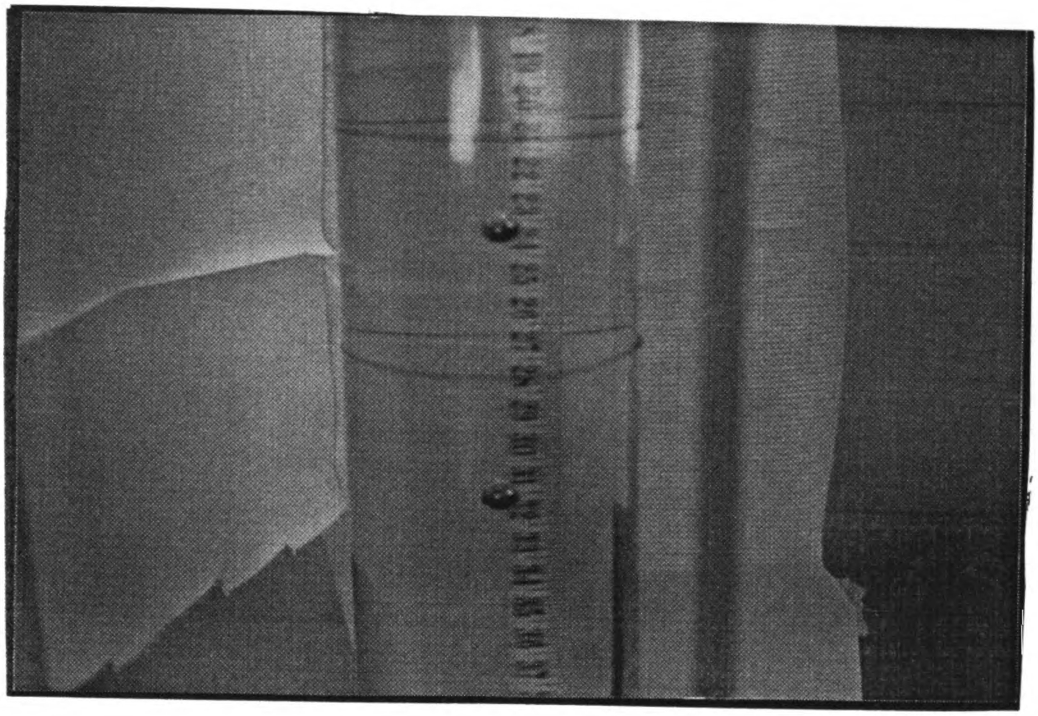

Figure 4.19. Photograph of particles separated by large critical distance at the top of the cylinder in a viscoelastic fluid.

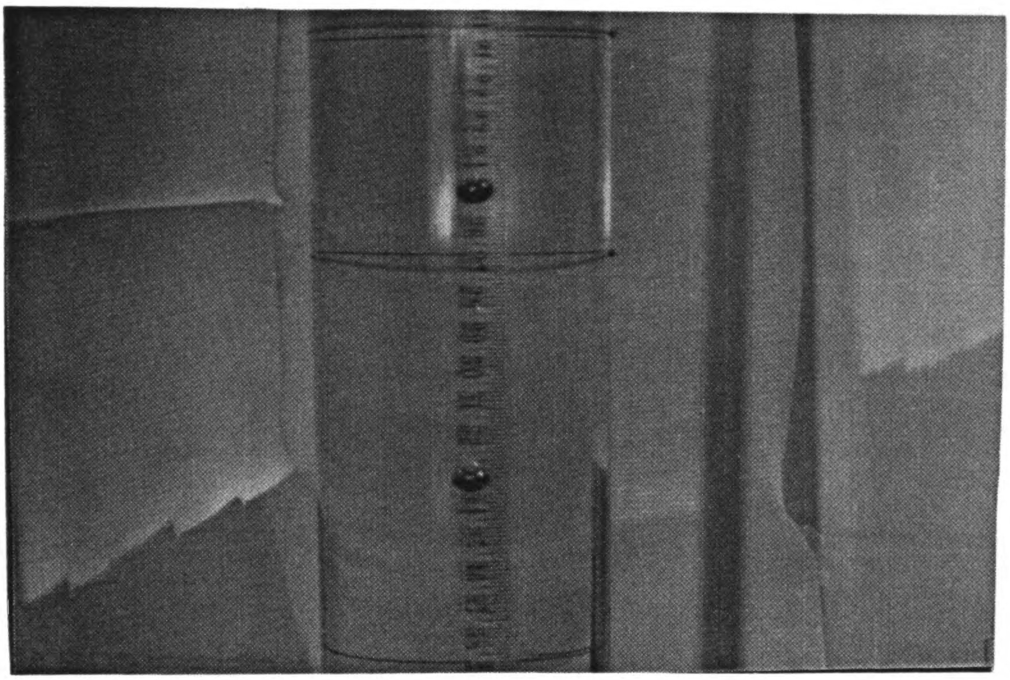

Figure 4.20. Photograph of same particles as they diverge down the tube.

4.6.2 Contacting Particles in Newtonian Liquid

The theoretical and experimental values of the correction factor f_N to STokes' law for doublets of various size ratios in the Newtonian corn syrup are summarized in Table 4.2. The

TABLE 4.2.--Newtonian fluid results. a = small sphere radius (cm). k = ratio of radii, f_{exp} = exp. drag correction factor, f_{theo} = theo-drag correction factor

a	k	$f_{exp.}$	f_{theo}
.1587 cm	1	1.216	1.29
.1587 cm	2	2.08	2.09
.1587 cm	4	3.97	4.02
.1587 cm	5	5.03	5.01
.1587 cm	7	6.99	7.01

experimental values have been obtained from the following equation

$$f_N = \frac{F_G}{6\pi\mu Ua} \tag{4.8}$$

where

$$F_G = (4/3)\pi(\rho_p-\rho_f)(1+k^3)\,a^3g$$

where

g is the acceleration

a is the small sphere radius

k is the ratio of radii ($k \geq 1$)

ρ_p and ρ_f are the particle and fluid densities

Theoretical values of f_N were given by O'Neill (1969a). The maximum discrepancy between the experimental and theoretical values of f_N is seen to be at k = 1; and amounts to 6%. This is believed to be due to experimental and wall effect error. Nevertheless, it should be mentioned that wall effect contribution to this value is very negligible. This conclusion is reached on the basis of the results of larger k values. So the error is mostly due to small errors in measuring the terminal velocities. It is to be noted that creeping flow was ensured since the values of Reynolds numbers are between 10^{-4} to 10^{-5}. The results obtained here confirmed the suitability of the cylinder design for carrying out the experiment for the elastic medium.

4.6.3 Contacting Spheres in Elastic Fluid

The results of this section are to be presented in terms of a correction factor which accounts for the deviation in drag coefficient from Newtonian value due to the presence of fluid elasticity. The correction factor was obtained for several values to the product of λ_o and the average shear rate which is in the case of doublets of spheres in creeping flow can be arbitrarily defined as

$$\lambda_o \dot{\gamma}_{av} = \lambda_o U/a(1 + k) \tag{4.9}$$

where

λ_o is a relaxation time in seconds and all other quantities are as defined before.

The various values of the product $\lambda_o \dot{\gamma}_{av}$ were obtained by varying the doublets size ratio. In general, for creeping flow, the drag coefficient can be written as:

$$C_d = \frac{2F}{\rho_f \, a^2 U^2 (1 + k^2)\pi} \tag{4.10}$$

where

F is the drag experienced by the doublets.

The correction factor can then be written as:

$$Xe = \frac{C_{de}}{C_{ds}} \tag{4.11}$$

where

C_{de} is the drag coefficient in the elastic fluid

C_{ds} is the drag coefficient for a Newtonian fluid of the same viscosity as that of the elastic medium

It is worth noting that in calculating C_{de}, we set

$$F = F_G \tag{4.12}$$

while in the calculation of C_{ds}, we set

$$F = 6\pi\mu Ua \; f_{N,theo} \tag{4.13}$$

with the viscosity μ and the observed terminal velocity U are taken from the experiment with the elastic fluid. Flow around a doublet of spherical shape in a non-viscometric and the shear rate at the surface varies from point to point over the surface. This case is the same as for flow around a single sphere. An average shear rate defined by

$$\dot{\gamma}_{av} = U/a$$

is usually used there. In our case $\dot{\gamma}_{av}$ is to be defined as

$$\dot{\gamma}_{av} = U/a(1+k) \tag{4.14}$$

At this point we will define

$$\dot{\gamma}_{av}\lambda_o \equiv We^* \tag{4.15}$$

In Table 4.3 the results for the elastic fluid are presented. These results include the size ratio k, the small sphere radius a, We*, the average surface shear rate $\dot{\gamma}_{av}$, the correction factor due to elasticity X_e for the doublets and the correction factor for the single spheres Xe_s given by Boger and coworkers (1980). These results cover a range of Reynolds numbers between 10^{-4} to 10^{-6} as shown in the Table of raw data in Appendix B. The results of Table 4.3 are also shown in Figure 4.21 and 4.22. The value of We^* was varied by changing the size ratio of the spheres. Thus in Figure 4.21 We^* values were obtained from doublets whose small sphere radius is 0.0794 cm and k was increased from 1 to 4. This arrangement covered a range of We^* from 0.0129 to 0.064. In Figure 4.22 the small sphere radius is 0.1587 cm and k is increased from 1 to 7 to cover a range of We^* from

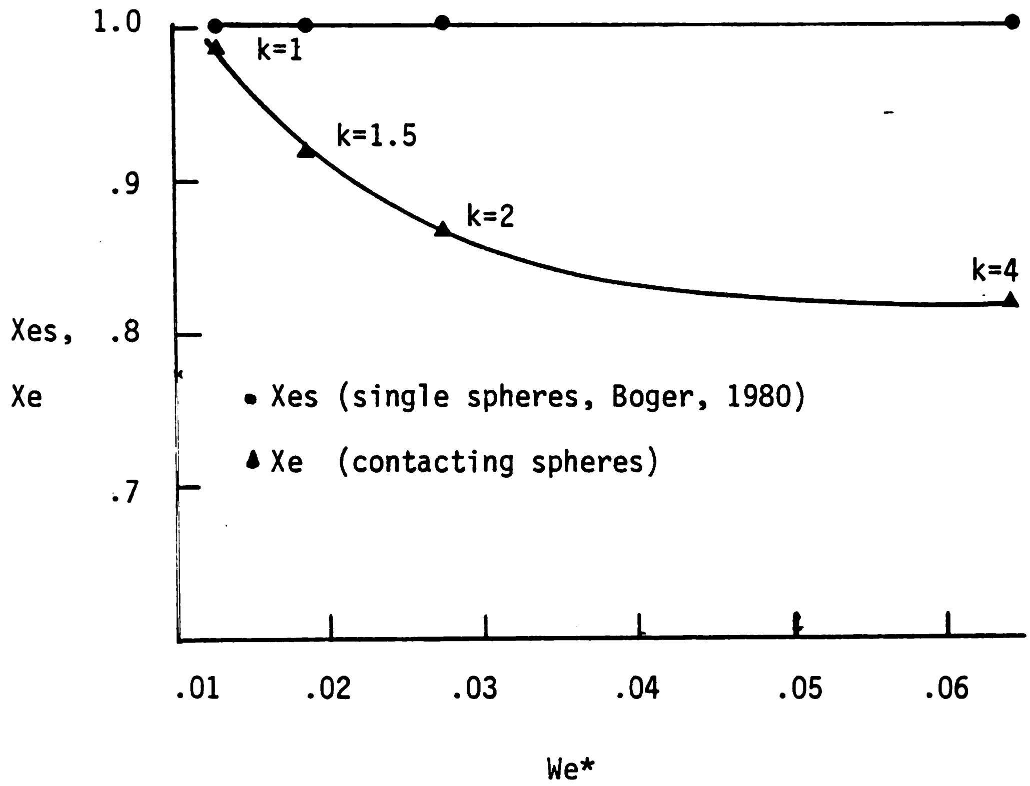

Figure 4.21. Correction factor for drag coefficient deviation from Newtonian Value due to presence of elasticity VS We*.

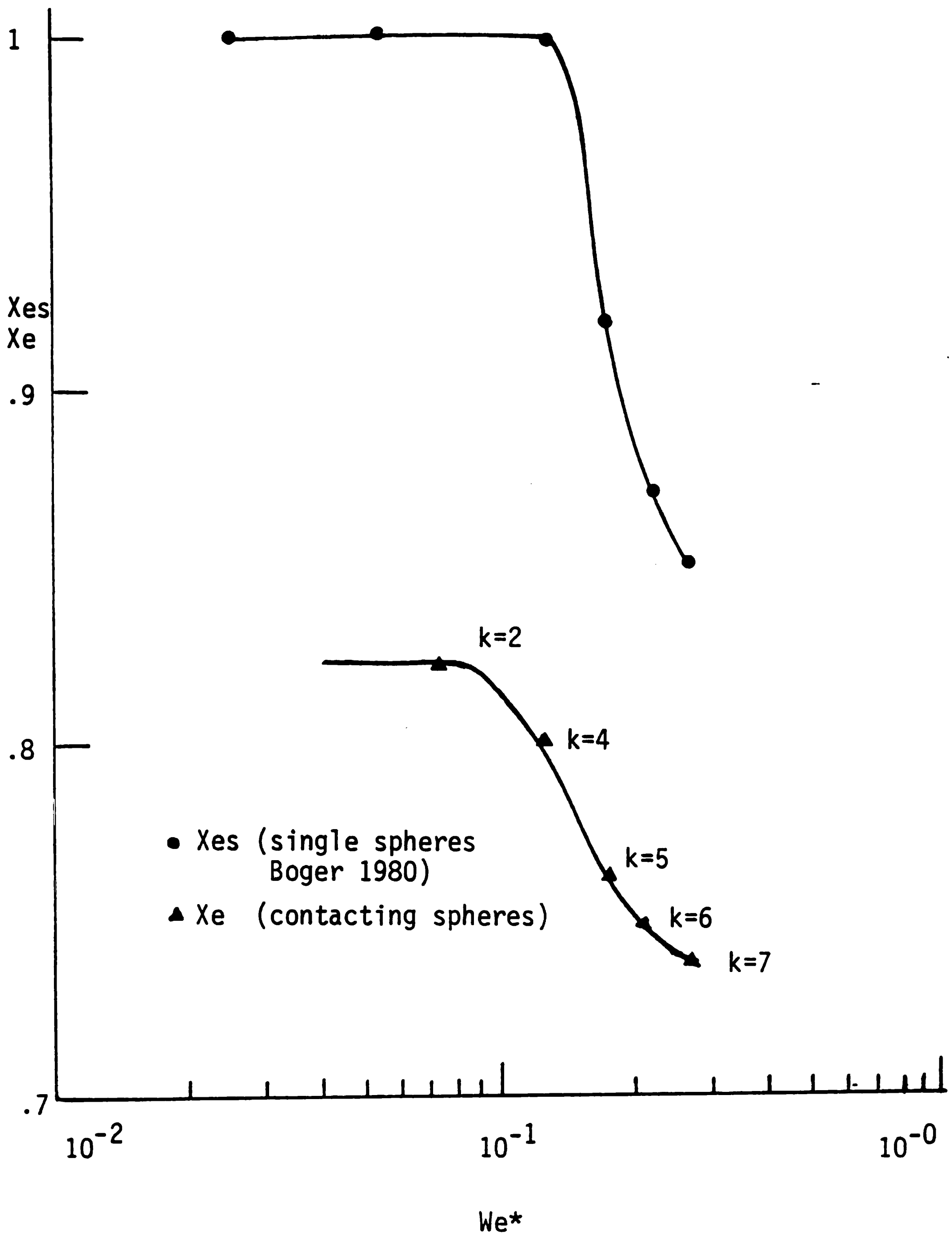

Figure 4.22. Correction factor for drag coefficient deviation from Newtonian values due to presence of elasticity vs We*.

Table 4.3.--Elastic fluid results

k	a(cm)	$\dot{\gamma}_{av}(sec^{-1})$	$\dot{\gamma}_{av}\ \lambda_o=We^*$	Xe	Xes
1	0.0794	.05	0.0128	.99	1
1	0.1587	.1	0.0261	.98	1
1.5	0.0794	.07	0.018	.91	1
2	0.0794	.104	0.027	.87	1
2	0.1587	.22	0.056	.84	1
4	0.0794	.25	0.064	.82	1
4	0.1587	.51	0.133	.80	1
5	0.1587	.695	0.178	.76	.92
6	0.1587	.879	.228	.74	.87
7	0.1587	1.05	.272	.74	.85

0.0261 to 0.272. These figures show that there is a significant reduction in drag coefficient of the elastic medium below that of Newtonian liquid for contacting spheres. It was further seen that this reduction is dependent on We^*. We observed that there is a linear reduction over We^* = 0.0128 to 0.035 where a reduction of 15% was seen. For We^* between 0.035 and 0.064 a leveling off is observed and a reduction of 18% is reached. As We^* is further increased above 0.064 we observed further reduction in the drag below the Newtonian value. The maximum reduction was seen to be 26% at We^* = 0.272. The case of single spheres doesn't show deviation except at We^* = .13. A linear reduction is seen there which reaches a maximum of 15% at We^* = 0.272.

At this point we would like to see how the elastic effect predicted by the numerical scheme of Chapter III compares to the results of this chapter. In particular, we will compare the results for the value of $k = 1.5$. In Chapter III we defined

$$We = (\nu_1 + 2\nu_2)\,\frac{U}{a} \tag{4.16}$$

where

$\nu_1 = \psi_1/\mu_o$

$\nu_2 = \psi_2/\mu_o$

ψ_1 and ψ_2 are the first and second normal stress coefficients

In this work we could measure only ψ_1. It is a common practice to assume that $\psi_2 = -\,.1\psi_1$, so

$$We = (\psi_1 - 2x \cdot 1\psi_1)\,\frac{U}{a\mu_o} = .8\psi_1\frac{U}{a\mu_o} \tag{4.17}$$

According to Equation (4.6)

$$\psi_1 = 2\mu_o\lambda_o \tag{4.18}$$

Therefore

$$We = 1.6\ \lambda_o\ U/a \tag{4.19}$$

So for $k = 1.5$ and $a = 0.0794$ cm, $U = 0.0145$ cm/sec. (from Appendix B) we get $We = 0.076$. Thus using F_{oz} and F_{1z} for $k = 1.5$ in Table 3.6, we can evaluate a corresponding theoretical value to Xe as Xt using

$$F = F_{oz} + WeF_{1z} \tag{4.20}$$

to get Xt = 0.944 while the experimental value Xe = 0.91. In Table 4.4 we present the results of k = 1.5 and 2. It is noticed that experimental values are in close agreement with those predicted by theory.

TABLE 4.4.--Comparison between theoretical drag coefficient ratio Xt and experimental drag coefficient ratio Xe

k	We	We*	1-Xt	1-Xe
1.5	0.076	0.018	.06 ± .03[a]	.09
2	.13	0.027	.1 ± .02[a]	.13

[a]This uncertainty is due to error in numerical scheme, already discussed.

CHAPTER V

CONCLUSION AND RECOMMENDATION

5.1 Conclusion

This investigation has focused on determining the elastic effect of a non-shear-thinning medium on the sedimentation of contacting particles. The flow conditions are those of creeping flow with Reynolds number in the range of 10^{-4} to 10^{-6}. As far as we know, we are the first to observe the elastic effect on the sedimentation of contacting particles with a non-shear-thinning (Boger) fluid. The suitability of our apparatus was checked with a viscous, Newtonian corn syrup in which our observations on orientation as well as sedimentation speed were consistent with previous reports in the literature. The experimentally observed settling speed on these particle pairs is reproducible to within 2 percent.

In the elastic fluid medium, this study provided new information about a stable orientation for unequal spheres. This orientation is that of the line of centers along gravity with the larger sphere leading. It was further observed that even if the initial orientation was not coinciding with the terminal orientation, the particles will reorient themselves to the terminal and stable orientation within a length of at most 15 cm. For completeness, we repeated the experiments which were carried out by Riddle et al.

(1977) on spheres separated by several distances. Convergence was seen for particles with small initial separation and divergence was seen with large initial separation. It is to be noted that while the fluid used by Riddle was considerably shear thinning, we observed similar behavior with the Boger fluid, so the above behavior might be attributed to elasticity of the medium alone.

Measured settling velocities for unequal spheres showed a significant reduction in the drag coefficient below the Newtonian values. The reduction was seen to be a function of $We^* = \dot{\gamma}_{av}\lambda_o$, where a deviation of 26 percent is observed over a range of We* between 0.0128 and 0.272, based on a dimension $(1 + k)a$ of the two spheres.

A theoretical analysis was carried out to investigate the translation of these contacting particles along their line of centers, in an effort to obtain the elastic effect of a second order fluid medium of a constant viscosity on the drag force on the contacting spheres surface. A volume integral was developed for the drag contribution at O(We) involving the zeroth order, Newtonian velocity field. Steps were taken to insure accuracy at each stage of the numerical solution by checking condition of matrix in solving a set of linear equations repeatedly; comparing asymptotic limits of all six Hankel transforms at both ends ($\eta \to 0$ and $\eta \to \infty$) with numerical estimates, taking care to obtain simple analytical approximations to the behavior of the integrand at large s as well as small s. Since the function $f(s,\xi)$ is evaluated thousands of times in the numerical scheme, accurate evaluation of f was the heart of the numerical steps in this work. Thus we carried out a detail error analysis and obtained an upper bound on the total error in evaluating $f(s,\xi)$. Our analysis revealed that the error increased with decreasing α over $0 < \alpha < 1$ and in the increasing s values above $s = 6$. Using the worst case error an upper bound on the error in the total result including 27,000 function evaluations, would be 10^{-4} for $\alpha = 0.2$ and 10^{-7} for $\alpha = 0.5$. In addition, there is the error in fitting exponentials to the large s behavior of f, $\frac{\partial f}{\partial \xi}$, $\frac{\partial^2 f}{\partial \xi^2}$. This fit was necessary to evaluate the complete Hankel transform of these functions. The error of the fit was worst for $\partial^2 f/\partial \xi^2$ and this error too increased with decreasing α over $0 < \alpha < 1$. We have tabulated results in Table 3.7 above $\alpha = 0.33$ for which these errors add up to only 20 percent of the final result for reduction in drag. These results indicate a definite nonzero elastic contribution to drag for the α values listed.

The contribution of the integrand involving η and ξ alone was investigated over the entire range of ξ and η. This investigation revealed that the region near the stagnation point on the larger sphere is the most important region for estimating the elastic effect. The region near the contact point of the two spheres has no contribution at all. These results are in accordance with findings of Leal (1975) in his analysis of the drag on slender cone in a second order fluid, Leal found that the major contribution to a similar volume integral was obtained from the fluid close to the particles; however, because of the slender body approximation, he was able to omit the stagnation points at both ends of the particle for very long rods.

The numerical results obtained for the integral of Equation (3.46) for $\alpha \geq 0.33$ show an appreciable elastic effect on the drag experienced by the unequal contacting spheres. This effect was larger for larger size ratio k. Comparing these theoretical predictions with the experimental values for k = 1.5 and 2 showed that experiments are in good agreement with theory.

5.2 Recommendation

The theoretical and experimental analysis carried out here has established the existence of an elastic effect due to the medium on the drag force of two contacting spheres of unequal size translating along their center line in creeping flow. The major problem and difficulty in the numerical solution is in evaluating the function $f(s,\xi)$ at large values of s and small values of α. The fitting procedure also involved an additional error with decreasing α over $0 < \alpha < 1$. Therefore, in order to obtain results for low α values some other methods for evaluating the function $f(s,\xi)$ and fitting $f(s,\xi)$, $\frac{\partial f(s,\xi)}{\partial \xi}$ and $\frac{\partial^2 f(s,\xi)}{\partial \xi^2}$ should be pursued in future work.

APPENDICES

APPENDIX A

PROOF OF VANISHING INTEGRAND OF EQUATION (3.20)

APPENDIX A

PROOF OF VANISHING INTEGRAND OF EQUATION (3.20)

Proving that

$$\int_{V_f} (\underline{\underline{\Pi}}_1 : \nabla\hat{\underline{v}}_o - \hat{\underline{\underline{\Pi}}}_o : \nabla\underline{v}_1) = 0 \tag{A.1}$$

Tensorial notations are going to be adapted for this proof. We consider the integrand term by term as follows

$$\underline{\underline{\Pi}}_1 : \nabla\hat{\underline{v}}_o = - P_1\underline{\underline{\delta}} + 2\mu\underline{\underline{D}}_1 : \nabla\underline{v}_o$$

$$= \left[-P_1 \, \delta_{ij} e_i e_j + \mu\left(\frac{\partial v_{1i}}{\partial x_j} \, e_i e_j + \frac{\partial v_{1j}}{\partial x_i} \, e_j e_i\right)\right]$$

$$: \frac{\partial \hat{v}_{om}}{\partial x_n} \, e_m e_n$$

$$= \left(-P_1 \delta_{ij} \frac{\partial \hat{v}_{om}}{\partial x_n}\right) (e_u e_j : \; e_m e_n)$$

$$+ \mu \left(\frac{\partial v_{1i}}{\partial x_j} \frac{\partial \hat{v}_{om}}{\partial x_n}\right)(e_i e_j : \; e_m e_n)$$

$$+ \mu\left(\frac{\partial v_{1j}}{\partial x_i} \frac{\partial \hat{v}_{om}}{\partial x_n}\right)(e_j e_i : e_m e_n)$$

$$= - P_1 \; \delta_{ij} \frac{\partial v_{om}}{\partial x_n} \; \delta_{in}\delta_{jm} + \mu\left(\frac{\partial v_{1i}}{\partial x_j} \frac{\partial \hat{v}_{om}}{\partial x_n} \; \delta_{in} \; \delta_{jm}\right.$$

$$\left. + \frac{\partial v_{ij}}{\partial x_i} \; \frac{\partial \hat{v}_{om}}{\partial x_n} \; \delta_{jn}\delta_{im}\right)$$

Since m = j and n = i

$$= - P_1 \; \delta_{ij} \; \frac{\partial \hat{v}_{oj}}{\partial x_i} + \mu \frac{\partial v_{1i}}{\partial x_j} \; \frac{\partial \hat{v}_{oj}}{\partial x_i} \qquad \frac{\partial v_{1j}}{\partial x_i} \; \frac{\partial \hat{v}_{oj}}{\partial x_i})$$

and i ≠ j

$$\therefore = \mu \; (\nabla \underline{v}_1 \cdot \nabla \hat{v}_o^{+} + \nabla \hat{v}_1^{+} \cdot \nabla \hat{v}_o) \qquad \text{(A-2)}$$

by the same procedure it can be proven that

$$\hat{\underline{\underline{\Pi}}}_o : \nabla \underline{v}_1$$

would yield the same quantity as in (A-2) thus the integrand of (A-1) vanishes.

APPENDIX B

EXPERIMENTAL RAW DATA

TABLE B.1.--Experimental Raw Data

a(cm)	k	t(sec)	U(cm/sec)	F_G (dynes)	F_N (dynes)	Re
0.0794	1	3854.8	0.0079	26.44	26.72	1.9×10^{-6}
0.1587	1	949.3	0.0316	208.96	213.74	7.7×10^{-5}
0.316	1	247.8	0.121	1692.66	1659.59	5.9×10^{-5}
0.0794	1.5	2067.7	0.0145	57.83	63.9	3.5×10^{-6}
0.0794	2	1214.7	0.0247	118.96	136.43	6.1×10^{-6}
0.1587	2	293.6	0.1022	952.1	1133.4	2.5×10^{-6}
0.0794	4	306.7	0.0978	857.2	1046.5	2.4×10^{-5}
0.1587	4	74.3	0.403	6871.79	8579.62	9.8×10^{-5}
0.1587	5	45.3	0.662	13329.11	17538.3	1.6×10^{-4}
0.1587	6	30.7	0.976	22955.69	31021.212	2.4×10^{-4}
0.1587	7	22.5	1.33	36390.6	49309.7	3.2×10^{-4}

BIBLIOGARPHY

BIBLIOGRAPHY

Acharya, A., R. M. Mashelkar, and Ulbrcht, J. Rheol. Acta, 15, 454 (1976).

Adler, P. M. Rheol. Acta, 17, 288-295 (1978).

Bacon, L. R. J. Franklin Inst., 221, 251 (1936).

Brenner, H. Chem. Eng. Sci., 16, 242-251 (1961).

Brenner, H., and Happel, J. Chem. Eng. Sci., 19, 599 (1964).

Brenner, H. Low Reynolds Number Hydrodynamics, Noordhoff (1965).

Broadbent, J. M., and Mena, B. J. Non-Newtonian Fluid Mech., 2, 1 (1974).

Brunn, P. Rheol. Acta, 15, 104-119 (1976).

Brunn, P. Rheol. Acta, 15, 163 (1976).

Brunn, P. J. Fluid Mech., 82, 529-547 (1977a).

Brunn, P. Rheol. Acta, 16, 461-475 (1977b).

Brunn, P. Rheol. Acta, 18, 229-243 (1979).

Brunn, P. J. Non-Newtonian Fluid Mech., 7, 271-288 (1980).

Caswell, B., and W. Shwarz. J. Fluid Mech., 13, 417-426 (1962).

Caswell, B. Chem. Eng. Sci., 25, 1167 (±970).

Caswell, B. Appl. Mech. Div., 22 ASME (1977).

Cooley, M. D. A., and M. E. O'Neill. J. Camb. Phil. Soc., 66, 407-415 (1969a).

Cooley, M. D. A., and M. E. O'Neill. Mathematika, 16, 37-49 (1969b).

Cox, R. G., and H. Brenner. Chem. Eng. Sci., 22, 1753-1777 (1967).

Chhabara, R. P., P. H. T. Uhlherr, and Boger, D. V. J. Non-Newtonian Fluid Mech., 6, 187-199 (1980).

Chan, P. C. H., and L. G. Leal. J. Fluid Mech., 92, Part 1, 131-170 (1979).

Dean, W. R., and M. E. O'Neill. Mathematika, 10, 13-25 (1963).

Faxen, H. Ark. Mathematik Astron. Fys., 17, 1 (1923).

Frankel, N. A., and A. A. Crivos. Chem. Eng. Sci., 22, 847-953 (1967).

Gauthier, F., H. L. Goldsmith, and Mason, S. G. Rheol. Acta, 10, 344-364 (1971a).

Gauthier, F., H. L. Goldsmith, and Mason, S. G. Trans. Soc. Rheol. 15:2, 197-330 (1971b).

Gieskus, V. H. Rheol. Acta, 3, 59-71 (1962).

Goldman, A. J., R. G. Cox, and Brenner, H. Chem. Eng. Sci., 21, 1151-1170 (1966).

Goldman, A. J., R. G. Cox, and Brenner, H. Chem. Eng. Sci. 27, 637-659 (1967).

Goren, S. L. J. Colloid Interf. Sci., 36, 94-86 (1971).

Goult, R. J., and Hoskins. Computational Methods in Linear Algebra. New York: John Wiley (1974).

Highgate, D. J., and Whorlow, R. W. Rheol. Acta, 9, 569-576 (1970).

Hoffman, R. L. J. Colloid Interf. Sci., 46, 481-506 (1974).

Kataoka, T., T. Kitano, M. Sasahara, and Nishijima, K. Rheol. Acta, 17, 149-155 (1978).

Leal, L. G. J. Fluid Mech., 69, 305-337 (1975).

Leslie, F. M. and R. Z. Tanner. 14, Pt. 1, 36-48 (1961).

Lin, C. J., K. L. Lee, and Sather, N. F. J. Fluid Mech, 43, 35-47 (1970).

Lorentz, H. A., Abhand. L. The Gret. Phys. 1, 23 (1906).

Michele, J., R. Patzold, and Donis, R. Rheol, Acta, 16, 317-321 (1977).

Nir, A., and A. Crivos, A. J. Fluid Mech., 59, 209-223 (1973).

Oldroyed, J. G. Proc. Roy. Soc. A, 245, 278 (1958).

O'Neill, M. E. Mathematika, 11, 67-74 (1964).

Papenhuijzen, J. M. P. Rheol. Acta, 11, 73-88 (1972).

Riddel, M. J., C. Narvaez, and Bird, B. J. Non-Newtonian Fluid Mech., 2, 23-35 (1977).

Russell, W. B. J. Rheol., 24, 287-317 (1980).

Sakai, K., Adachi, K., and N. Yoshioka. J. Non-Newtonian fluid Mech., 3, 107-125 (1977/1978).

Sigli, D., and Countanceau, J. J. Non-Newtonian Fluid Mech., 2, 1-21 (1977).

Soni, K., and Soni, R. P. SIAM J. Math. Anal., 4, 466-481 (1973).

Stimson, M., and Jeffery, G. B. Proc. R. Soc., A111, 116-119 (1926).

Sun, K., Jayaraman, K. J. Chem. Eng. Commun., 20, 137-155, (1982).

Sutterby, J. L. Soc. Rheol, 17:4, 559-573 (1973).

Thomas, R. H., and Walters, K. Rheol. Acta, 5, 23-27 (1966).

Zeichner, G. R., and Schowalter, W. R. AICHE J., 23, 243-254 (1977).